Titre: Title:	PMG: Numerical Model of a Fault Tolerant Permanent Magnet Generator for High RPM Applications
Auteur: Author:	Alexandre Bertrand
Date:	2014
Type:	Mémoire ou thèse / Dissertation or Thesis
Référence: Citation:	Bertrand, A. (2014). PMG: Numerical Model of a Fault Tolerant Permanent Magnet Generator for High RPM Applications [Mémoire de maîtrise, École Polytechnique de Montréal]. PolyPublie. https://publications.polymtl.ca/1356/

UNIVERSITÉ DE MONTRÉAL

PMG: NUMERICAL MODEL OF A FAULT TOLERANT PERMANENT MAGNET GENERATOR FOR HIGH RPM APPLICATIONS

ALEXANDRE BERTRAND

DÉPARTEMENT DE GÉNIE ÉLECTRIQUE

ÉCOLE POLYTECHNIQUE DE MONTRÉAL

MÉMOIRE PRÉSENTÉ EN VUE DE L'OBTENTION

DU DIPLÔME DE MAÎTRISE ÈS SCIENCES APPLIQUÉES

(GÉNIE ÉLECTRIQUE)

FÉVRIER 2014

UNIVERSITÉ DE MONTRÉAL

ÉCOLE POLYTECHNIQUE DE MONTRÉAL

Ce mémoire intitulé:

PMG: NUMERICAL MODEL OF A FAULT TOLERANT PERMANENT MAGNET GENERATOR FOR HIGH RPM APPLICATIONS

présenté par : BERTRAND Alexandre

en vue de l'obtention du diplôme de : Maîtrise ès sciences appliquées

a été dûment accepté par le jury d'examen constitué de :

M. KARIMI Houshang, Ph.D., président

M. MAHSEREDJIAN Jean, Ph.D., membre et directeur de recherche

M. SIROIS Frédéric, Ph.D., membre et codirecteur de recherche

M. KOCAR Ilhan, Ph.D., membre

ACKNOWLEDGMENTS

I would like to thank my director and co-director, Professor Jean Mahseredjian and Professor Frédéric Sirois for their guidance, support and expertise.

I also would like to say special thank to Ulas Karaagac for his help and support throughout the project. I will always be grateful for the technical advice and experience he generously shared with me.

I also would like to thank Mr. Kevin Dooley from Pratt & Whitney Canada for his crucial contribution to the project.

RÉSUMÉ

L'industrie aéronautique fait face aujourd'hui à de nombreux défis. Ces défis, tant sur les plans environnemental qu'économique et social, ont forcé l'industrie à se tourner vers de nouvelles façons de faire et de penser. C'est dans ce contexte qu'est né le concept de l'avion plus électrique (aussi appelé dans la littérature More Electrical Aircraft – MEA). Ce concept vise à augmenter la contribution de l'énergie électrique au sein des aéronefs en comparaison avec les sources d'énergie plus traditionnelles telles que l'énergie hydraulique ou mécanique.

Afin de pouvoir supporter cette demande croissante en énergie, la génération d'électricité à bord des appareils doit aussi subir une réingénierie. C'est donc en support au MEA que le moteur plus électrique (aussi appelé dans la littérature More Electrical Engine – MEE) a vu le jour. C'est précisément dans le cadre des moteurs plus électriques que le présent projet s'inscrit. Ce projet, réalisé en partenariat avec Pratt & Whitney Canada, se veut une première approche à la modélisation électrique de cette nouvelle génération de générateurs destinés aux aéronefs. Les principaux objectifs de ce projet sont d'étudier le fonctionnement du NAEM (New Architecture Electromagnetic Machine) et de bâtir un modèle simplifié de ce générateur sous EMTP-RV capable de reproduire le comportement du NAEM en régime permanent.

Ce mémoire contient les résultats obtenus dans le cadre d'un premier projet de modélisation du générateur développé par Pratt & Whitney Canada (New Architecture Electromagnetic Machine – NAEM) sous un logiciel de simulation électrique. Le modèle construit par Pratt & Whitney Canada sous MagNet, un logiciel de simulation par éléments finis, a été utilisé comme référence dans le cadre de ce projet. Il a été possible de développer un modèle électrique qui calque bien le comportement du modèle magnétique de référence pour des conditions d'opération en régime permanent. Quelques pistes de solutions techniques sont abordées dans la discussion afin de dresser une liste sommaire des travaux à considérer pour la poursuite du projet.

ABSTRACT

The aerospace industry is confronting an increasing number of challenges these days. One can think for instance of the environmental challenges as well as the economic and social ones to name a few. These challenges have forced the industry to turn their design philosophy toward new ways of doing things. It is in this context that was born the More Electrical Aircraft (MEA) concept. This concept aims at giving a more prominent part to electrical power in the overall installed power balance aboard aircrafts (in comparison to more traditional power sources such as mechanical and hydraulic).

In order to be able to support this increasing demand in electrical power, the electric power generation aboard aircrafts needed reengineering. This is one of the main reasons the More Electrical Engine (MEE) concept was born: to serve the needs of the MEA philosophy. It is precisely under the MEE concept that this project takes place. This project, realized in collaboration with Pratt & Whitney Canada (PWC), is a first attempt at the electrical modelling of this new type of electrical generator designed for aircrafts. The main objectives of this project are to understand the principles of operation of the New Architecture Electromagnetic Machine (NAEM) and to build a simplified model for EMTP-RV for steady-state simulations.

This document contains the results that were obtained during the electrical modelling project of the New Architecture Electromagnetic Machine (NAEM) by the author using data from PWC. The model built by PWC using MagNet, a finite element analysis software, was used as the reference during the project. It was possible to develop an electrical model of the generator that replicate with a good accuracy the behaviour of the model of reference under steady-state operation. Some technical avenues are explored in the discussion in order to list the key improvements that will need to be done to the electrical model in future work.

TABLE OF CONTENTS

LIST OF TABLES

LIST OF FIGURES

LIST OF ABBREVIATIONS

DLL	Dynamic Link Library
EMF	Electromotive Force
FE	Finite Element
FFT	Fast Fourier Transform
ISG	Integrated Starter Generator
MEA	More Electrical Aircraft
MEE	More Electrical Engine
NAEM	New Architecture Electromagnetic Machine
PMSM	Permanent Machine Synchronous Machine
PWM	Pulse-Width Modulation
RMS	Root Mean Square

LIST OF ANNEX

INTRODUCTION

The aerospace industry has never faced more challenges since its creation. Rising oil prices, rising environmental concerns and awareness, and a constant need to improve the reliability of all aircrafts are among the biggest challenges this industry has to deal with. In such a complex and challenging context, there is a constant need to improve and reinvent the technologies used aboard aircraft. This is where the More Electrical Aircraft (MEA) [1-3] concept comes into play. As its name implies, the MEA philosophy is based on the valorization of electrical power embedded in aircrafts.

One of the back bones of the MEA philosophy is a similar concept, applied this time to the gas engines of the aircrafts: the More Electrical Engine (MEE) [4-6]. As one can easily imagine, a growing demand in electricity requires a growing capacity in terms of production of electrical power. This is one of the goals achieved by the MEE. This project is part of the industry's efforts towards the implantation of the MEE philosophy aboard aircrafts.

The scope of the current project is, first, to present the theoretical concepts that underlie beneath the NAEM design in regards to the state of the art of the technology. Second, this project is an initial attempt to model the electrical behaviour of the New Architecture Electromagnetic Machine (NAEM) developed by Pratt & Whitney Canada (PWC) for steady-state operation in EMTP-RV. This project is directly in line with the MEE philosophy that the industry is now pursuing as the electrical modelling of the NAEM will make it possible in the future to include this generator in a complete aircraft power system. For this first model, the main objectives were to understand the mechanisms behind the NAEM design and to produce a simplified model for EMTP-type simulations of the NAEM using the magnetic model as a reference.

The present report presents the academic path followed to achieve the objective of the project and is divided into 5 main sections. The first section presents the state of the art in the industry regarding MEA and MEE. This will give the reader a fair idea of what is the current position of the industry as well as the context in which the NAEM project takes place. In addition, this section contains the methodology of the modelling project (the objective and the project methodology).

Chapter 2 familiarizes the reader with the NAEM finite element (FE) model. This model was built by PWC using the software MagNet by the Infolityca Corporation. By presenting the magnetic model, the technical details that lay behind the design of the NAEM will also be explained, and the behaviour of the NAEM will be demonstrated using MagNet. It is in this section that the reader will also find the details about the simulations that were run using MagNet during the project. This section completes the literature review and, therefore, the first objective of the project. After this chapter, the reader will be able to put the technological advances of this new generator design, developed by Pratt &Whitney Canada, in perspective in regards to the state of the art.

The next chapter presents the electrical model, the main objective as well as the original contribution of the project. The process that led to the building of the electrical model is first presented. This includes for instance the modelling assumptions (as well as the justifications for those assumptions) and the calculation details for each of the components in the model. Therefore, at the end of this chapter, the reader should be able to fully understand the electrical model built by the author during the project.

Chapter 4 presents the results. Results coming from both MagNet and EMTP-RV are superposed for 4 different test scenarios. Both models are compared and the accuracy of the electrical model is analyzed taking the results from MagNet as the reference.

Chapter 5, contains a technical discussion of the results showed in the previous section. It is in this section that the main differences are explained and discussed as well as the limitations of the current EMTP-RV model. Some possible improvements for future work on the model are also discussed here.

CHAPTER 1 STATE OF THE ART & METHODOLOGY

This chapter presents the state of the art of the more electrical aircraft (MEA) project in the industry. It attempts to make a concise summary of the context in which the MEA project evolves and what are the main technical challenges related to the implantation of such philosophy in tomorrow's aircraft.

1.1 More Electrical Aircraft (MEA)

As its name indicates it, the MEA is a will of the industry to increase the importance of electrical components in aircrafts. The most obvious examples of such increase are the on-board entertaining systems and comfort related systems in modern aircrafts, but the MEA also covers more valuable and vital systems of the aircraft. One can think for instance of the fly-by-wire programs (where the hydraulic links between the cockpit and the various components are replaced by an electrical link), or the power-by-wire philosophy (where mechanical components are replaced by their electrical counterparts). These two philosophies are somewhat new in the aerospace industry where the technology of choice has historically always been mechanical. It is essential to note that the MEA program is not limited to the two areas mentioned above; as a matter of fact, virtually every task accomplished aboard by a mechanical component can be accomplished by an electrical component.

By replacing mechanical components with their electrical counterpart, one can achieve significant improvements. One of the most significant improvements is related to the efficiency of aircrafts. For instance, by replacing the mechanical actuators by electrical ones, it is possible to reduce the consumption of fuel during a flight due to reduction of weight and size of the required equipments. The elimination of gearboxes aboard the aircraft is one of the most relevant examples. Numerous studies have proved this fact beyond any doubt [1, 7-12] as it is one of the main goals pursued by aeronautic corporations to improve their financial situation as well as reducing their footprint from an environmental point of view. Another crucial point is the improvement of the reliability of key systems. Electrical components are often more reliable than their mechanical counterpart (for instance, electrical actuators in comparison with typical hydraulic/mechanical ones [13]), and their conception makes it often easier to achieve redundancy, which also increases the reliability. As other advantages of electrical components

over mechanical ones, one could think of lower maintenance costs, easier monitoring and assessment of each component and lower weight.

1.2 More Electrical Engine (MEE)

Such an ambitious undertaking comes with a lot of technical challenges. One of the main challenges is to be able to meet this growing demand for electricity on-board of aircrafts. Indeed, the more tasks accomplished by electrical components, the more electrical power the aircraft needs on board. As the tasks performed by some of those electrical components are crucial to the safety of the aircraft and its passengers, this electrical power supply needs to be reliable. This is precisely where the more electrical engine (MEE) comes into play.

The MEE is therefore an integral part of the MEA project. It could even be considered as the backbone of the MEA philosophy as it is the MEE which will support the growing electrical demand on-board. Speaking of growth in electrical demand, one may note that some authors are starting to talk about the “megawatt dream” [14] aboard aircraft. Although this milestone is still to achieve, it clearly shows that the place of the MEA concept and, therefore, the MEE, is expected to grow significantly in importance in the years to come.

The essence of the MEE is truly the integrated starter generator (ISG) [15]. As the name implies it, an ISG plays both the role of starter (which is required only for a few seconds at the starting of the engines) and the role of a generator which will provide electrical supply throughout the different phases of the aircraft flight.

1.3 New Architecture Electromagnetic Machine (NAEM)

The New Architecture Electromagnetic Machine (NAEM) developed by Pratt & Whitney Canada falls directly into the MEE philosophy. In fact, the technological choices behind the design of this new generator were all driven by the needs and the requirement of the MEE. This section is intended to present the NAEM and to give the reader a strong overview of the design particularities that make the NAEM an innovative technology, and the ways it is linked to the MEE philosophy. As it will be discussed, the NAEM can be either controlled actively or passively. The two modes will be presented here, but the current project focuses on the actively

protected NAEM. The technical theory that supports those technological improvements is explained in details using the FE model of the machine in a subsequent section.

First, the permanent magnet synchronous machine (PMSM) was chosen as the base design due to, among other factors, its high power density. As weight is a key element in aircraft design, it is of crucial importance to achieve the higher power production per unit of weight possible to avoid carrying dead weight during the whole operational life of the aircraft, which would result in higher fuel consumption. In addition to that, a PMSM has no wearing parts such as brushes and rigging system because it has permanent magnets in the rotor to create the field flux instead of field windings [15]. This leads to a more reliable generator while keeping the maintenance costs low. The outside rotor configuration was privileged by PWC for the NAEM.

In the actively controlled NAEM, one of the most significant technological progresses in comparison to a regular PMSM design is the addition of a control winding inside the machine. In the past, the PMSM has not been a popular choice in the aerospace industry. Even thought this type of machine makes it possible to achieve a high power density, it has been put aside due in part to the destructive potential of an internal fault. The control coil embedded inside the NAEM is giving a strong control over the output of the machine in various operational conditions (no-load, full-load, overload and in a faulty scenario to name a few). This improvement of the traditional PMSM architecture therefore has opened the way to permanent magnet machines into the aerospace industry. The control over the output of the generator is done by connecting this control coil to external circuitry that controls the current flowing through the control coil and thus controlling the saturation of the magnetic core of the machine. This is the reason why this type of control in the generator is referred to as “active control”.

This active control shares some similarities with the principles of operation of a saturable reactor. In saturable reactors, the injected direct current on the DC side of the reactor controls the level of saturation of the core. As the inductance value of the core is fixed by the saturation level, there is a direct relationship between the impendence of the core and the magnitude of the injected direct current. The same principle applies for the saturable-core inductances in the control portion of the NAEM. A visual representation of this phenomenon is shown in figure 1-1.

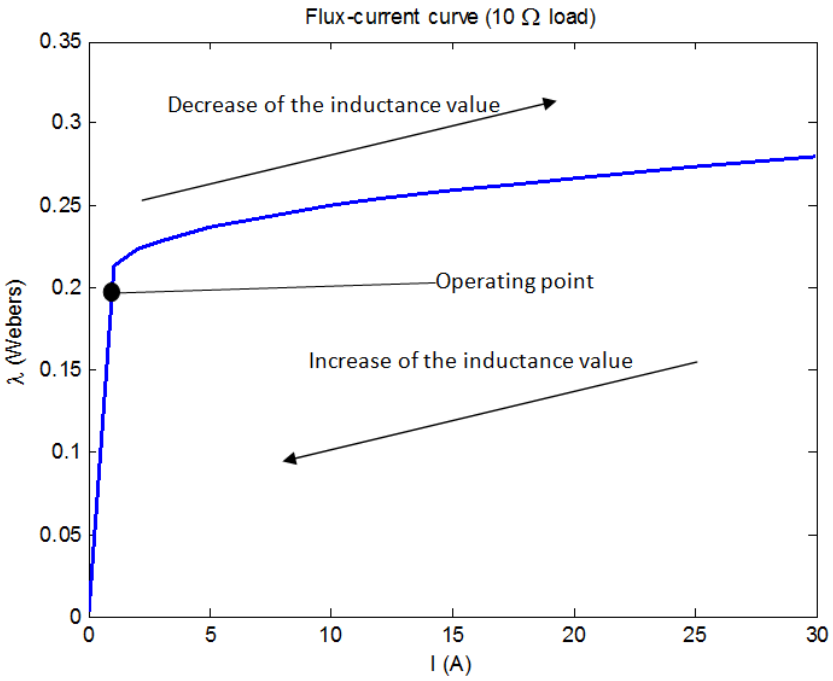

Figure 1-1 Visual representation of the behaviour of a saturable-core inductance

There is another type of control which can be embedded in the machine and referred to as "passive control". This protection is a two-level protection and, as its name implies, does not require any external action to take place. The first level of protection is a direct consequence of the materials used in the construction of the generator and is known as the Curie point, or the Curie effect [16]. More precisely, around 425°F, the core's magnetic susceptibility decreases and the magnetic material becomes paramagnetic. This automatically has the effect of reducing the generated voltage of the machine and thus the output current [17]. This effect is 100% reversible, and if this first protection level is effective enough and the temperature of the machine decreases, the magnetic core regains its magnetic properties, and the generator can continue to operate normally. The rate at which the generator can regain its normal properties depends on the cooling of the generator (the properties are restored once the temperature of the core is below the Curie point). But, if this first level is insufficient and the internal temperature still continues to rise, the second level of passive protection comes into action. This second level is the activation of an eutectic fuse that has the effect of increasing the internal impedance of the machine. This change is permanent, and the NAEM cannot recover its original properties after the activation of the eutectic fusible. The goal here is to reduce permanently the output current of the NAEM should

the temperature rises around 530°F [18]. The passively protected generator was presented here to give the reader a complete overview, but this mode of protection was not considered in the modelling of the machine for this project.

One must also note that the NAEM uses a single-turn solid copper winding arrangement for the output winding. This improves the overall reliability of the machine by simultaneously reducing two separate hazards. First, as the winding is made of a single-turn coil design, the possibility of a turn-to-turn failure inside the stator is virtually inexistent. This is a crucial point as this type of internal fault can be particularly destructive. Second, again due to the single-turn architecture, the machine operates at a low voltage level. Thus, the dielectric stress on the insulation is lower, and the risk of an electric arc is correspondingly diminished.

Another key element is that, as it will be explained in details, the NAEM uses a three-channel configuration that ensures a full redundancy of the generator. In other words, there are, in fact, three generators in one physical unit; each of which is able to produce electrical power independently from the two other units. It is therefore possible to use different generating configurations depending on the situations the aircraft may face. It goes without saying that this three-channel configuration significantly increases the redundancy of the system and thus the reliability of the power generation.

Figure 1-2 summarizes the main characteristics of the NAEM in comparison to a regular PMSM. From this figure, one can easily see that the main difference between both concepts truly is the control winding (illustrated in green).

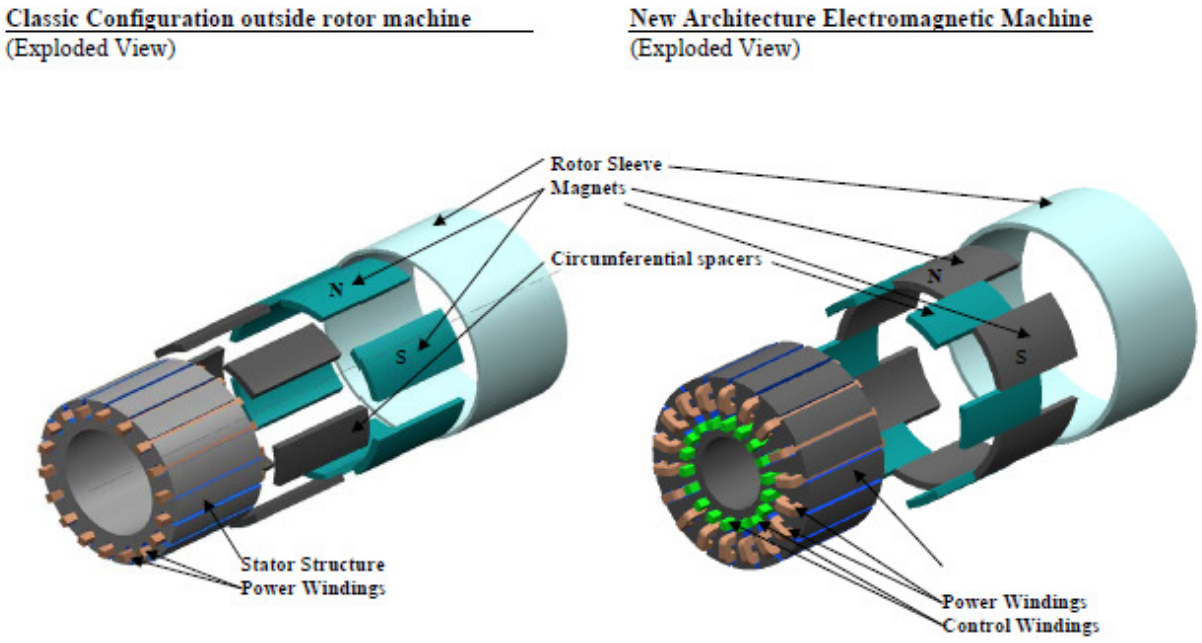

Figure 1-2 Comparison between a regular PMSM and the NAEM [15]. Used with permission.

1.4 Methodology

The focus of this subsection is to expose the methodology of the project and its main objectives. One must note that the modelling assumptions are presented further in the document.

1.4.1 Main objectives

This project pursues one main objective: to develop a first electrical model of the NAEM. This objective was achieved by going through the following steps. The first one was to establish the state of the art regarding the MEE. This first step was mandatory to position the NAEM in its technological context. This literature review is summarized above and concludes in chapter 2 with the presentation of the NAEM design.

The second step was to develop the electrical model per say of the NAEM, using the finite element (FE) model as a base. In other words, the magnetic model built by PWC was to be transposed into an electrical model, using the relevant modelling assumptions. The developed model is intended to be a steady-state model in time-domain. This means that it will be possible to simulate the machine mainly in steady-state conditions with this model: fixed speed and fixed

load. This electrical model of the machine was developed in EMTP-RV. This objective was the backbone of the project.

The third and final step was the validation of the developed model. The validation was done using the FE model developed in MagNet by PWC. This validation of the developed electrical model was essential to be able to assess the level of fidelity of the model (with respect to the magnetic model). Therefore, it was needed to be able to identify the next steps to undertake in order to produce a more accurate model in a future project. This is the topic of the last two subsections of the present document.

1.4.2 Methodology

In order to achieve the objective presented above, the following methodology is used:

1) Do a complete literature review and gather all the data available from the industrial partner: PWC.
2) Study of the FE model of the NAEM.
3) Development of the electrical model using EMTP-RV.
4) Validation of the EMTP-RV model using the simulations ran in MagNet.

CHAPTER 2 FINITE ELEMENT MODEL

This chapter is dedicated to the presentation of the finite element model of the NAEM developed by PWC. It also explains the architecture of the generator and explains its behaviour. Some results coming from the FE model are presented at the end of this chapter to illustrate the capabilities of the NAEM. Figure 2-1 is an exploded view of the NAEM to which the reader can refer throughout the document to understand the geometry of the model. The figure was extracted from [15].

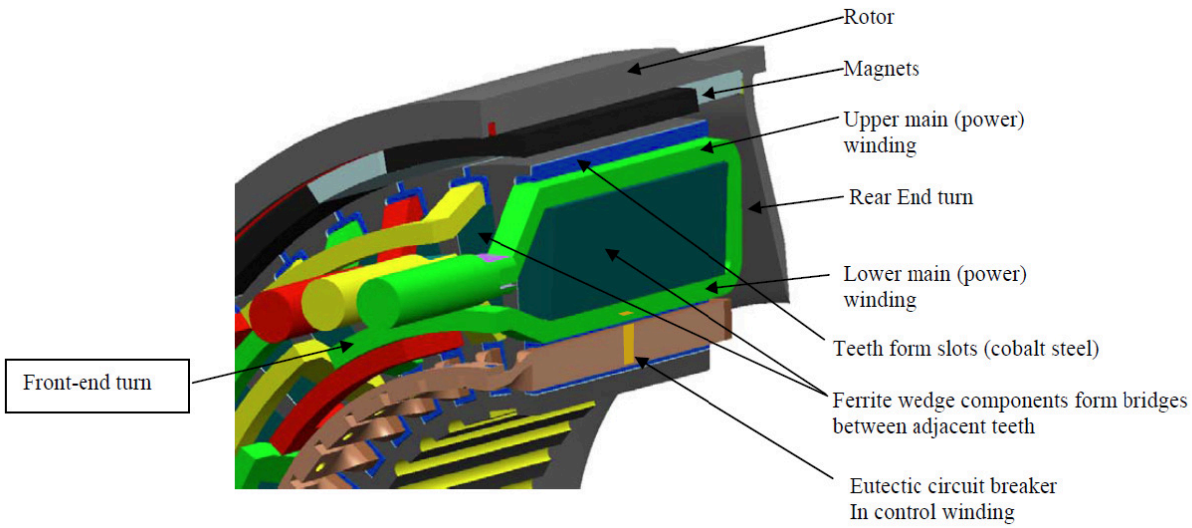

Figure 2-1 Exploded view of the NAEM [15]. Used with permission.

2.1 Brief presentation of MagNet

This subsection presents a brief overview of the FE element software (MagNet) [19] used to model the electromagnetic behaviour of the NAEM.

MagNet is a FE element software developed by the company Infolytica and was used by PWC to build the initial model of the NAEM. The software makes it possible to couple an electromagnetic model (which takes into account the real geometry of the device as well as the response of the different materials used in the machine to electromagnetic fields) with an external electrical circuit. From this point, it is then possible to compute a complete set of electrical and magnetic parameters: flux, magnetic field, voltage across components, current flowing through

each component, etc. These results have been used to compare the performances of both electrical and magnetic models of the generator.

2.2 Overview of the FE model

As mentioned before, the FE model was built by PWC in the design phase of the NAEM. The version of the model that was used throughout the whole project is the PW625Me model, revision B [15]. Should there be any substantial revision of the model issued, it would need to be assessed to ensure the best correlation possible between the developed electrical model and the magnetic one.

2.2.1 NAEM model geometry in MagNet

The magnetic model was built by PWC using a series of assumptions. As these assumptions affect directly the results obtained, it is essential for the reader to acknowledge and understand them. The NAEM was approximated using a 2D model [15]. This leads to a null flux in the z axis and the calculations of the fluxes are performed in the x-y plane. Figure 2-2 below shows the geometrical representation of the machine model built in MagNet by PWC.

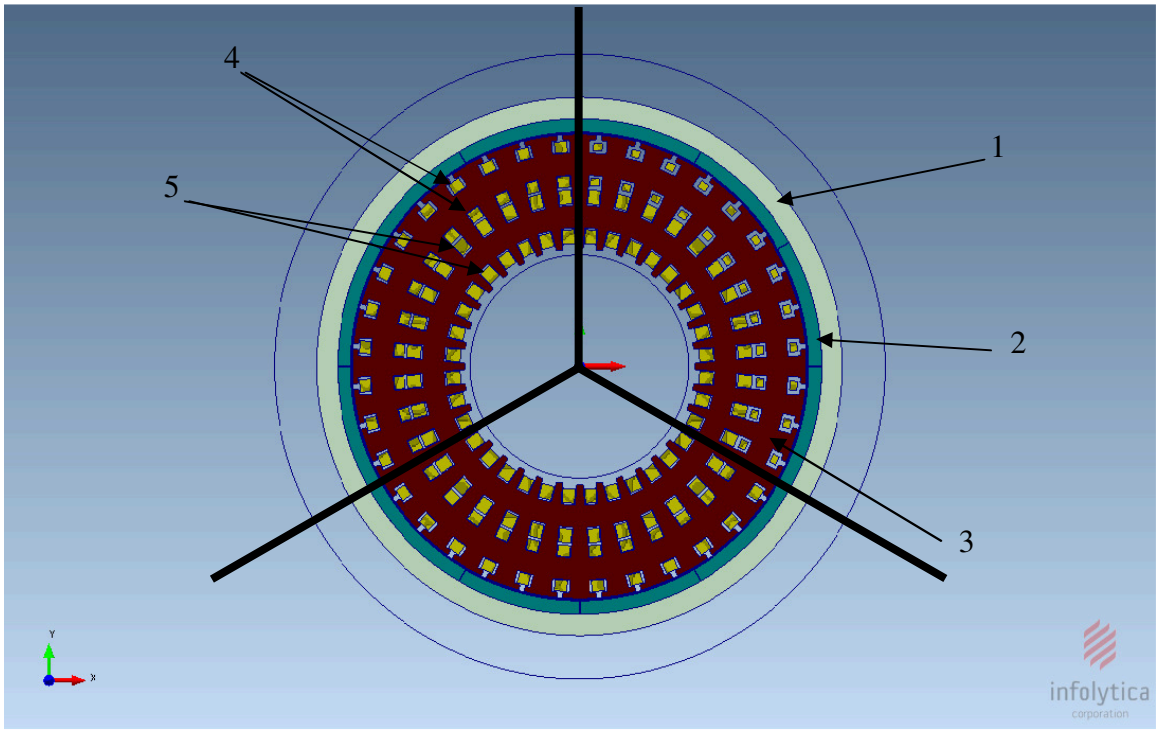

Figure 2-2 Physical representation of the machine in MagNet

One must first notice that this is an “outside rotor” configuration. In other words, “1” and “2” constitute the rotor, being the rigid part of the rotor and the permanent magnets respectively. Item “3” is the magnetic core of the stator. Components “4” and “5” are the phase windings and the control windings respectively. It is important to note that both windings are passing through an upper and a lower slot. In addition, the phase windings consist of single-turn solid copper coils, but the control winding is constituted of 24-turn coils.

Another important aspect to note is the presence of three machines in one (three-channel generator). The bold black lines indicate the separation of these three machines. This ensures redundancy inside the NAEM and, therefore, is a step further in improving reliability. The two machines in the upper and lower left are low-voltage AC machines (28 volts, main systems supply), and the third one on the right is a high voltage AC machine (115 volts, intended to be mainly used as a heating power source). In other words, the output of the two low voltage AC machines is first rectified by a three-phase diode bridge before being distributed in the aircraft in opposition to the output of the third AC machine that is distributed in AC (not rectified). It is assumed in this project that there is no coupling between the three machines; this allows the development of a model for a single channel without any regard for the other ones.

Each of the materials contained in the geometrical model is defined by an internal material library from MagNet. For instance, here are the main characteristics of the stator core material.

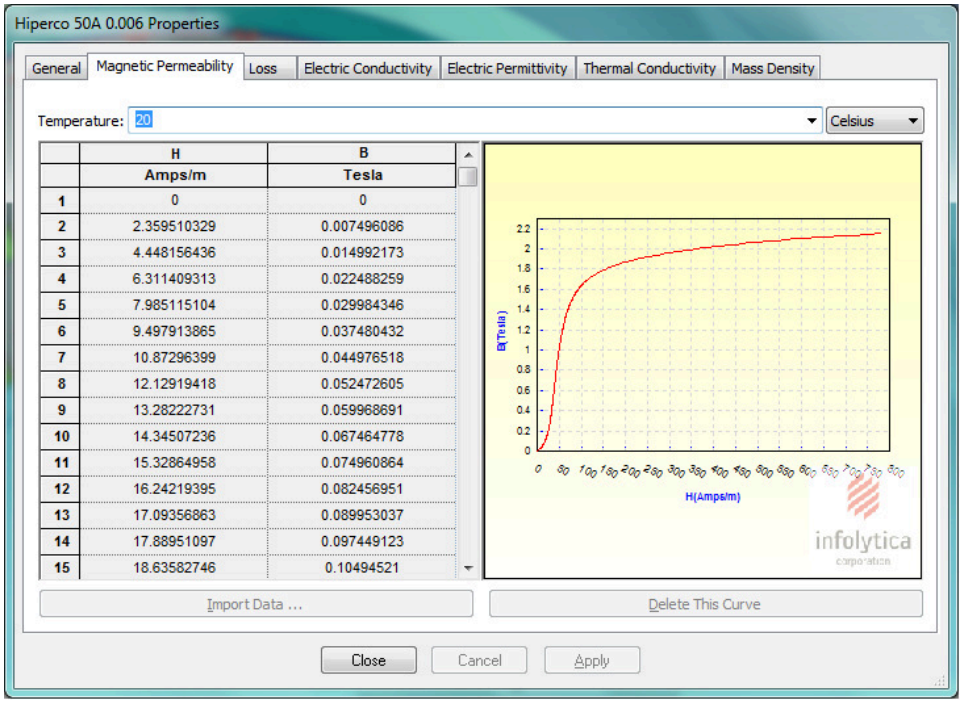

Figure 2-3 Magnetic permeability of the stator core material

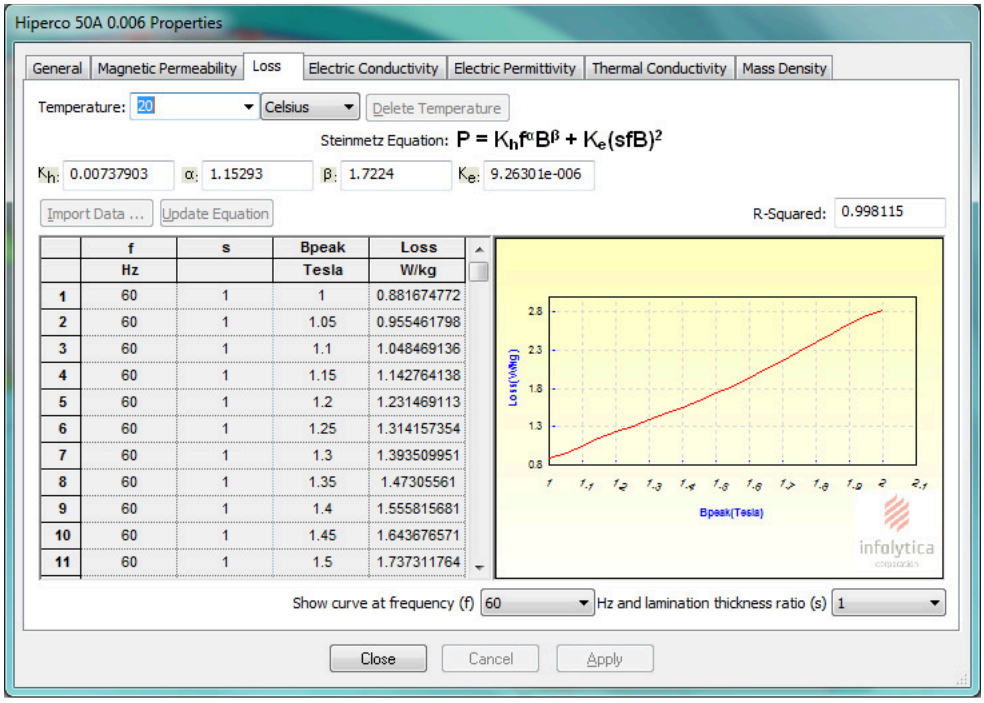

Figure 2-4 Losses of the stator core material

Each material in the geometrical model can be parameterized the same way as the magnetic stator core material presented above. This increases the accuracy of the model as it is possible to build a geometrical model using the exact same materials that are used in the actual generator.

To better understand the path taken by each coil, figure 2-5 and figure 2-6 illustrate the paths of phase A and of the control coil. Phases B and C follow the same pattern as phase A in the other slots. The concerned windings are highlighted in yellow in each case.

From figure 2-5, it is possible to see the path followed by phase A winding from the start of the coil to its end (both identified on the figure). A slot marked with a dot is indicating that the current is coming towards the reader, and a slot marked with a cross indicates the opposite. By knowing this, it is now possible to understand the path followed by the winding. First, the winding is going from the connector (behind the machine) to the top of the generator in what is called the lower slot. The winding is then bent to return to the back of the machine in the upper slot (nearest to the rotor). In the back of the generator, the winding is then re-introduced into the following slot (the next "upper slot" while going up on the figure). The same process is then repeated for each slot until the end, where the winding is attached to the second connector (at the back of the machine).

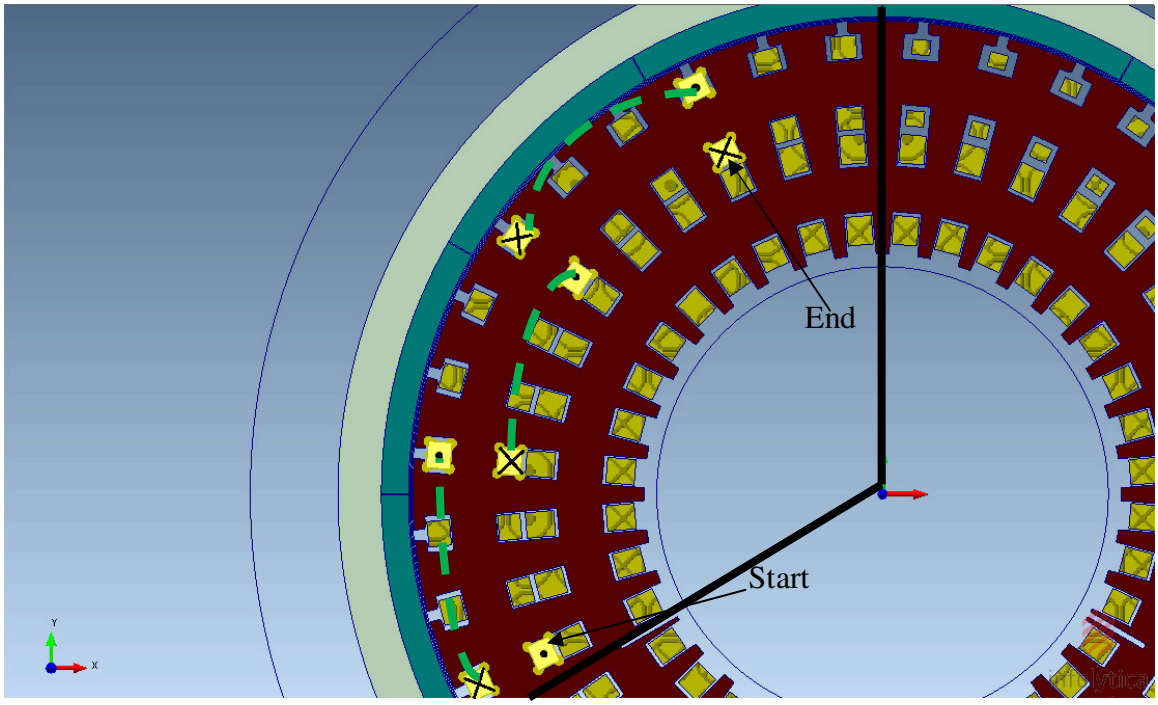

Figure 2-5 Phase A winding path

The connections between the slots are shown by the green dashed lines. Each channel of the NAEM is configured in a 12-poles arrangement.

Figure 2-6 shows the connection strategy for the control coil. Even if the philosophy here is slightly different, one must note that the same “upper” and “lower” slot configuration is used here. Connected at the back of the machine, the first winding comes towards the reader from the identified slot to be bent in the corresponding lower slot (the one at the bottom of the figure) to go back on the other side of the machine. The winding is then going to the next upper slot (as opposed to the phase winding, which was going back to the next corresponding slot without changing level) where it comes back towards the reader again. From there, it is bent to fit in the lower slot to go back on the other side of the machine. The process is afterwards repeated until the end of the coil, where it is bonded to a connector. The connections between the slots are shown by the green dashed lines.

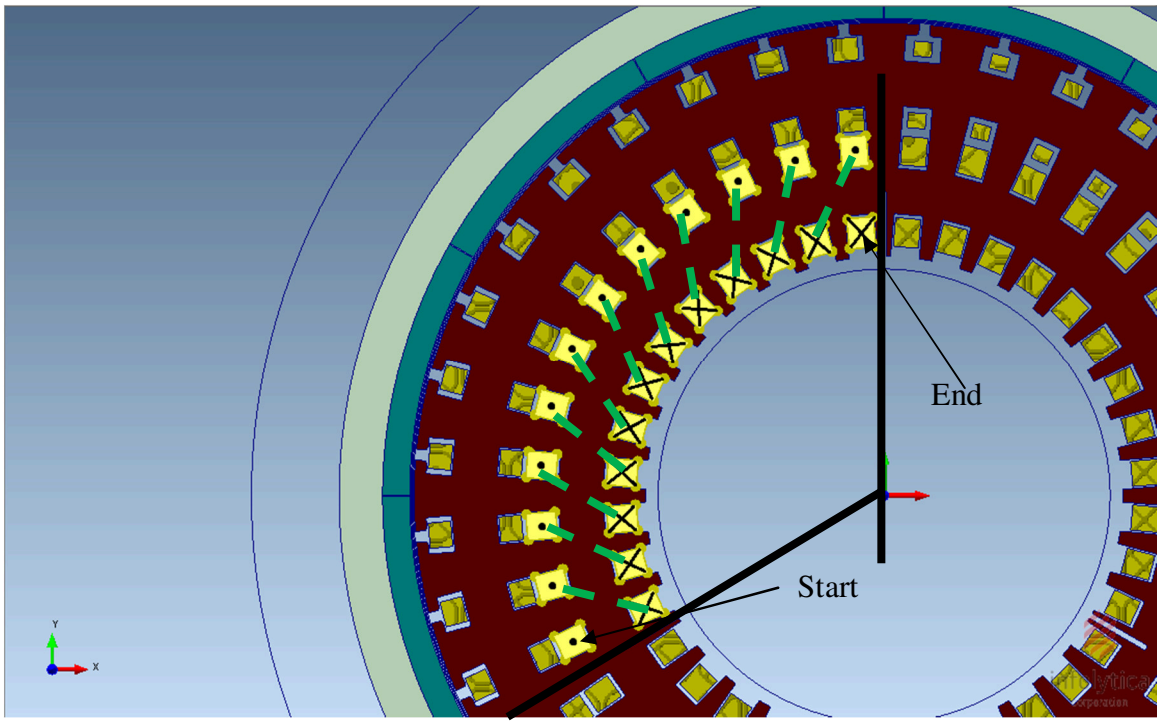

Figure 2-6 Control coil close-up

Both connection schemes are summarized in figure 2-7, showing one channel of the NAEM.

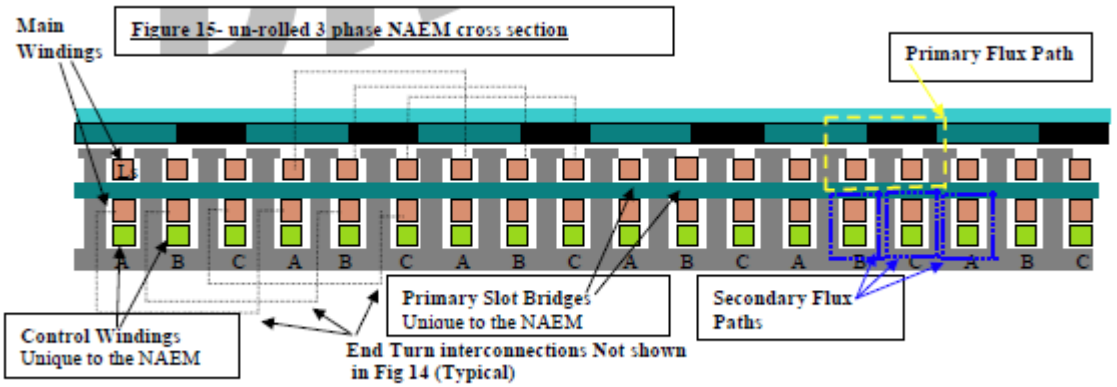

Figure 2-7 Unrolled 3-phase NAEM cross-section [15]. Used with permission.

Following that logic, it can be seen that the control coils beneath each phase winding are connected in series, in the same direction (in figure 2-7, the lower part of the control coil is not shown). This type of connection causes a cancellation of the net AC flux that is created in the control coil by the phase coils. This cancellation can be understood by seeing that each coil in a "pair" of coils has a phase shift of 180° with its neighbour; thus, when a given slot is seeing a maximum positive peak of the AC flux, the slot beside it is seeing a maximum negative peak of the AC flux and vice-versa. This phenomenon is repeated for the complete control coil winding, cancelling the net AC flux that would be created otherwise across the control coil's terminals. Furthermore, the connection in series of the control coil for phase A, B and C allow the usage of only one control circuit to control all three phases as only one signal of direct current is needed.

This means that by modifying the magnitude of the control current, one modifies the saturation level of the secondary magnetic path. As a portion of the stator coils is coupled with this secondary magnetic path, they are affected by this change in the saturation level. This change results in a modification of the overall impedance of the generator stator (a modification in the saturation level changes the operating point on the saturation curve of the material) as seen by the network at the output of the generator. It is this principle of operation that makes it possible to control the output current for a given load and speed.

For comparison purposes, figure 2-8 shows the same unrolled cross section, but of a typical synchronous machine this time.

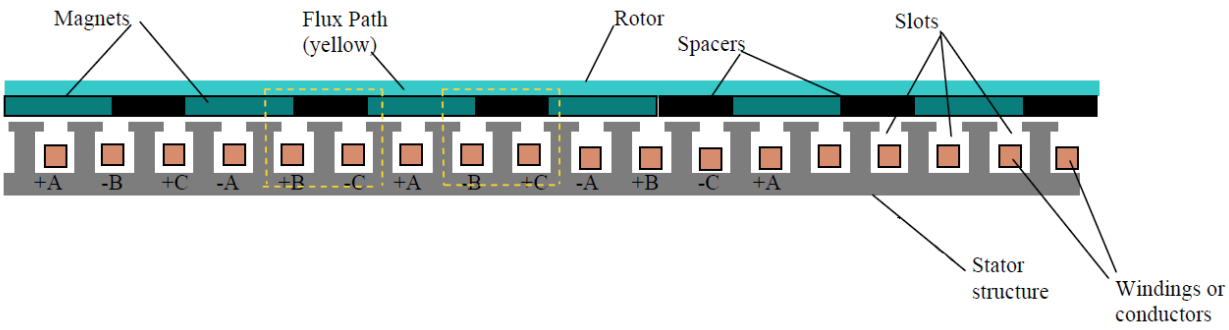

Figure 2-8 Unrolled 3-phase conventional synchronous machine cross-section [15]. Used with permission.

In figure 2-8, one can clearly see that there is only one magnetic path. This path is composed of the permanent magnet of the rotor and the stator coils. Thus, here, it is not possible to modify the internal impedance of the machine.

2.2.2 External circuitry

In addition to the physical model shown above, an external electrical circuit model is also attached to the geometrical model. As discussed previously, this is done directly in MagNet and permits to emulate the behaviour and the effects of some of the external components of the machine such as the DC source and the line cable inductance. Figure 2-9 is showing the external circuit for a single channel of the machine; the circuit was set for a steady-state test at the time of capturing the screenshot. There is one such circuit for each channel of the machine.

At first sight, it is easy to identify the four coils of the channel that are the three-phase coils named “LowV1-PhA Coil”, “LowV1-PhB Coil” and “LowV1-PhC Coil” and the control coil named “LowV1-Ctrl Coil”. The characteristics of these coils are defined by the geometrical construction previously seen, as well as by the different material properties. The coils are then included in the electrical circuit by connecting them via their two respective connectors; it is the coil-type components that are linking together the geometrical model (solved by FE) and the electrical circuit.

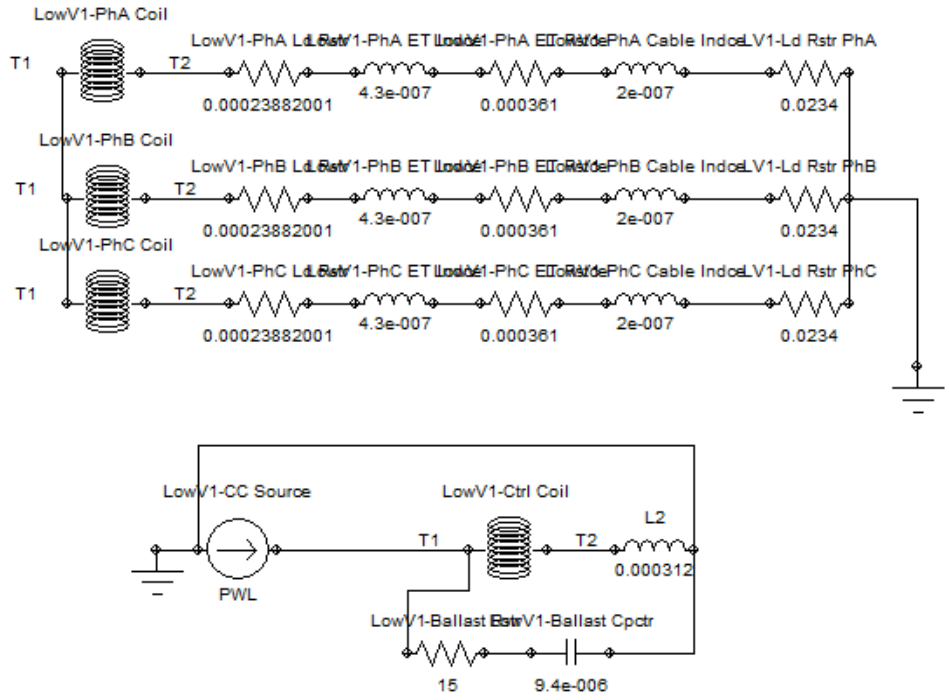

Figure 2-9 External circuit of one channel of the NAEM

One can see that these coils are connected to two different sub-circuits. The circuit with the phase coils is the "power" circuit, which account for power generation by the machine and consumption by the load ("LV1-Ld Rstr PhA"). The other elements are there to take into account the end turn inductance and resistance as well as the connector resistance and inductance. In fact, this sub-circuit is simulating all the elements that are not simulated by the FE model (this is the reason why some components, as the leakage inductance for instance, are not shown in the circuit above). This sub-circuit is coupled with the control one via the magnetic coupling between the phases and control coils. This coupling is taken into account and simulated in the FE portion of the model.

The second sub-circuit, as one might expect, is the electrical representation of the control circuit. It contains the control coil and the DC source which permit the modulation of the machine's internal impedances. The RC branch was added there by the designer of the model (PWC) to damp some high frequency transient effects and is not of substantial importance here as the current project focuses on steady-state modelling.

Each of the components shown in figure 2-9 is customizable with its respective parameters. For instance, figure 2-10 shows some of the possible options for the coil-type component.

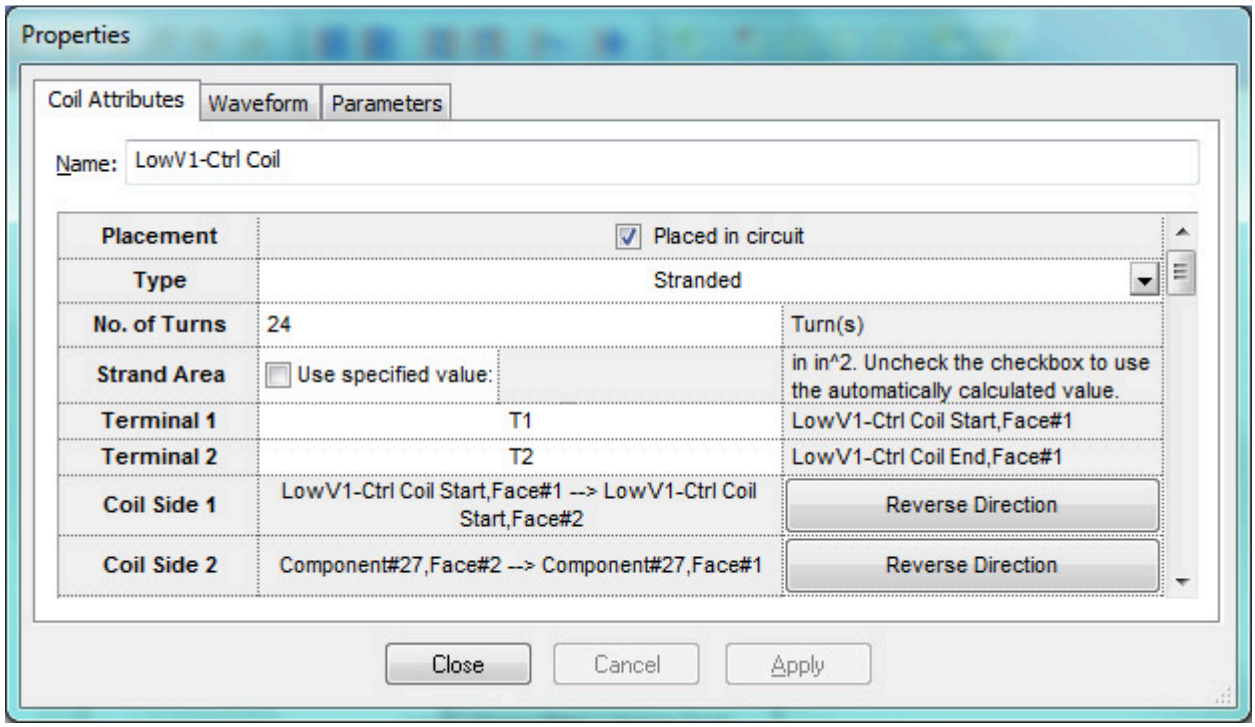

Figure 2-10 Some of the customizable parameters for a coil in a MagNet electrical circuit

2.3 Performances of the NAEM

The following section describes the behaviour of the NAEM. It is necessary to clearly understand the goals pursued by the NAEM as well as the mechanisms in place to achieve them in order to be able to understand the modeling phase of the project later on.

The main objective of this new machine architecture is to be able to control the output current of the machine under various circumstances. This is of crucial importance when one wishes to directly connect the generator to the combustion engine of the aircraft (instead of coupling the two using a gearbox like it was traditionally done). This goal can be achieve by injecting a direct current into the control coil, which modifies the saturation level of the secondary magnetic circuit, thus modifying (or modulating) the machine internal impedance and output current. To get a better understanding of this phenomenon, it is essential first to analyze the two main magnetic circuit paths present in the machine.

2.3.1 Primary and secondary magnetic flux paths

Figure 2-11 is showing a close-up view on one channel of the alternator. From this view, it is possible to clearly see the primary magnetic flux path (dotted red line) as well as the secondary magnetic flux path (dotted blue line). The primary flux path includes the permanent magnets as well as the upper half of the phase winding and the air gap. The secondary flux path, in turn, includes the second half the phase winding and the control coil. It is the first magnetic circuit that is responsible of the power generation.

It can be seen on the figure that the secondary flux path encounters the region delimited by the green solid line: this is precisely the region where the saturation modulation takes place. All around the machine, as the direct current is increased (inversely, decreased), the saturation of this portion of the stator core is increased (inversely, decreased). In consequence, as the saturation is increased (inversely, decreased), the inductance value of the second half of the phase winding decreases (as its magnetic flux path encounters the saturated region) (inversely, increases).

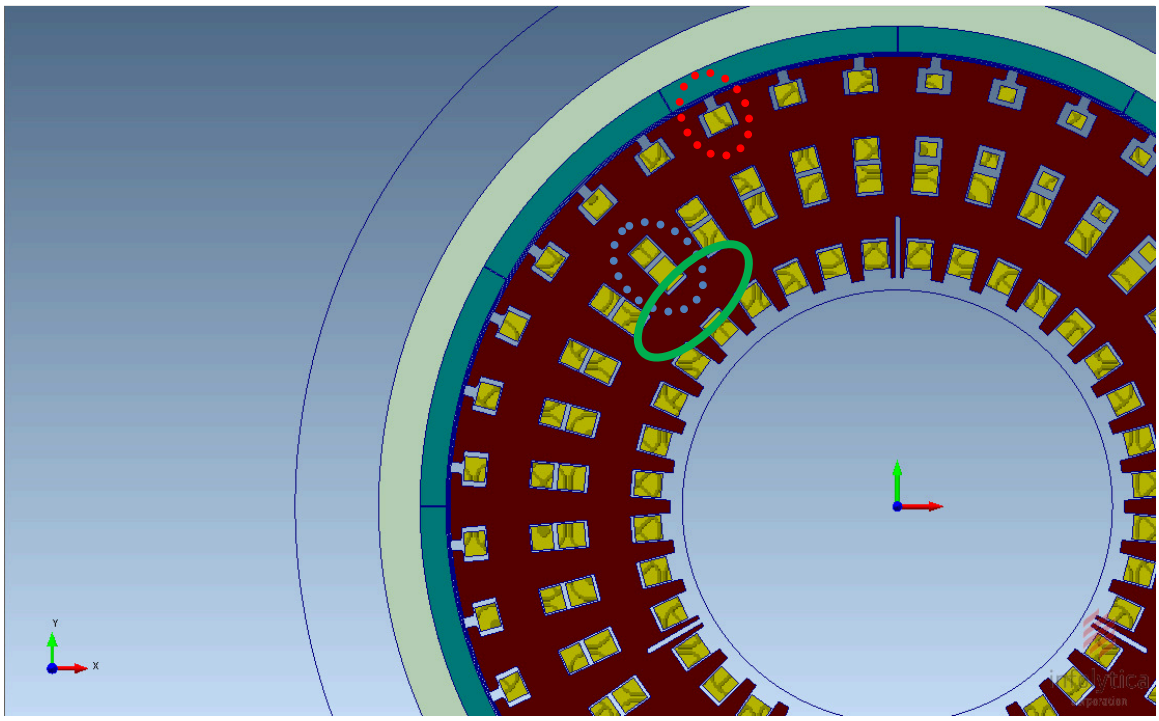

Figure 2-11 Magnetic flux paths in the machine

This phenomenon is clearly shown in figure 2-12 and figure 2-13 . Both figures present the relative permeability of the NAEM under the same load, but with a control current of 0 A for

figure 2-12 and a control current of 20 A for figure 2-13. One can observe that the relative permeability in the region enclosed by the solid green line of figure 2-11 significantly decreases as the control current increases; reaching almost unity at full saturation.

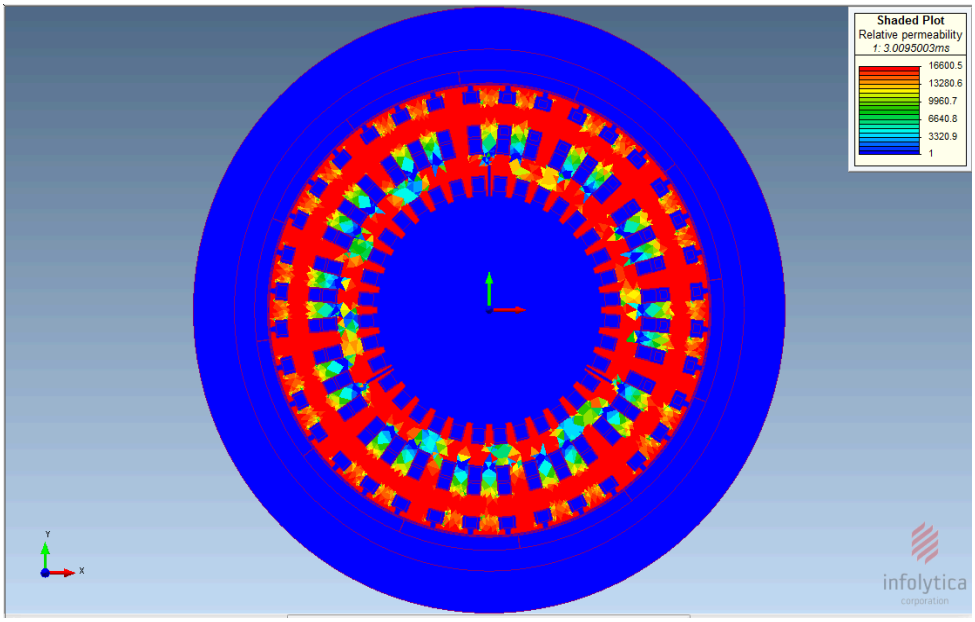

Figure 2-12 Relative permeability of the ferrous materials in the NAEM for a control current of 0 A and a load of 2 p.u. (0,0234Ω)

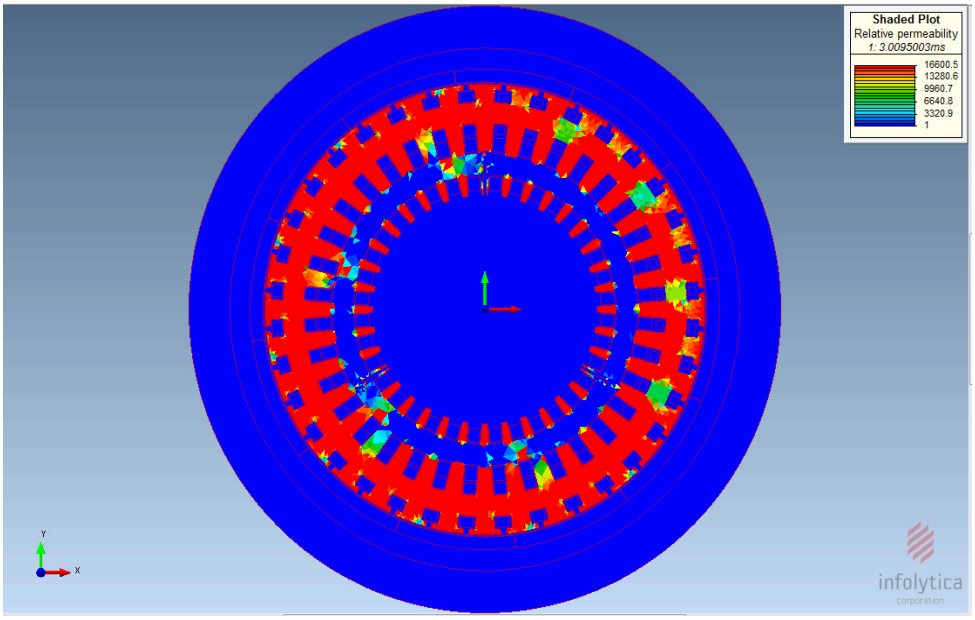

Figure 2-13 Relative permeability of the ferrous materials in the NAEM for a control current of 20 A and a load of 2 p.u. (0,0234Ω)

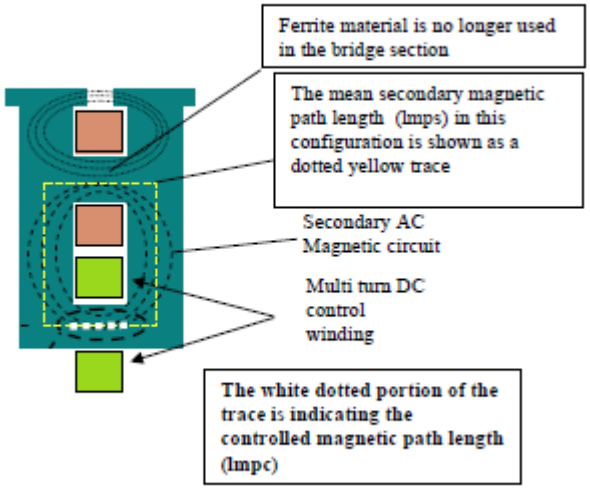

Figure 2-14 : Cross-sectional representation of the two magnetic paths in the NAEM [15]. Used with permission

Each turn of the phase windings occupies both an upper and a lower slot. Therefore, a modification in the inductance value of the portion of the winding in the lower slot causes systematically a modification of the net inductance value of the phase windings. A representation of this phenomenon is presented in figure 2-14.

2.3.2 Dynamic operation of the NAEM

Figures 2-15 and 2-16 show the flux lines during dynamic operation of the machine. On figure 2-15, the control current is set to zero, and it can be see that the saturation of the previously identified green region is low. In opposition, figure 2-16 is showing the same machine under the same loading conditions, but with a control current of 10 amperes. In this second view, we observe that the saturation level of the secondary magnetic flux path has increased, forcing all flux lines to flow in the upper portion of the magnetic circuit. The loading scenario chosen here is an arbitrary one.

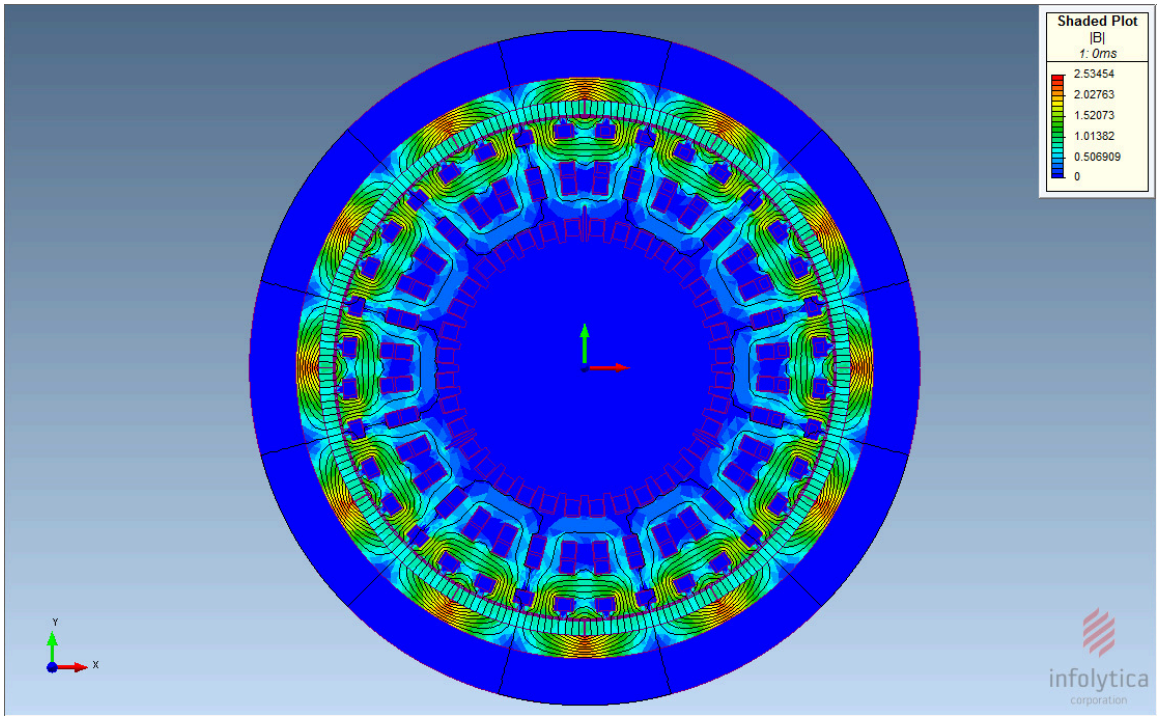

Figure 2-15 Flux density for a control current of 0 A and a load of 2 p.u. (0,0234Ω)

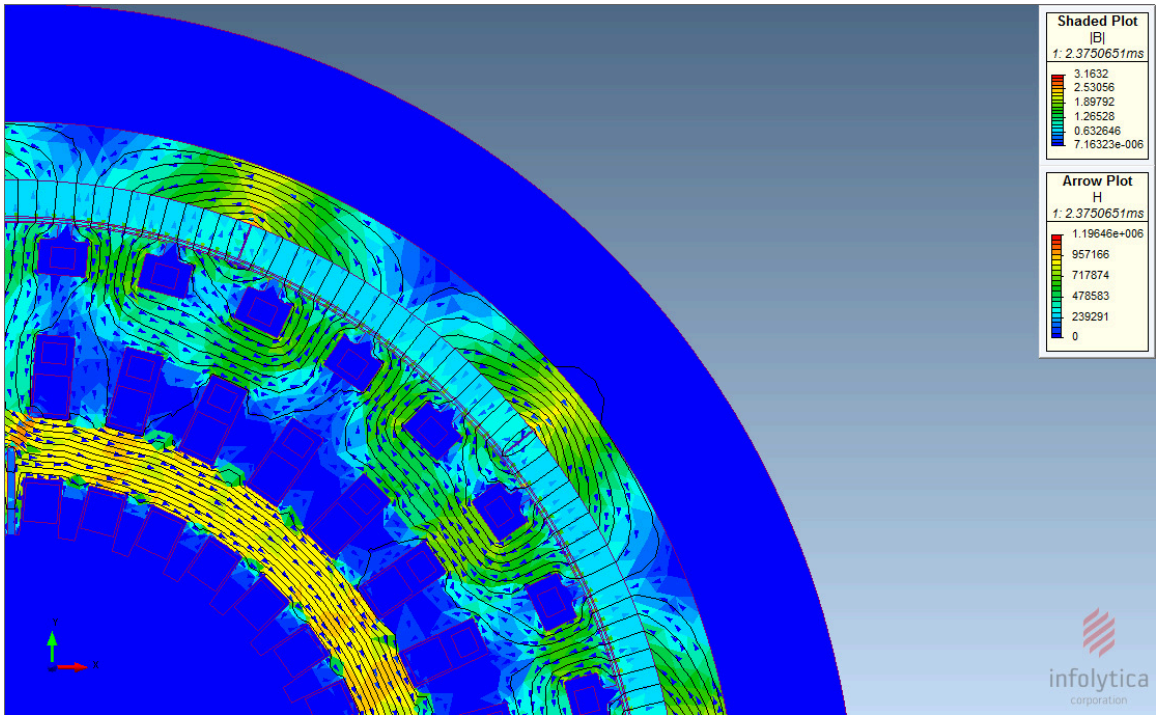

Figure 2-16 Flux density for a control current of 10 A and a load of 2 p.u. (0,0234Ω)

Figure 2-14 to figure 2-16 also clearly demonstrate the assumption that the primary and secondary flux paths are uncoupled (discussed above in the modeling assumptions used by PWC) is correct. It is necessary to note that although the two magnetic circuits are decoupled, the upper and lower phase coils are connected in series. This explain why the saturation of the secondary magnetic circuit affects the impedance of the machine seen at its output even if there is not direct magnetic coupling between the primary and the secondary magnetic paths.

When there is no control current flowing in the control coil, the secondary magnetic circuit stays unsaturated as the flux lines from the primary circuit encompass the machine stator coils and the permanent magnets only. On the other hand, when current is flowing into the control coils, the flux lines of the secondary magnetic circuit are mainly trapped between the control coils and the lower part only of the machine stator coils. The flux lines from the primary magnetic circuit still encompass the permanent magnets and the upper part of the machine stator coil. Thus, it is valid to assume that there is no coupling between those two magnetic circuits; this only introduces a small error due the few flux lines leaking from the secondary magnetic circuit to the primary circuit as shown in figure 2-16.

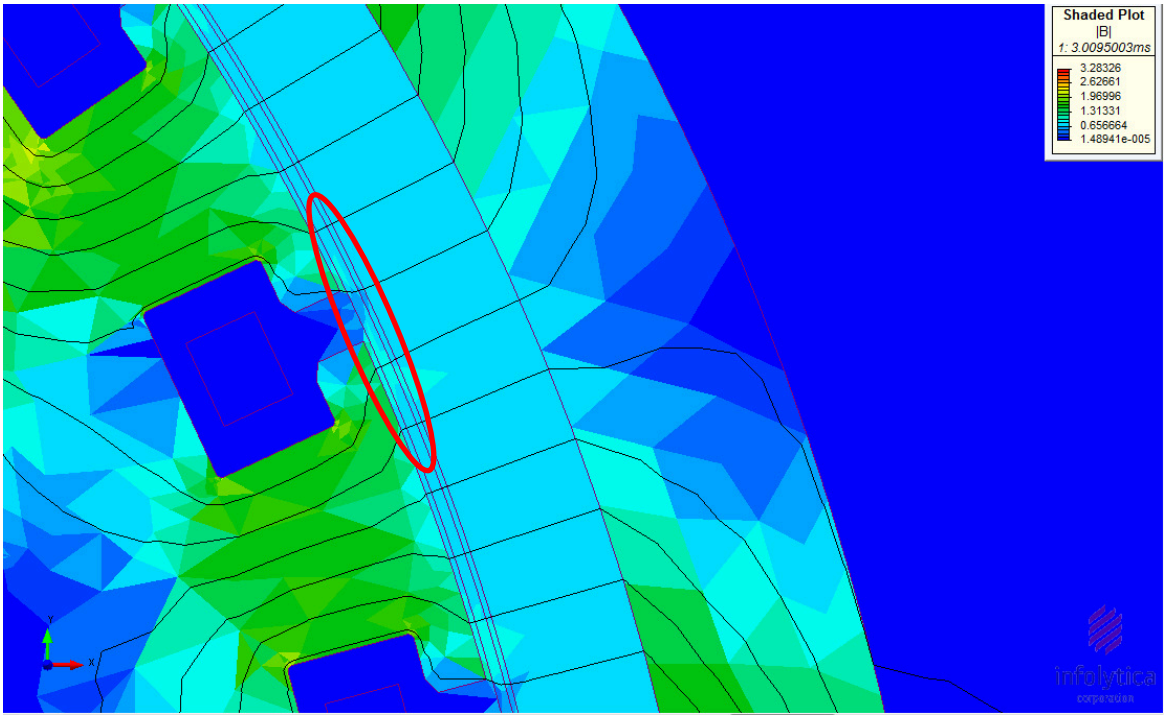

Figure 2-17 Air gap flux lines for a control current of 20 A and a load of 0.5 p.u. (0.1 Ω)

Figure 2-17 shows, for information, a close-up view of the air gap flux lines (the air gap is identified by the red circle). The flux lines are crossing the air gap perpendicularly to the stator and the rotor as it is the case in a typical synchronous machine. Although the figure is showing the result for a given loading scenario, this behaviour is typical to all loading conditions.

2.4 Simulations performed

This section is divided into two subsections. The first one presents some typical simulation results to show the behaviour of the NAEM under various circumstances. This validates the fact that the output current of the NAEM can be controlled using the control current. The second subsection documents the simulations ran for the current project. These simulations were a significant part of the project and generated a noteworthy amount of data. This data had to be documented in order to make easier the continuation of this project.

In order to obtain results, the model presented above had to be meshed first. The meshing is a crucial step as it is the mesh that determines the accuracy of the results. The default meshing of MagNet was used here. Once the model is meshed, the result shown in figure 2-18 is obtained.

During simulations, at each time step, the program solves the geometry by minimizing the magnetic energy in the discretized model.

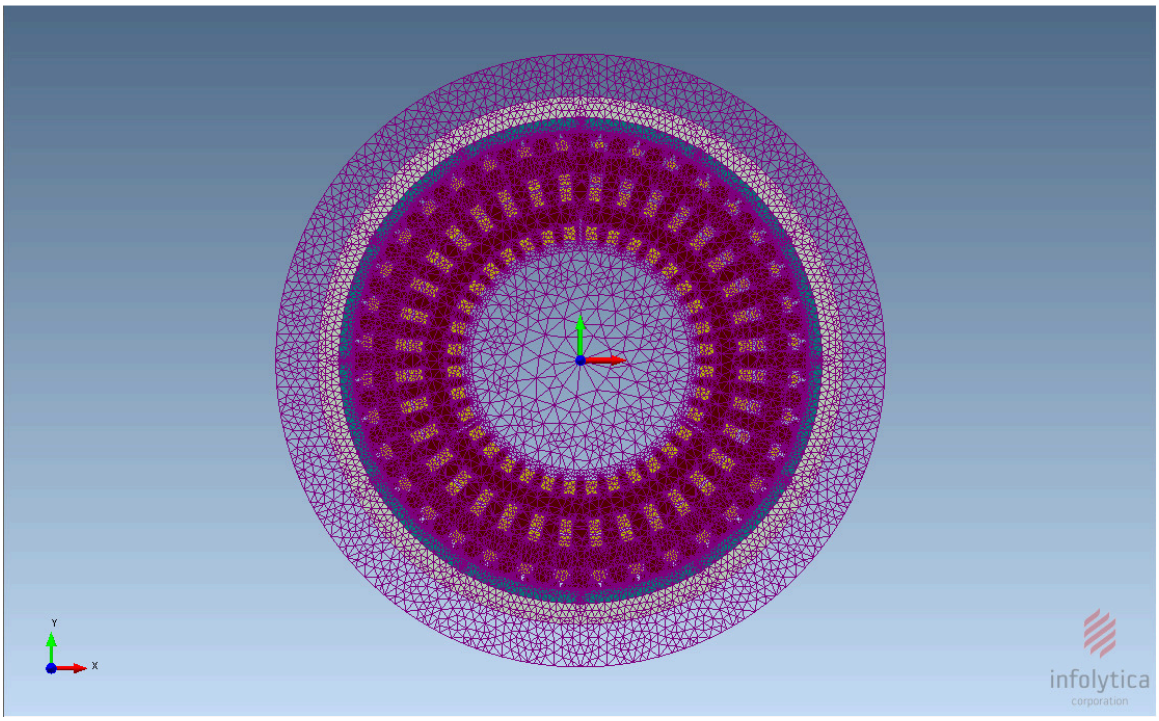

Figure 2-18 Initial 2D mesh of the model

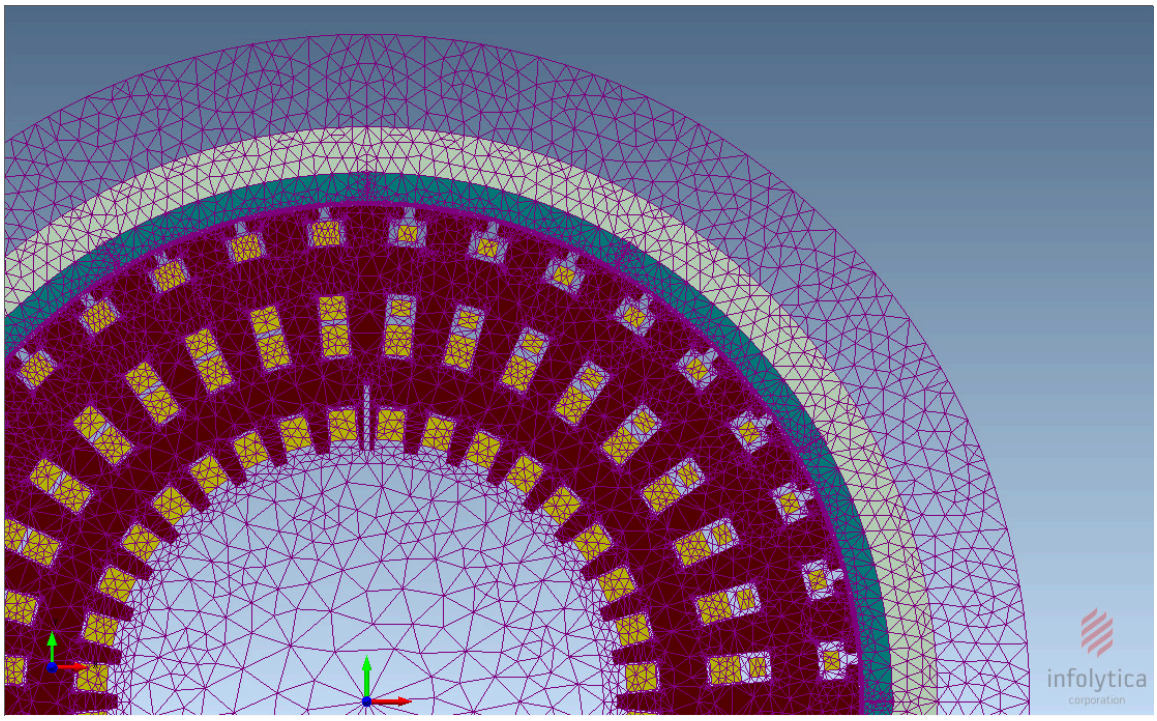

Figure 2-19 Initial 2D mesh close-up of the model

In figure 2-18, the initial mesh of the geometrical model of the NAEM is visible. The outer ring in this model is an “air region” created automatically by MagNet. This infinite box encloses the environment to be simulated by the FE solver. Figure 2-19 shows a close-up of figure 2-18 to have a more precise idea of the mesh used in the model.

In figure 2-19, it is possible to see that the mesh is finer in the regions of interest (in an area where a high magnetic activity is expected for instance) and becomes coarse when approaching the edge of the infinite box. The results presented throughout this document were obtained using this 2D mesh.

2.4.1 Behaviour of the NAEM

The control coil allows changing the magnitude of the output current under a given load and a given speed. The next set of figures shows this behaviour of the machine. One must note that the variations in the magnitude of the output current in those next figures are only due to the variation of the control current. In other words, all other conditions (load, speed, etc.) have been kept constant throughout the simulations. To avoid overloading the text, only one test case is presented here to demonstrate the principle of operation.

The set of three figures show the operation of the machine under a given load condition (in this case, 0.0234Ω was arbitrarily chosen as load) with three different values of control current. Remember that the control current is a continuous current injected into the control winding of the machine. In the FE model, the control current source is modelled by an ideal DC voltage source. The figures were cropped to show only the steady-state operation of the machine as the current project focuses on this regime. In all cases, the speed of the generator is constant and equal to 15 368 rpm. This value was imposed by PWC and is in the typical order of magnitude for the engine under cruising conditions. The frequency of the signal is approximately 1 537 Hz; which confirm the 12-pole configuration of the NAEM.

In the first case, the load is applied to a generator with a completely unsaturated secondary magnetic circuit. The control current is equal to zero, and the direct current source is acting as an open circuit. It is possible to observe here, as it is indented as per design, that under such operating condition the output current of the machine is significantly low. This is even clearer

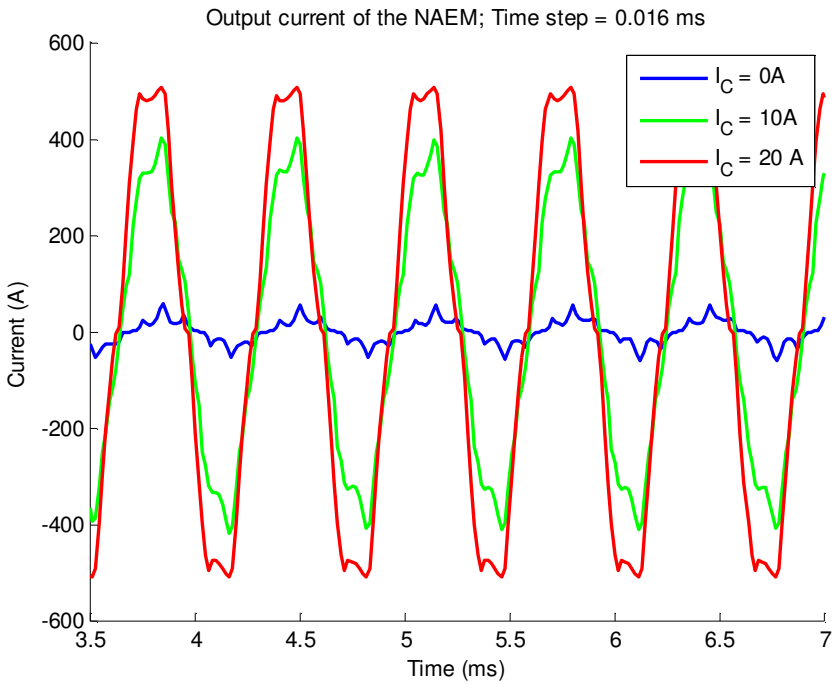

Figure 2-20 Load current of phase A for a control current of 0 A, 10 A and 20 A and a load of 2 p.u. (0,0234Ω)

when one looks at figure 2-20 showing the output of the machine for the same loading condition and speed, but with different values of control current.

As the saturation of the secondary magnetic circuit increases (refer to previous sub-section for visual representations of the magnetic saturation of the generator under various control current levels), the output current of the generator follows the same trend. In fact, one can see a significant difference between the output current for a control current of 10 A (peaking around 400 A) and the output current for a null control current (peaking around 59 A).

The last curve in figure 2-20 shows the generator when the control circuit is fully saturated. As expected, the output current of the generator increases again. In this situation, the peak output current is around 506 A. The behaviour observed here is a non-linear relationship between the output current and the control current. This behaviour was also to be expected as the role of the control current is to modify the operation point of the machine on its saturation curve. This implies a steeper slope in early unsaturated stages and a more moderated slope as saturation is reached. This particular design is intended to reach its nominal saturation point at around 20 A. Beyond that point, as figure 2-21 shows, the magnetic circuit is saturated and an increase in

control current has only a marginal effect on the output current. It is therefore irrelevant to operate the NAEM at higher control current values as it will mostly increase the losses in the control winding and the external circuitry for no significant gain on the output of the machine. The reader can refer to section 3.3.2.3 for further details on the saturation characteristics of the generator.

Considering the preceding results, it was found that the two more relevant states for the control winding is either fully saturated or unsaturated; the control circuitry acts as a virtual switch that can limit the output current of the machine. In normal conditions (e.g. normal speed and load, and no fault), the NAEM will operate with its secondary magnetic circuit fully saturated in order to produce as much power as needed (within the operating limits of the generator). However, should an abnormal situation occurs (a fault or a dangerous overload condition for instance), the control current will be reduced to zero in order to avoid damaging the generator and feeding a potential fault. Therefore, a particular attention was put on these two states during the modeling phase.

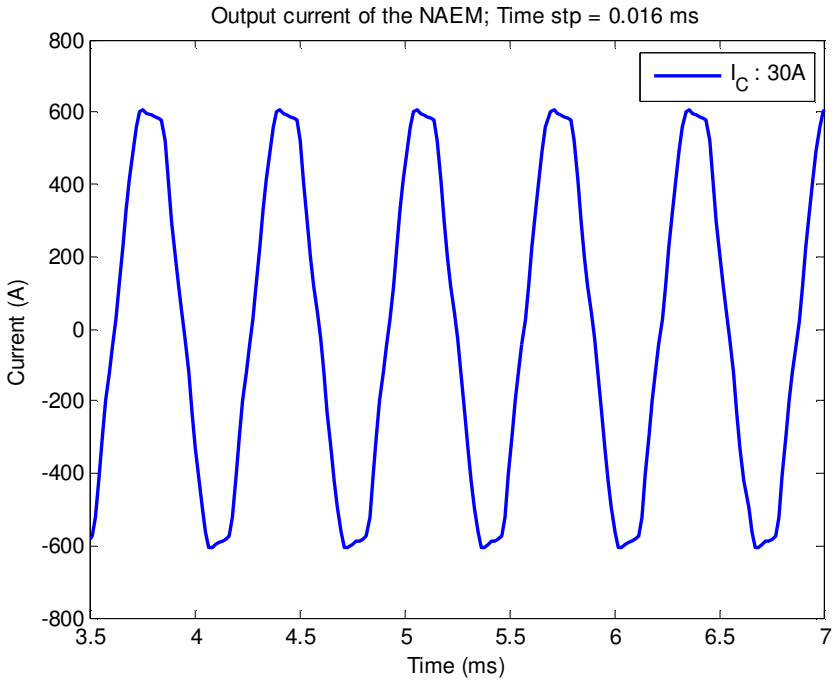

Figure 2-21 Load current for a control current of 30 A and a load of 2 p.u. (0,0234Ω)

For demonstration purposes, a short-circuit scenario is presented in figure 2-23 using the circuit shown in figure 2-22 in MagNet. The three switches are set to close at t = 3 ms (all at the same time). They are closing on a really small load that is simulating a short-circuit. For numerical stability purposes in MagNet, it was impossible to use a "genuine" short-circuit and link directly the three phases together. The closing time of the switches is long enough for the NAEM to reach its full steady-state operation. The control current is kept at 0 A throughout the simulation.

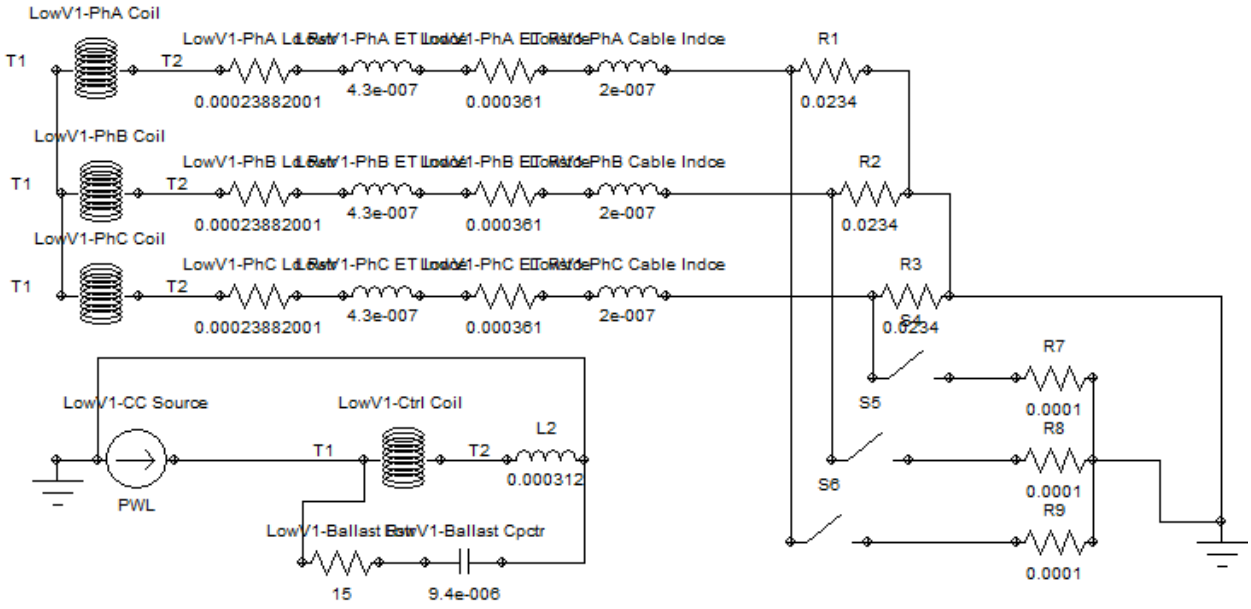

Figure 2-22 Short-circuit scenario in MagNet (file *ParametricalStudy.mn*)

The output current of phase A for this scenario is shown in figure 2-23.

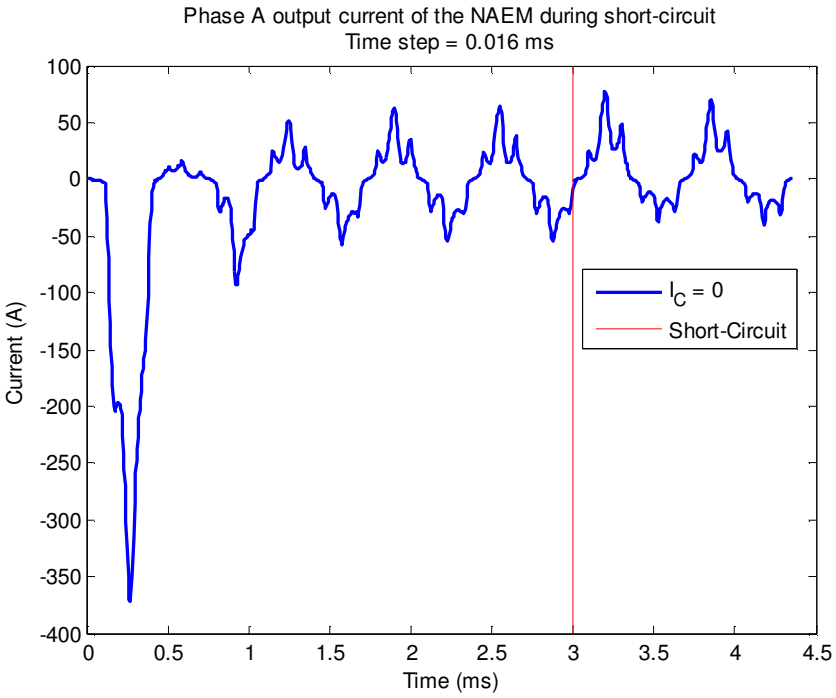

Figure 2-23 Phase A output current of the NAEM under short-circuit condition

As one can observe, the peak output current in steady-state before and after short-circuit (identified on the graph by the red vertical line) is virtually the same. This is a strong demonstration that the most critical parameter to influence the output current in the NAEM is the control current. Here, as one can see, it would be feasible to operate continuously the generator under a short-circuit condition. It would therefore be possible to keep the generator running and let it feed the others output channels of the machine while avoiding significant damages to the portion in fault (the reader has to remember that the NAEM is a multi-channel architecture machine) which was precisely one of the objectives pursued by the design of the NAEM.

2.4.2 Calibration data

This section presents the data available from PWC to build and validate the model. It also contains documentation on the FE simulations that were run during the project. The last subsection briefly introduces the available data in transient mode, which was also provided by PWC. This section is only an overview and is presented here to ease the knowledge and experience transfer for future work on the model.

2.4.2.1.1 **Simulation results from the MagNet model**

2.4.2.1.2 MagNet parametric study file

A significant part of this project consisted in retrieving simulation results from the existing MagNet model. These results were the building blocks of the current project and will be used in future projects to complete the electrical modelling of the NAEM.

The raw simulations results are available in the file named *ParametricalStudy.mn*. This file is, as its name implies, a parametric study of the MagNet model. This type of simulation under MagNet allows the user to make a value sweep of chosen parameters. In this case, the following parameters were varied, for a total of 130 different test scenarios summarized in table 2-1.

Table 2-1 Parametric sweep of the MagNet model

Parameters	**Tested Values**
Control Current Value (A)	0; 1; 2; 3; 4; 5; 10; 12; 15; 18; 20; 25; 30
Load Resistor Value (Ω)	10; 5; 1; 0.5; 0.1; 0.05; 0.01; 0.005; 0.001; 0.00001

Reminding that the developed model here is a steady-state model, the speed of the machine was always kept constant, as were the load resistor value and the control current for a given simulation.

2.4.2.1.3 Matlab data extraction and post-processing

As MagNet uses a finite element approach, the files it generates rapidly become large and are a burden to manipulate (around 85 GB for the parametric study). Therefore, the strategy that was employed here was to write a Matlab file that controls the MagNet model to (1) launch a series of test cases and (2) extract the useful data and send it to a Matlab data file (a .mat file). The files created for this project can be use as a template to run virtually any scenarios in MagNet and easily post-process the data in Matlab afterwards.

The Matlab script in appendix 1 shows a typical procedure to connect Matlab to MagNet using an Active X applet. This code was programmed by the author for the purposes of the project. As

indicated by the comments embedded in the coding, the procedure to connect both software is a 3-step procedure and everything is performed in Matlab. First, the user needs to create an Active X Server object to handle MagNet from Matlab. Once the object has been created, the MagNet constants are set (the variables that will be later retrieved from MagNet). In the current example, all variables are invoked. The last initialization step is to open the MagNet file. Once the MagNet file is opened and configured to be used by Matlab, various actions can be performed in MagNet from the Matlab file using predetermined commands that are transferred to MagNet in string format as shown by the figure in appendix 2.

For informational purposes, appendix 2 shows typical commands to transfer data from MagNet to Matlab. Once the data is transferred into a .mat file type, it is easy to execute any post-processing task directly in Matlab. The extraction procedure can also be broken down into 3 operations. The reader must note that the example of appendix 2 must be executed after a MagNet file was opened and solved. First, the user needs to identify the problem ID for which he wishes to retrieve the data (the problem ID can also be seen as the scenario number in MagNet). Once the problem ID has been called, the simulation points to be extracted are identified and called. The last operation is to extract the data in a Matlab-compatible format. In the example of appendix 2, the flux linkage data for the 41 last time steps is extracted for all the problems solved in the active MagNet file. This procedure is easily customizable in order to extract any data from already solved simulations (MagNet can calculate virtually any electrical and magnetic quantity for each component of both the geometrical model and the external electrical circuit). All the possible commands are listed in the MagNet help.

2.4.2.2 Real-time response of the prototype

This section briefly presents the transient response curves given by Pratt & Whitney Canada. These curves come directly from field tests on an actual prototype of the generator. The data was recorded using a HBM Genesis HighSpeed apparatus on the prototype. This data is saved under a proprietary format and can be viewed using the Perception software or can be exported using the DLL files of the company provided in an available toolkit [21]. In the present case, a Matlab script was written by the author to use the DLL toolkit to import the data under Matlab for eventual post-processing. Some of the figures extracted are shown below. This data is not currently used in the project but could be use for comparison purposes (mainly for transient

operation) between (1) the MagNet model and the prototype and (2) the EMTP-RV model and the prototype. The purpose here is to inform the reader that such data exists and that an extraction script in Matlab has also been developed during this project.

The following figures show some of the curves which were extracted from the original files. The sampling rate for the current waveforms is 20 kHz. The quantities of interest measured on the prototype were: current of phases A, B and C, control current, rotor speed and the voltage at the output of the machine. The machine was submitted to various loading conditions during a time span of approximately 2500 seconds. Those tests have been done on a prototype of the generator to show its capabilities.

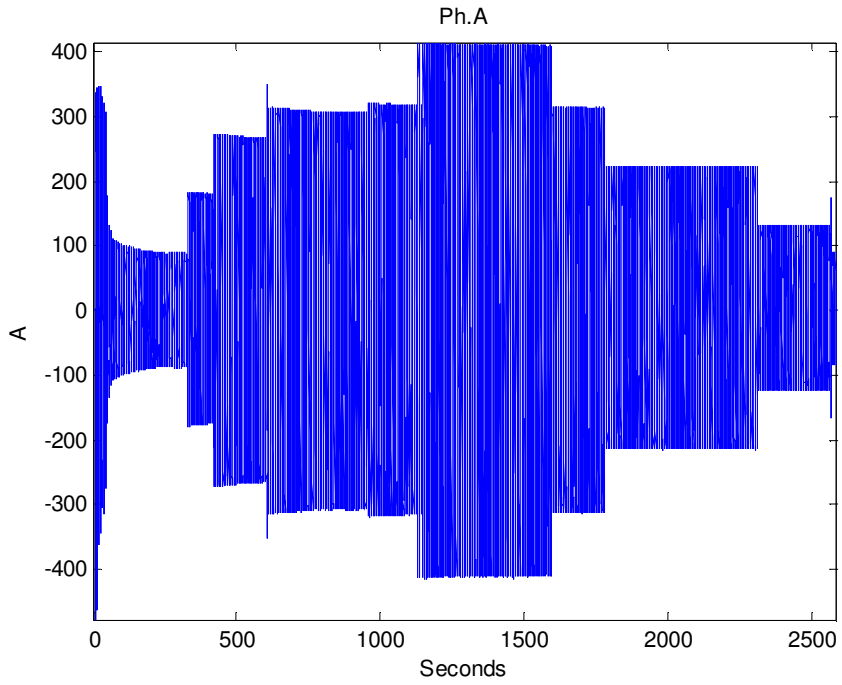

Figure 2-24 Output current on phase A of the prototype during a test run; file *recording237.nrf*

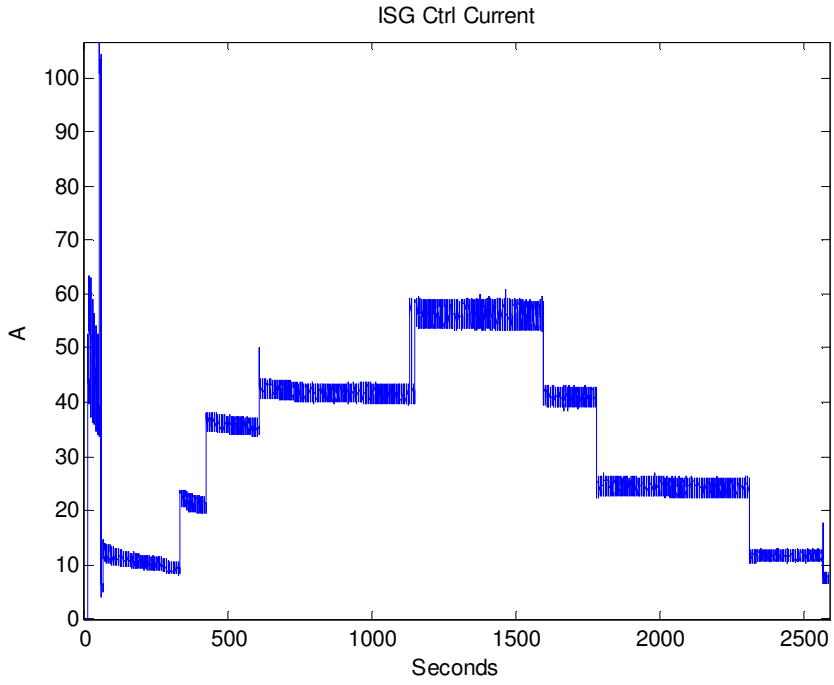

Figure 2-25 Control current of the NAEM prototype during a test run; file *recording.nrf*

CHAPTER 3 ELECTRICAL MODEL

This section covers the structure of the EMTP-RV electrical model of the NAEM and the modelling process. After a brief presentation of EMTP-RV, the reader is guided to the whole modelling process, from the modelling assumptions behind the model to the presentation of the final model. This model represents one of the two main original contributions of this project. Results are presented in the next chapter.

3.1 Brief presentation of EMTP-RV

The Electromagnetic Transients Program (EMTP-RV) software is focused on power system type of problem analysis. This is one of the reasons it was chosen to develop the model discussed in this thesis: it will allow an easy coupling of the NAEM model to an existing power system model. Calculations in EMTP-RV are performed using the modified-augmented nodal analysis theory, which allow the program to be highly adaptive to a large range of situations. The reader is invited to consult the references [22, 23] to learn more about EMTP-RV.

3.2 Modelling assumptions

The following subsections contain the modelling assumptions that were taken during the project. These assumptions will be the subject of comments and discussion in a following chapter.

3.2.1 Steady-state model

The developed model in this project is a steady-state model. In other words, the modelling of the transient phase of the generator is left for a subsequent project. This decision was taken during the project because of the complexity of the relationship between the internal fluxes, the output current and the control current. Therefore, the model developed here is only valid in steady-state operation (the transient phase will be presented in the results of chapter 4 for information only).

3.2.2 Magnetic coupling between machine stator coils and the control coil

Another assumption that was taken in the process of modelling the machine is to consider that there is no magnetic coupling between the control coil and the machine stator coils in the upper slots. In other words, there is no direct magnetic influence of one coil on another. This is an

acceptable assumption as it is stated in the PWC documentation [15] that there is virtually no magnetic coupling between those coils. In fact, the magnetic circuit of the machine can be divided into two distinct magnetic circuits: the primary magnetic circuit (in which the power is generated into the machine stator coils) and the secondary magnetic circuit (in which the internal impedance variation of the machine takes place as a function of the control current). This fact is verified by finite element analysis results (see chapter 2) and is illustrated here in figure 3-1 below, taken from [15]. The figure shows a stator slot cross section (the permanent magnets of the rotor would be at the top of the figure, but are not shown here). The machine coils are represented in red, and the control coil winding is pictured in green. Here, one can clearly see the secondary magnetic flux path in dotted yellow line; going around the upper portion of the control coil and the lower portion of the machine coil. The primary magnetic path, not shown here (refer to section 2.3.1 Primary and secondary magnetic flux paths for further details), is a closed contour between the upper coil section and the permanent magnets of the rotor. It can be assumed that there is no direct magnetic coupling between both magnetic paths. This assumption was taken prior to start the modelling of the NAEM in EMTP-RV and was verified by finite element analysis in the previous chapter.

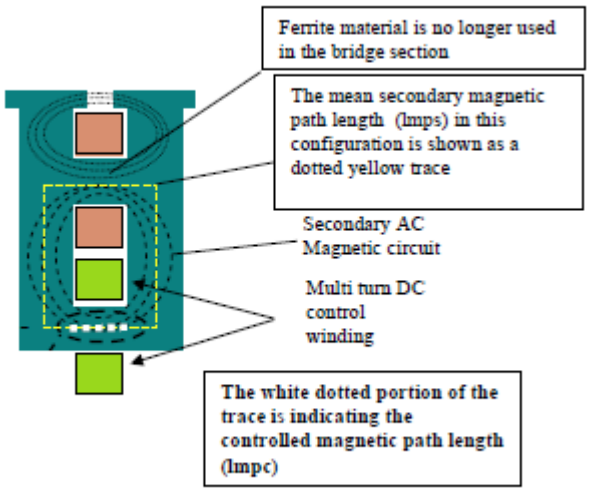

Figure 3-1 Cross-sectional representation of the two magnetic paths in the NAEM [15]. Used with permission.

3.2.3 Purely sinusoidal EMF

This assumption is somewhat in direct correlation with the first one presented in this section (the scope of this project is limited to a steady-state model). A purely sinusoidal emf means that space harmonics were neglected as well as the distortion that can affect the voltage waveform produced by the generator depending on the loading conditions.

In addition to the previous assumption, the emf of the generator is kept constant at all times, regardless of the loading current. There is thought, as one may know, a demagnetizing effect taking place in the permanent magnets of a PMSM [24] that grows with the output current. This counter effect, also called armature reaction, is the result of the cross-magnetizing force created in the armature windings during operation. This effect has an impact on the generated emf inside the machine, but was not taken into account here.

Furthermore, the reader should note that the geometry of the NAEM is significantly different from that of a traditional PMSM (the NAEM is a 3-channel generator). The particular geometry of the NAEM leads to a more distorted voltage waveform at the output of the generator than a typical permanent magnet synchronous generator (typical PMSM have a stator winding distributed all around the circumference of the machine for instance) due to higher space harmonic contents. This was not taken into account in the scope of this project.

3.2.4 External control circuitry

Although the external circuitry governing the control current is most likely to take the form of a PWM on the final system, this part is not included in the scope of this project. Therefore, the control current is modelled using an ideal direct current source that makes it possible for the end-user to easily run simulations using the desired control current value.

3.3 New Architecture Electromagnetic Machine electric model

The developed model is presented here, block by block. Each subsection contains the details behind the modelling of a specific component as well as the calculations used to determine their value.

3.3.1 Generator model overview

Figure 3-2 below shows the model of the NAEM from the end-user point of view.

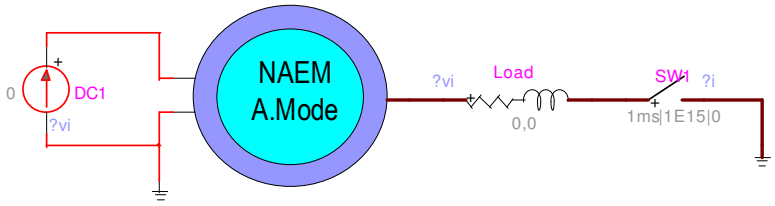

Figure 3-2 End-user view of the NAEM model; file *NAEM.ecf*

From left to right, one can observe (1) the control current source, (2) the NAEM (where "A. Mode" stands for "Actively Protected Mode"), (3) a user-determined loading conditions. Thus, from the end-user point of view, the NAEM has two input pins (corresponding to the two ends of the control winding) and a three-phase output pin that corresponds to the output of the generator. The parameters of the generator to be used are entered in a contextual menu as shown in figure 3-3. These parameters are the ones calculated throughout this chapter.

The "Initial values" zone contains the value of the desired speed of the machine (in rpm). The "Rules" zone is responsible for lunching the mask (establishing the necessary values to run the model). Finally, the "Variables to transmit" text zone indicates which variables will be transmitted from the mask to the model components for execution.

The model of the NAEM can be divided into two distinct portions. The first one would be the generator portion of the machine. It is in this portion of the model that the power generation takes place. This part of the model is analogous to a classical PMSM and is presented in 3.3.1.1. The second part of the model is the control portion of the NAEM (presented briefly in chapter 1). As mentioned before, this constitutes the main innovation of the NAEM in relation with a typical PMSM. This is where the active control of the machine is modelled.

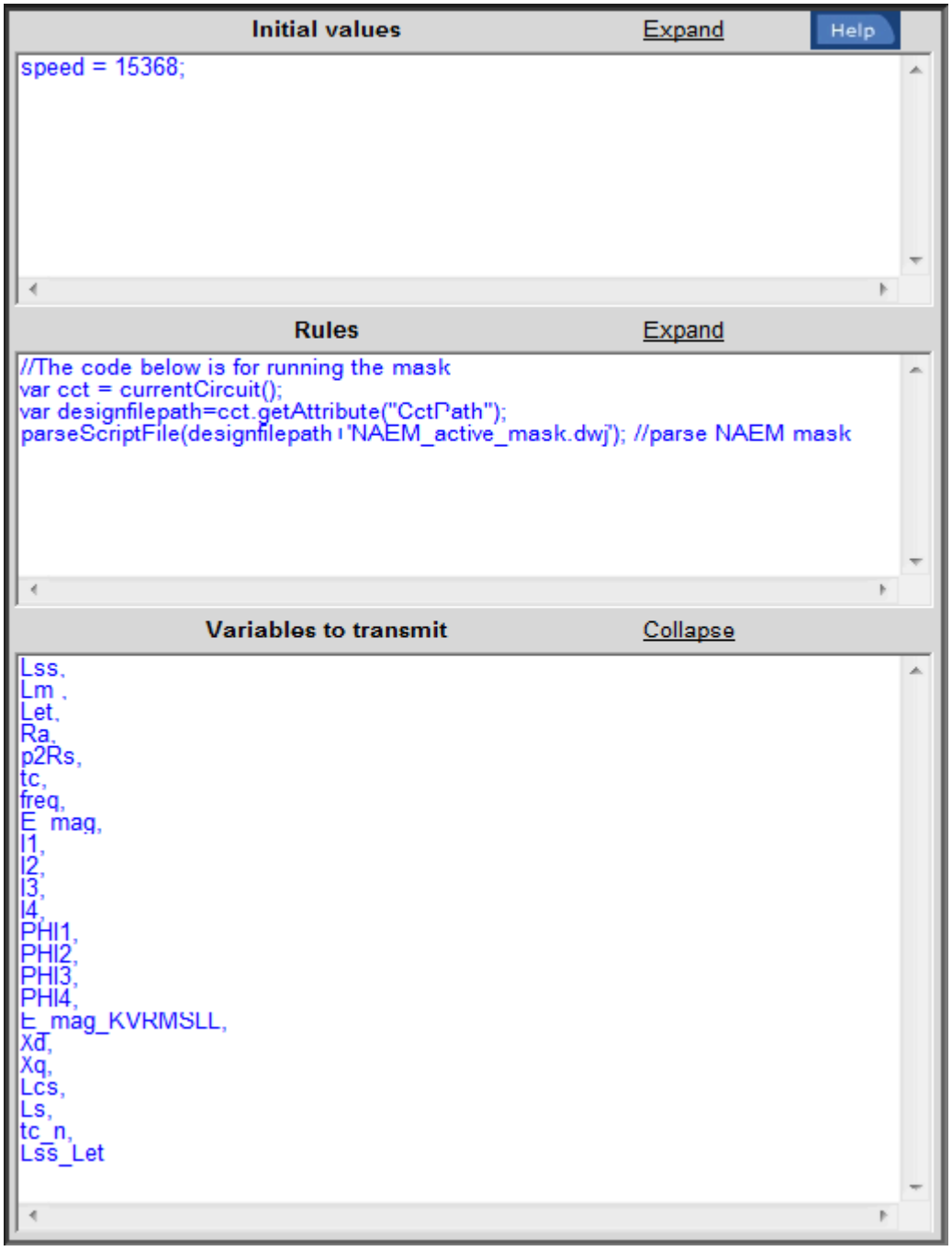

Figure 3-3 Contextual menu of the NAEM model block

3.3.1.1 Generator portion of the NAEM

Figure 3-4 shows an overview of the machine portion of the NAEM model. When looking at the model from left to right, one first encounters the ideal AC voltage source that models the voltage generation inside the generator. As a purely sinusoidal emf is assumed in the generator, the voltage generation can be modeled by an ideal source with its associated impedance (the coupled R-L branch at the right of the source; see section 3.3.2.4 for the mathematical details).

At the output of the RL branch, one can see that the three-phase bus is separated into three distinctive branches for phases A, B and C. Each phase then goes through saturable core inductances that are there to model the influence of the control current over the internal impedance of the generator. The level of saturation of the core of those inductances is controlled by the control current. Those saturable core inductances are referred to as the "control portion" (figure 3-6) of the machine.

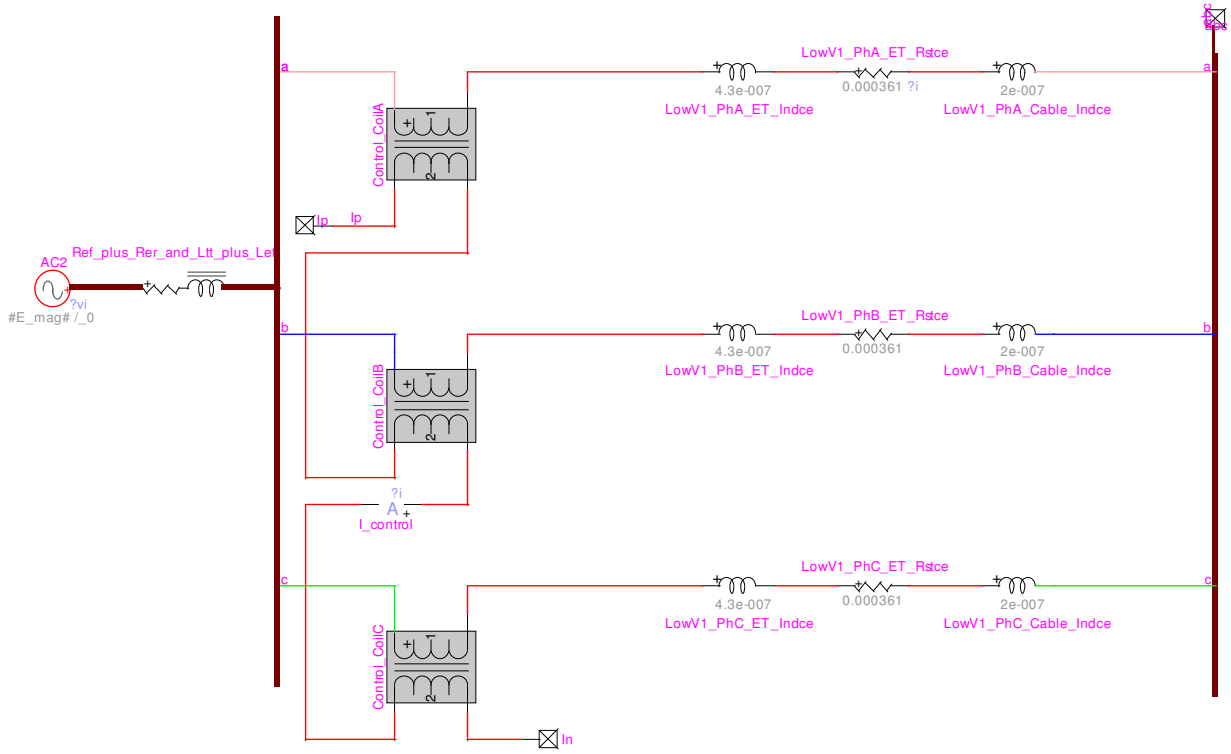

Figure 3-4 Machine portion of the NAEM model; file *NAEM.ecf*

In series with the saturable core reactors, there are resistors and inductors that are there to model, respectively, the inductance and resistance of the end turn of the coil (the end turn of the coils are not modeled in MagNet for a 2D geometric model; they are only represented by ideal wires which explains the need of adding them manually here), and finally the cable inductance which is there to model the inductance associated with the connectors of the machine to the aircraft's network cables. These components were taken directly from the external circuit in MagNet (figure 2-9) and added into the EMTP-RV model. All three phases are then recombined into a three-phase bus to deliver the power at the output of the generator.

3.3.1.2 Control portion of the NAEM

Figure 3-6 shows internal circuit arrangement in each of the transformer unit of figure 3-4. The left side of the circuit is the AC side, or primary side, (current flowing from pin AC_in to pin AC_out) and the right side is the DC side, or secondary side, (current flowing from pin DC_in to pin DC_out).

The first thing one may note is the presence here of two ideal transformers in each unit. The reason of their presence is that each transformer has the same turn ratio, but inversed polarities in such way that there is no net AC voltage going from the AC side to the DC side. This behaviour is desirable and was first explained in section 2.2.1 NAEM model geometry in MagNet. With this configuration, each saturable inductance "Sat1" and "Sat2" will both be affected individually by the AC flux coming from the primary side, but no net AC flux will be seen across pins DC_in and DC_out. Refer to figure 3-5 for a typical example of the voltages developed across the main components on the DC side of the model. The curves are named in accordance with the nomenclature used in figure 3-6.

These two saturable inductances are the only non-linear components in the model. They are defined by a flux-current curve which characterizes their behaviour. Their net inductance value is given by the saturation level associated with the operation conditions. These conditions include the direct current amplitude, which will move the operation point on the flux-current curve, and the AC voltage generated across them (which will tend to push it further into saturation for one half of the cycle and will tend to cancel in part the saturation on the other half of the cycle). It is the net effect of the two combined fluxes that dictates the operating point and thus the net inductance value of Sat1 and Sat2.

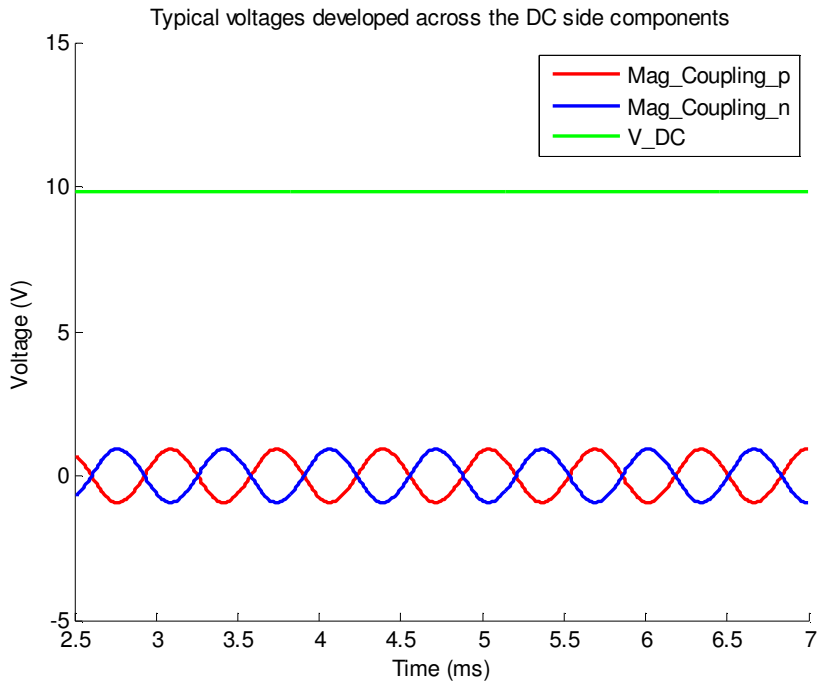

Figure 3-5 Voltages developed across the main components of the DC side of the model

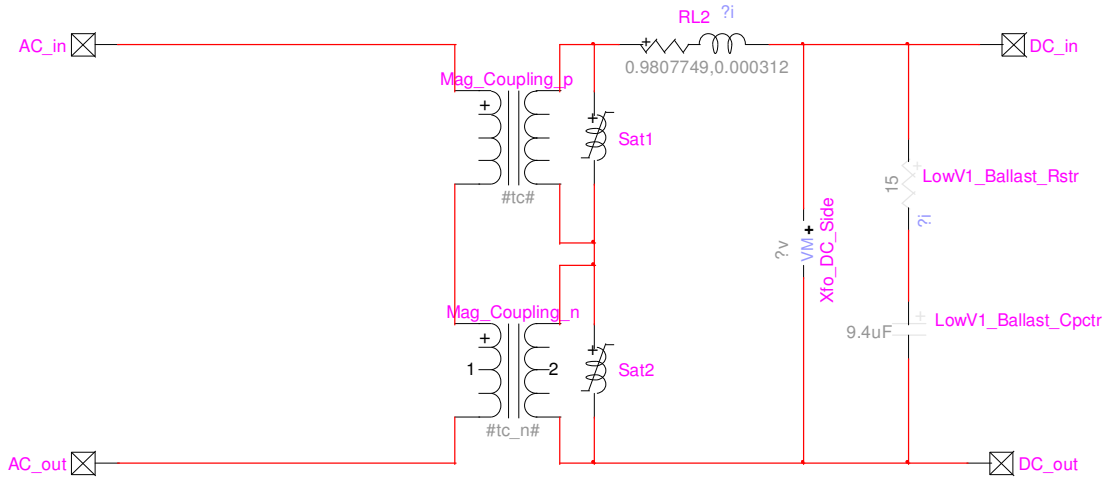

Figure 3-6 Control portion of the NAEM model; file *NAEM.ecf*

This is one of the most critical aspects of the model as it makes it possible to modulate the impedance seen on the primary side (i.e. the AC side or phase winding side) and thus change the internal impedance value of the machine to modulate the output current value.

To the right of these two transformers is a RL uncoupled branch. This branch accounts for the resistance and leakage inductance values of the control coil per say. For now, no coupling is

assumed between the different branches of the control coil (between the three phases). The values were determined using MagNet directly.

3.3.2 Parameters determination

This subsection details the technical approach followed to determine and characterize the elements composing the electrical model of the NAEM.

3.3.2.1 Internal voltage source

As mentioned previously, the internal voltage generation in the NAEM model is represented by an ideal voltage source. Thus, the only two quantities that need to be dimensioned are the frequency and the magnitude of the voltage source.

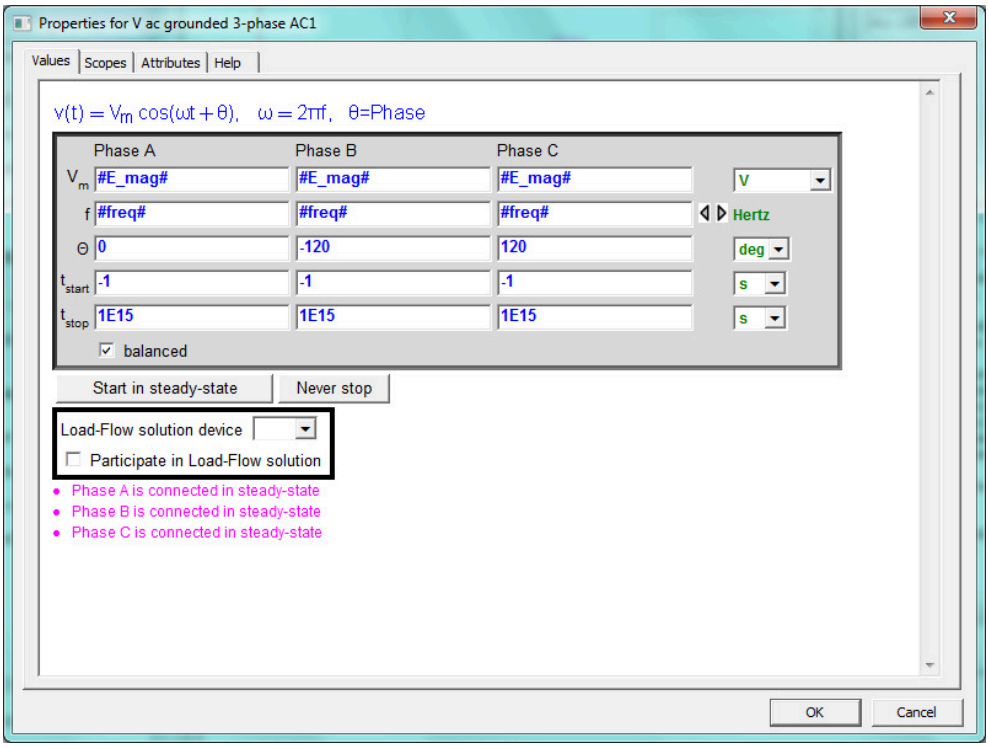

Figure 3-7 Characterization of the internal voltage source of the NAEM electrical model

The frequency is simply fixed by the relationship between the speed of rotation (in revolutions per minute) and the number of poles of a synchronous machine:

$$n = \frac{120 * f}{p} \Rightarrow f = \frac{n * p}{120}$$

The number of poles is fixed by design, (12 poles, or 6 pairs of poles) and the speed of rotation is fixed by the user using the contextual menu shown in figure 3-3. The model's mask is updated accordingly to the value entered by the user.

The second parameter of the voltage source, the magnitude of the voltage sine wave, is first approximated using the proportional relationship that exists between the speed of rotation and the voltage generated in a synchronous generator. This first approximation yielded to an initial value of (calculi are shown for a generator speed of 15 368 rpm; the speed at which the results of section 4 below have been obtained):

$$V_{mag} = \frac{V_{ref} * n}{n_{ref}} = \frac{5.12\ V * 15\ 368\ rpm}{3\ 275\ rpm} = 24.03\ V$$

One must note that the reference value (5.12 V, 3 275 rpm) was given in [15]. This value was afterward fine-tuned in order to calibrate the NAEM electrical model to get to the most representative behaviour possible in the steady-state near or at full saturation.

3.3.2.2 Transformer ratio and arrangement

The turn ratio of the transformers modelling the relationship between the control coil and the phase coils in the machine is set to 24. This value is imposed by the physical arrangement of the NAEM in which there are physically 24 turns in the control coil and 1 turn in the phase coil in each slot. As one may recall, the phase windings are conceived in a single-turn arrangement to avoid potential inter-turn faults. On its side, the control winding is set in a different arrangement as one wishes to maximize the saturation effect for a given current. For this reason, the control coil is a 24-turn per slot arrangement; which gives the 1:24 ratio of the transformers.

The other relevant detail to note is that the polarities of the two transformers are inversed. In other words, the variable "tc" is set to 24 and "tc_n" (see the lower transformer of figure 3-6) is set to "-24". A negative turn ratio results in the inversion of the polarity of the transformer. Therefore, as the polarities of the two transformers oppose each other, the AC flux induced in

Sat1 is 180° out-of-phase with respect to the AC flux generated in Sat2. Thus, while the AC flux is affecting the two saturable inductances individually, there is no AC flux visible between pins DC_in and DC_out.

3.3.2.3 Saturable inductances characteristics

The determination of the flux-current curve was an important procedure as it is a crucial part of the project. It is those saturable inductances that are responsible for the internal impedance variation in the generator. Due to the geometry of the NAEM, it is the equivalent impedance of the control coil reflected on the AC side that affects the internal impedance of the generator seen at its output terminals.

Numerous tests were conducted in order to test as much different saturation curves as possible to be able to determine which one fits the most the behaviour of the magnetic model. The way of conducting those tests was standardized as follows. For 10 different loads (loads were always perfectly balanced three-phase, purely resistive loads), 13 simulations were done to cover all the relevant range of control current from 0A to 30A. The control current vector used in the simulations is the following:

$$I_c = [0,1,2,3,4,5,10,12,15,18,20,25,30]\ A$$

One may note that the step between each control current was smaller for low current values (as the curve is rapidly changing around those points) and is larger for higher values. At the end, there were 130 simulations conducted in MagNet. The data has been extracted for each simulation afterwards and has been post processed in Matlab in order to compute the rms value of flux as a function of the current inside the control coil. The results are shown in figure 3-8.

We can clearly see that the output current of the machine significantly affects the resulting RMS saturation curve of the control coil. After analysis and tests, it was determined that the curve obtained in the less loaded condition has to be used in order to have the most representative saturation characteristic. To come to this result, a series of simulations were performed in EMTP-RV using each curve shown in figure 3-8. For each scenario, only the saturation curve

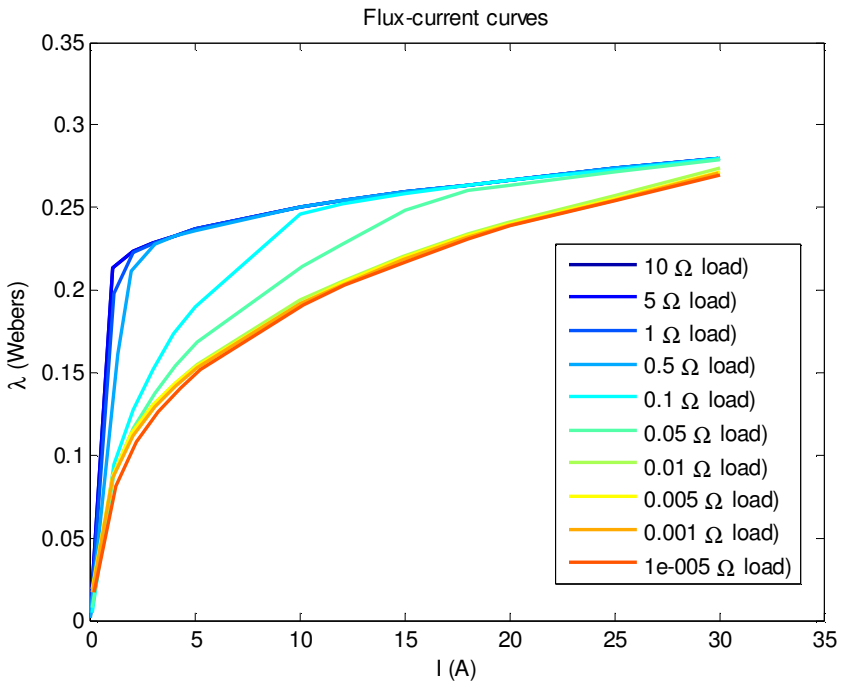

Figure 3-8 The 10 different saturation curves – rms flux in the control coil - plotted from MagNet simulation results

of the non-linear inductances was changed, keeping all the other parameters of the model as is. The results obtained using the EMTP-RV model were afterwards compared to the results obtained with MagNet, computing each time the mean square error. Figure 3-9 illustrates the process for three different test cases. At this stage of the project, the saturation curves implemented in the model were not optimized, this is the reason why there are some discrepancies between the results shown in figure 3-9 for the 10-ohm saturation curve and the results presented in the subsequent chapter. For the three cases in figure 3-9, only the saturation curve of the EMTP model is changed; all the other parameters of the model are kept constant for all cases. This analysis was performed for all the saturation curves shown in figure 3-8 and lead to the conclusion that the 10-ohm saturation curve was the one giving the most accurate results. It appears irrelevant to go beyond the 10-ohm loading condition as changes in the saturation curve are negligible passed this point.

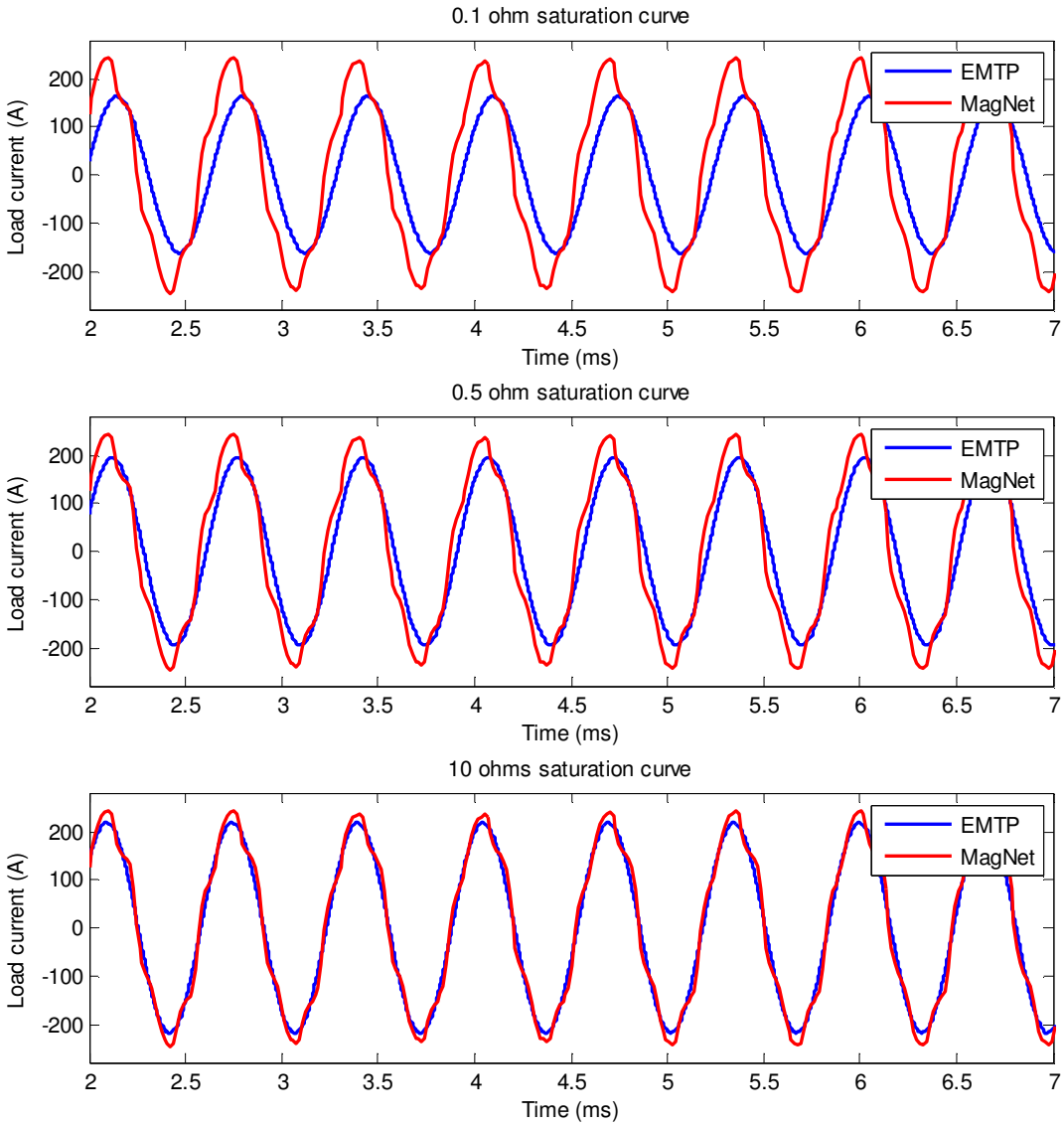

Figure 3-9 Phase A output current of the generator using different saturation curves

As there is a dependency that exists between the control coil and the AC side of the generator, the saturation curves built using simulation results with the generator connected to a load are "contaminated" by the influence of the output current of the generator on the control side. The tests performed in various loading conditions while building the saturation curves proved that hypothesis as the results show that the rms-value of the flux in the control coil is different under different loading conditions for the same control current. Therefore, the curve corresponding to

the 10-Ω load was used (which corresponds to a no-load condition for the NAEM) in order to characterize the control coil in an almost isolated state (from the rest of the generator). The curve is reported in more details in figure 3-10.

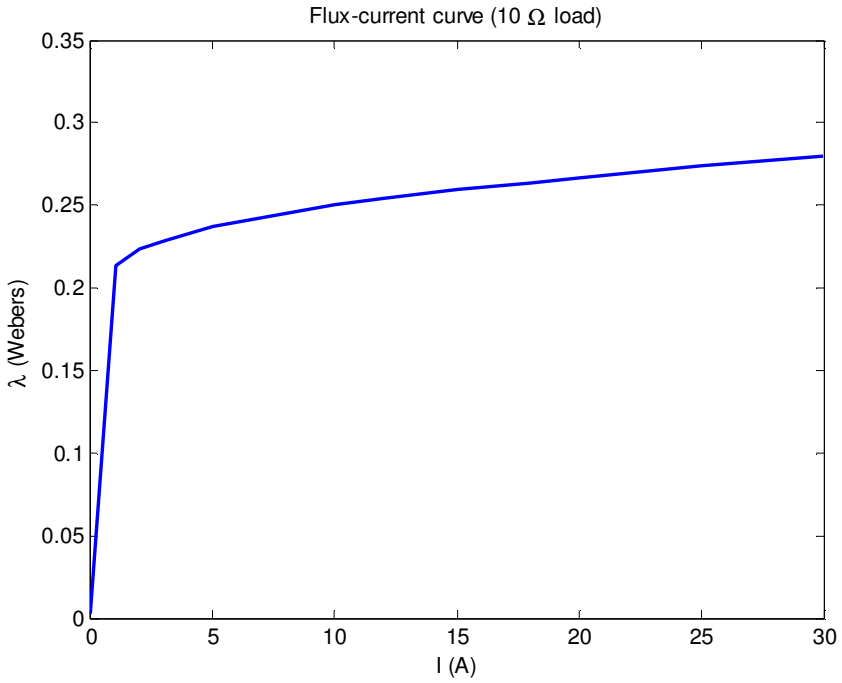

Figure 3-10 Saturation curve - rms flux - obtained from the 10 Ω load (e.g. no-load condition) MagNet simulation

Table 3-1 : Implemented saturation curve (RMS values)

I (A)	**λ (Wb)**
0	0
5	0.04
15	0.045
45	0.055

In the curve shown in figure 3-10, there are 13 knee points or, in other words, 14 different segments. This can cause problems during numerical simulations in terms of stability since the operation point might be changing too frequently. To solve this problem, the curve was

simplified to use only four knee points. After some adjustments, the curve's points that have been implemented in the model are shown in table 3-1.

It is essential to note here that the points in table 3-1 are the results of an iterative process. In fact, due to the modelling assumptions, the saturation characteristic had to be adjusted in order to take into account some effects that were left aside. This is why the operating points in table 3-1 are not directly coming from the original 10 Ω load curve. The points in this table are the one giving the best results in terms of waveform shape and were used to produce the results shown previously. They were obtained by means of an iterative process, comparing the waveforms produced by EMTP-RV to the ones produced by MagNet each time a point was modified computing the mean square error between both curves (considering the results from MagNet to be the vector of true values). The iterative process used here is quite similar to the one presented in figure 3-9 above: for each modification of the saturation curve in the EMTP-RV model, the results were plotted against the ones coming from MagNet to evaluate the error.

3.3.2.4 Stator and control coils inductance and DC resistance values

Only the values of the machine stator coil inductances were calculated. Indeed, there is no need to compute the inductance of the control coil in steady-state as this coil is excited by a direct current and as there is no AC flux reflected on the control side of the circuit in this mode of operation; thus eliminating the potential impedance of an inductance. This AC flux would not change the magnitude of the current injected by the direct current source, but would affect the losses in the control circuitry. This inductance would need to be assessed if one would like to study the transient response of the control coil of the generator. During transient, it is this inductance that dictates and limits the behaviour of the active protection in terms of rapidity of operation.

The calculation of the inductance values in the document [15] is based on the geometry of the magnetic flux path associated with each coil. The theory in the work from [15] was used to compute those values. For instance, the four next equations are taken from the document and are giving the value of these inductances. These equations describe the relationship between the length of the magnetic path and the cross-section that the magnetic flux passes through for a given coil. Therefore, they are all imposed by the geometry of the generator. A visual representation of these quantities is shown in figure 3-11.

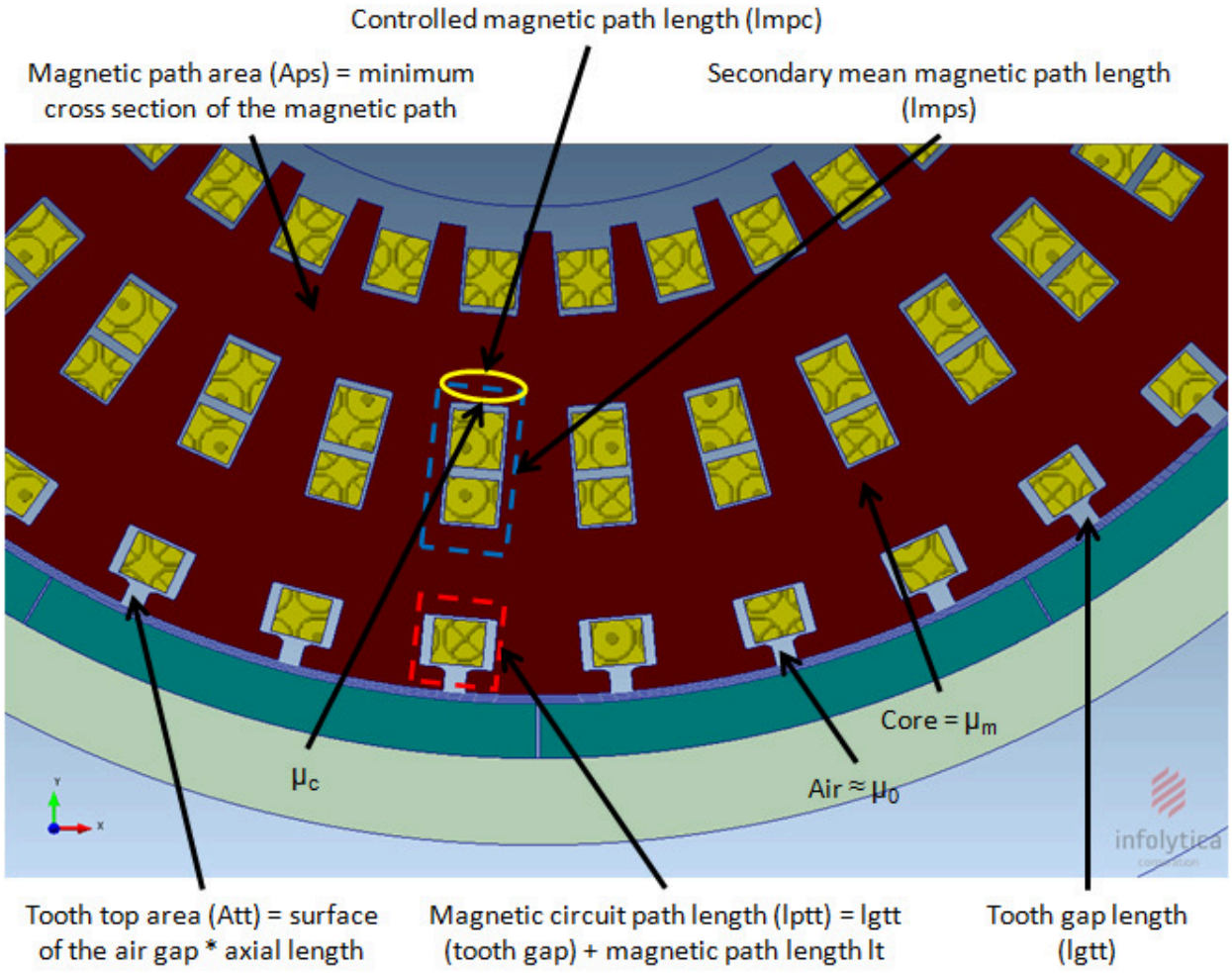

Figure 3-11 Visual representation of the geometry of the NAEM

$$L_{tt} = \left(l_s * \mu_0 + \frac{A_{tt} * \mu_0}{l_{ptt}}\right) * S \qquad (3-1)$$

$$L_s = \left(l_s * \mu_0 + \frac{A_{ps}}{l_{ps}/\mu_0}\right) * S \qquad (3-2)$$

With

$$lps = \frac{lmps}{\mu_m} + \frac{lmpc}{\mu_c} \qquad (3-3)$$

$$L_{et} = l_{er} * \mu_0 + c_f * l_{ef} * \mu_0 \qquad (3-4)$$

$$L_{cs} = t_c^2 * L_s + t_c^2 * \left(\frac{A_{ps}}{\frac{\frac{l_{mps}}{\mu_{mat}} + \frac{l_{mpc}}{\mu_c}}{\mu_0}} + t_c^2 * l_{eta} * \mu_0 \right) \qquad (3-5)$$

where L_{tt} is the top tooth inductance (primary magnetic path), L_s is the slot inductance, L_{et} is the end turn inductance and L_{cs} is the control coil inductance. In figure 3-11, there is segregation between μ_c and μ_m although they both refer to the same material and thus the same permeability. This segregation is done only to remind that the local permeability μ_c reduces as the saturation of the control portion of the NAEM is increased during operation of the generator

Using a matrix representation of the following form [25]:

$$L = \begin{bmatrix} L_s & L_m & L_m \\ L_m & L_s & L_m \\ L_m & L_m & L_s \end{bmatrix} \qquad (3-6)$$

Where

$$L_s = \frac{L_0 + 2L_1}{3} \qquad (3-7)$$

$$L_m = \frac{L_0 - L_1}{3} \qquad (3-8)$$

Then, the self and mutual inductances can be defined by the following equations ($Z_0 = 0$ and $Z_1 = Ltt$ =tooth top inductance):

$$L_{self} = \frac{2}{3} * L_{tt} \qquad (3-9)$$

$$L_{mutual} = -\frac{1}{3} * L_{tt} \qquad (3-10)$$

one obtains the following results for the above inductances:

$$L_s = 6{,}799 * 10^{-7}$$

$$L_m = -2{,}502 * 10^{-7}$$

$$L_{et} = 5{,}964 * 10^{-7}$$

These values represent the internal impedance of the machine's voltage generation part. The self and mutual inductances were implemented in the couples RL branch of figure 3-4 in the form of an inductance matrix. The end turn inductance was added to the self inductance value considering a linear relationship and no coupling. In other words, a linear inductance was added directly in series to model the effects of the end turn inductance calculated using equation 3-4.

In a second step, the DC resistance values of both the stator and control coils were computed using a MagNet script. This value can be calculated using the following relation:

$$R_C = \rho * \frac{L}{S} \qquad (3-11)$$

In the equation above, ρ is the resistivity of copper (in Ω•m), L the length of copper (in meters) and S is the cross sectional area of the copper wire (in m^2). One must note that all these parameters are fixed by the geometrical dimensions and properties of the used materials (these properties are defined in MagNet materials libraries). The DC resistance values in ohms of both the phase and control coil were determined by evaluating this equation for both coil arrangements. The following values were obtained:

$$R_{stator\ coil} = 7{,}174 * 10^{-4}\ \Omega$$

$$R_{control\ coil} = 0{,}981\ \Omega$$

The previous value for the stator coil resistance presupposes that the skin effect in the winding conductors can be neglected. To verify this assumption, the skin depth is approximated using the following equation. As the generator is a variable-frequency generator, a frequency of 1 536.8 Hz is used as a mean value. The value of the copper resistivity in the PhD document [15] is $2.812 * 10^{-8}\Omega \cdot m$ at 180°C. According to standard ASTM B48 [26] (standard specification for soft rectangular and square bare copper wire for electrical conductors), the maximum allowable resistivity for copper at 20°C is $1.7241 * 10^{-8}\ \Omega \cdot mm$. Using a linear approximation to compute this resistivity at 180°C according to this standard leads to:

$$\rho(T) = \rho_0[1 + \alpha(T - T_0)] \qquad (3-12)$$

$$\rho(180) = 1.7241 * 10^{-8}[1 + 0.003862(180 - 20)] = 2.789 * 10^{-8}\Omega \cdot m$$

As the discrepancy between both values is less than 1%, the value of resistivity from the PHD document will be used in the following calculations.

The skin depth can be evaluated using the following formula [27] :

$$\delta = \sqrt{\frac{2\rho}{\mu_0 \mu_r * 2\pi f}} \qquad (3-13)$$

$$\delta = \sqrt{\frac{2 * 2.812 * 10^{-8}}{4\pi * 10^{-7} * 1 * 2\pi * 1536.8}} \approx 1.97\ mm$$

In the geometrical model of the NAEM, in MagNet, the stator winding conductors are represented by rectangular conductors of the following dimensions:

$$h_{stator\ conductor} = 0.125\ in \approx 3.175\ mm$$

$$w_{stator\ conductor} = 0.140\ in \approx 3.556\ mm$$

An equivalent circular conductor of the same cross-section would have a diameter of:

$$D = 2 * \sqrt{\frac{3.175mm * 3.556mm}{\pi}} \approx 3.791\ mm$$

As $D < 2\delta$, it is therefore a valid approach to neglect the skin effect for the stator winding conductors.

3.3.2.5 Other components

The four other components (at the right of the transformer in figure 3-4) in the EMTP-RV model (LowV1_PhA_Ld_Rstr, LowV1_PhA_ET_Indce, LowV1_PhA_ET_Rstce, LowV1_PhA_Cable_Indce) were directly built using the corresponding values found in MagNet (see figure 2-9). One must recall that these values account for end turn resistance and inductance and for the cable line inductance. They were introduced in the EMTP-RV model in order to replicate with as much fidelity as possible the MagNet model.

All the loads used during this project are 3-phase balanced loads. Furthermore, all scenarios were run using purely resistive loads.

CHAPTER 4 RESULTS

This section presents the results obtained from the EMTP-RV electrical model for 4 specific test cases. These test cases were chosen in order to show some of the most representative modes of operation of the NAEM. In all cases, the results obtained from EMTP-RV are compared to their counterpart from MagNet (the reference). First, in a regular-load condition (scenario #1), to then in a heavy-load condition (scenario #2) and in a light-load condition (scenario #3), the EMTP-RV model showed good results in steady-state operation compared to the MagNet model.

Each test case presents various control current values for a given loading condition. The speed of the machine is always kept constant throughout the simulations. All loads presented here are three-phase balanced loads. These loads are purely resistive.

One must note that, according to the assumptions stated previously, the most interesting cases are those were the control portion of the NAEM is operating near or at full saturation for two main reasons. First, the NAEM should always operate in this mode under normal circumstances, which represents the most common state during the lifetime of the generator. Second, the assumption that the internal voltage generation in the generator can be modelled by an ideal voltage source coupled with a RL impedance makes it impossible to cover all cases, as the output current of the generator significantly affects the internal emf of the machine (armature effect). The calibration of the NAEM in the EMTP-RV model was therefore done assuming operation near or at full

Table 4-1 Summary of the simulations presented in chapter 4

Test case	Load (Ω)	Load (p.u.)	Control current (A)
1	0.05	0.9	0
			10
			20
2	0.01	4.6	0
			10
			20
3	0.1	0.5	0
			10
			20
4	5	≈ 0	0
			20

saturation for this project. This assumption was taken at the beginning of the project since the scope has been limited for this first model to simulate the behaviour of the NAEM in steady-state.

In order to evaluate the performances of the EMTP-RV model in regards with the reference, the normalized root mean square error (also known as the normalized root mean square deviation) is computed for each scenario. The normalized root mean square error is defined as follow:

$$nrmse = \frac{\sqrt{\frac{\sum\left(\widehat{\Theta} - \Theta\right)^2}{n}}}{y_{max} - y_{min}} \qquad (4-1)$$

where $\widehat{\Theta}$ is the estimator (data coming from the MagNet model), Θ is the predicted value (data coming from the EMTP-RV model), n the number of points and y_{min} and y_{max} are respectively the minimum and the maximum values observed for a given scenario. The objective here is to be able to compare the performances of the EMTP-RV model in various scenarios. As the root mean square error is scale-dependant [28], the normalized root mean square error was used to allow the comparison of the error between both models for different set of data (with different set of scales). The normalized root mean square error in steady-state for each scenario is shown on the corresponding figure.

Another important point to note is that the transient phases of the signals are shown here for discussion purposes only. Transient-phase will be discussed in the next section as an objective for a future project.

4.1 Test case #1: 0.05 Ω (0.91 p.u.) load

In this first scenario, the NAEM is loaded with a 0.05 Ω load. This load simulates a standard loading condition near nominal power. Each figure showing the results in EMTP-RV for a particular loading scenario is accompanied by a figure showing the flux lines and the magnetic field magnitude (shaded areas) as calculated by MagNet for the same conditions.

The first figure shown here is the output current under the stated load for a null control current. As mentioned before, figure 4-1 shows the worst case scenario in terms of matching results. This is due mainly to one of the modeling assumptions explained earlier: the fact that the voltage

sources in the electrical model are assumed constant no matter what are the loading conditions. This assumption is not true in all cases and can create a discrepancy between both models as in this case. In fact, as the next figures suggest it, the lower the output current is, the more significant are the effects of space harmonics. In this particular case, although the load is near the nominal value, the control current is set to zero (the direct current source becomes an open circuit) which reduces the output current of the generator. The case with a control current equals to zero will be shown in the next two scenarios for discussion purposes only in the last section.

In figure 4-3, the controlled portion of the NAEM is near full saturation as the control current is raised to a value of 10 A. The effects of the space harmonics are less significant on the output current waveform as the control current increases. This figure shows an interesting phenomenon of the EMTP-RV model. As one may observe, the electrical output waveform is not purely sinusoidal in this case. In fact, for a control current value near 10 A, the slope of the curve changes, creating a bending point in the sine waveform and then resuming its original trajectory. This effect is explainable by looking at the modelling of the non-linear inductances saturation curves (refer to section 3.3.2.3). As the saturation curves are modelled here using only 4 segments to avoid numerical time step dependant imprecision for this first model, the difference between two segments is significant. Therefore, what the reader can observe here is a back-and-forth change of the saturation slope (in other words, a change in the relative permeability μ_r of the magnetic material). This results in a momentary modification of the internal impedance of the generator and thus affects the output current of the machine. This behaviour was expected to happen around this value of control current as the generator is operating near the saturation curve's knee; saturation is not yet achieved. This effect is also visible in the next loading scenario.

One can note that both waveforms, from EMTP-RV and from MagNet, are similar in terms of global shape and peak values. The most significant discrepancy resides in the harmonics visible in the MagNet curve. Besides that, the EMTP-RV curve is representing with a good level of fidelity the behaviour of the NAEM during the steady-state phase.

Figure 4-5 presents the output current when the control portion of the NAEM is fully saturated. The portion of the stator core in the controlled magnetic path is considered fully saturated when the control current reaches 20 A as increasing the control current any further than 20 A has no

significant effect on the output of the machine. This scenario is the case where the match between the electrical model and the finite element model is the best. This is due to the fact that the EMTP-RV model has been calibrated using this particular mode of operation (for the calibration of the internal voltage source for instance that is the most significant calibration parameter of the model; the magnitude of the voltage source has been adjusted to fit as best as possible the waveform from MagNet for this particular scenario). The calibration of the model has been done only once, and the same saturation curve is used everywhere.

One can notice that, in this case, the output waveform of the FE model contains fewer harmonics than the two other ones presented above. This is because as the control current increases, it keeps the controlled magnetic circuit path (associated with the control coil) saturated at all times, resulting in quasi-constant (thus linear) machine series impedance. It is in this particular scenario that the electrical model is best fitting the results compared to its magnetic counter-part. Both waveforms peak around the same value and have similar shapes in steady-state.

From this first loading scenario, it is possible to see that the behaviour of the EMTP-RV model in steady-state corresponds with a good precision to the one of the MagNet model. For instance, the normalized root mean square error for steady-state phase is below 3% for this loading scenario and a control current of 20 A. It is therefore visible here that the objective of the modelling process has been reached: to have a model that exhibits an acceptable behaviour of the NAEM in steady-state condition. It can also be seen that as the control current increases, the error between both models tends to decrease. The next test cases in the following subsections will also confirm this.

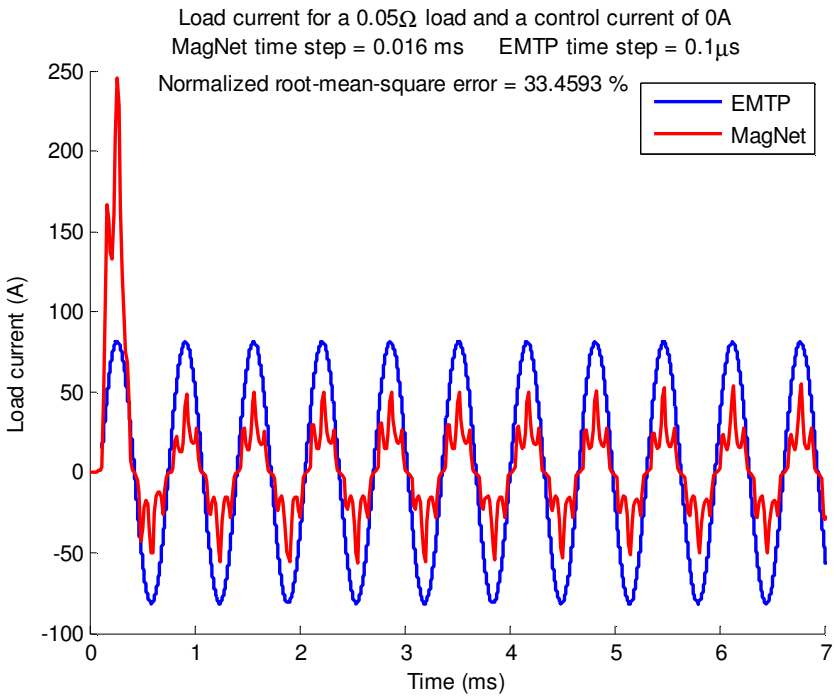

Figure 4-1 Load current for a control current of 0 A and a load of 0.9 p.u. (0,05Ω)

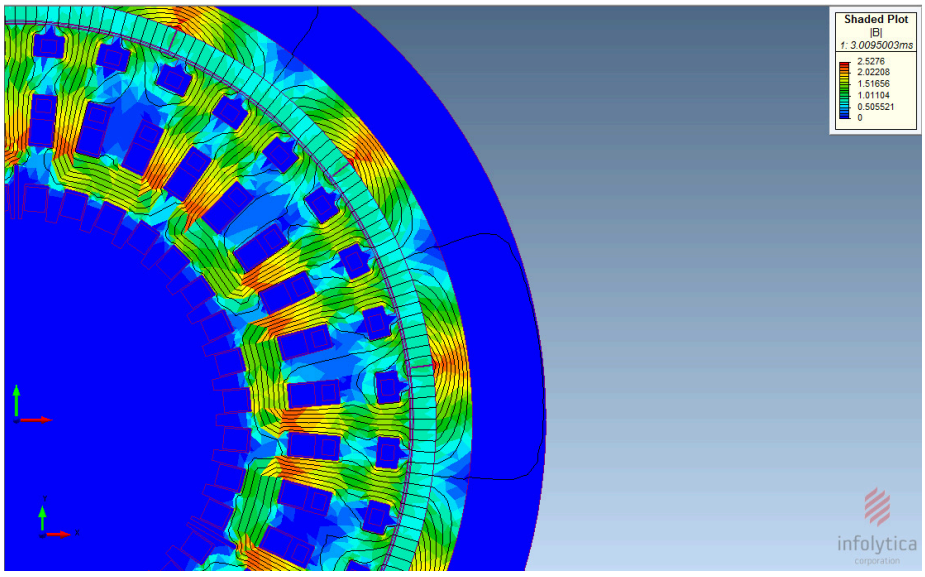

Figure 4-2 Flux lines and magnetic field magnitude calculated by MagNet for a control current of 0 A and a load of 0.9 p.u. (0,05Ω)

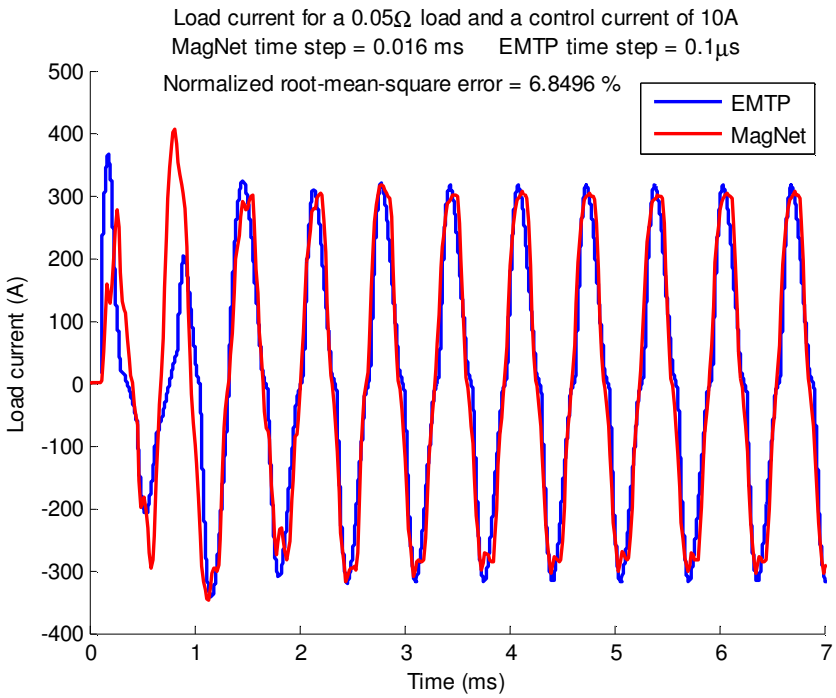

Figure 4-3 Load current for a control current of 10 A and a load of 0.9 p.u. (0,05Ω)

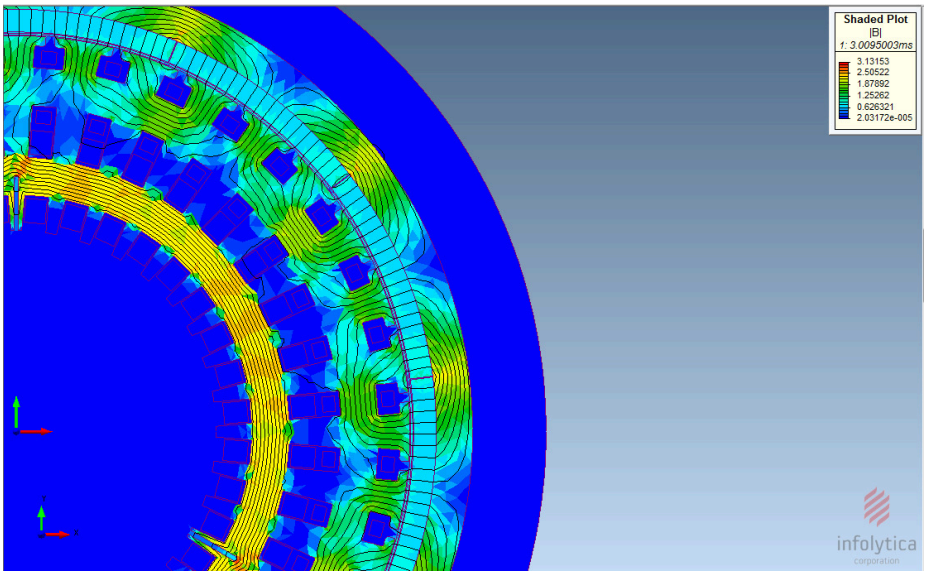

Figure 4-4 Flux lines and magnetic field magnitude calculated by MagNet for a control current of 10 A and a load of 0.9 p.u. (0,05Ω)

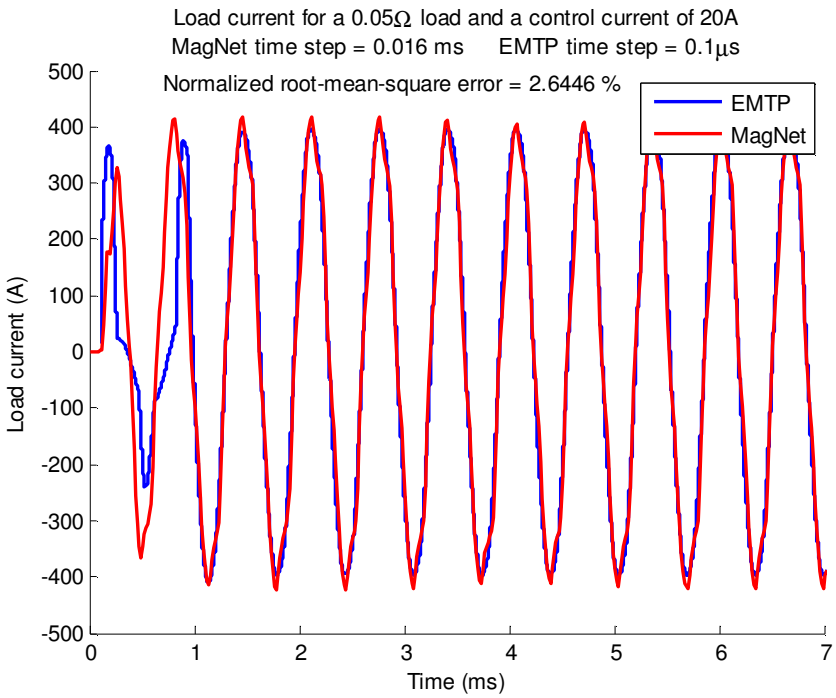

Figure 4-5 Load current for a control current of 20 A and a load of 0.9 p.u. (0,05Ω)

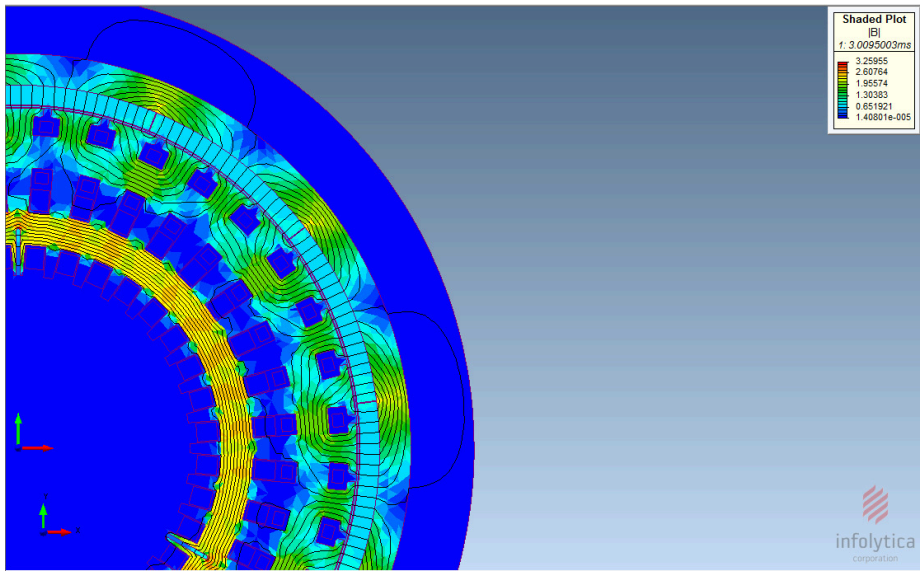

Figure 4-6 Flux lines and magnetic field magnitude calculated by MagNet for a control current of 20 A and a load of 0.9 p.u. (0,05Ω)

4.2 Test case #2: 0.01 Ω (4.6 p.u.) load

In this scenario, the NAEM is loaded with a 0.01 Ω load (4.6 p.u.), an overloaded condition. As it was the case in the previous section, each figure showing the results for a particular loading scenario is accompanied by a figure showing the flux lines and the magnetic field magnitude as calculated by MagNet for the same conditions. As figure 4-8, figure 4-10 and figure 4-12 show, the behaviour of the NAEM under this loading scenario is similar as the one observed for the previous loading scenario, thus explaining the similarities in the correlation between the precision of the electrical model and the magnitude of the control current.

The output current of the machine for a 0 A control current is shown in figure 4-7. This is the worst scenario in terms of matching results for the reasons mentioned in the previous section.

Using a control current of 10 A for the given load condition yield to the output shown in figure 4-9. One can observe that the peak value of the output current here is higher than it was for the previous loading condition for the same control current. This result was expected as the NAEM is putted here in this more heavily loaded condition. The same behaviour is observable for the NAEM with a control current of 20 A. Also, as it was the case in the previous loading scenario, the more saturated is the generator's secondary magnetic path, the more accurate is the electrical model compared to the FE one. Figure 4-11 shows the results obtained for a fully saturated control winding.

The results presented here for this second test case confirm once again that the behaviour of the EMTP-RV model, in steady-state, corresponds well to the one of the reference. The main discrepancies visible are due to the modelling assumptions stated previously.

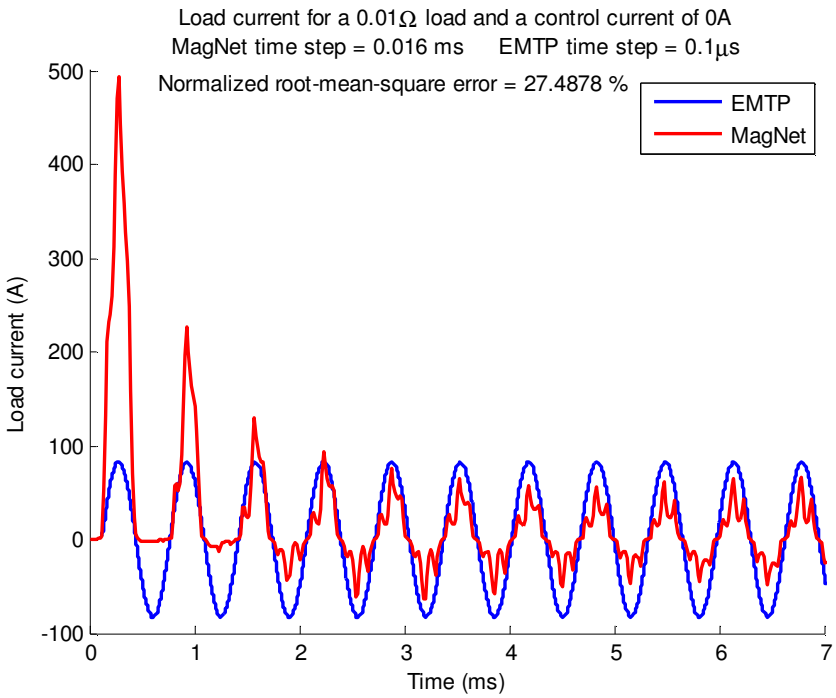

Figure 4-7 Load current for a control current of 0 A and a load of 4.6 p.u. (0,01Ω)

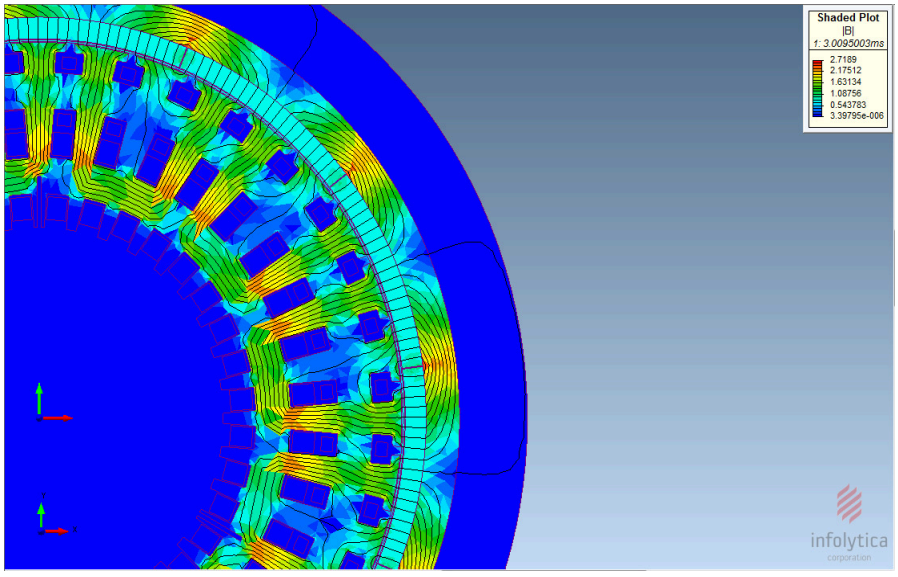

Figure 4-8 Flux lines and magnetic field magnitude calculated by MagNet for a control current of 0 A and a load of 4.6 p.u. (0,01Ω)

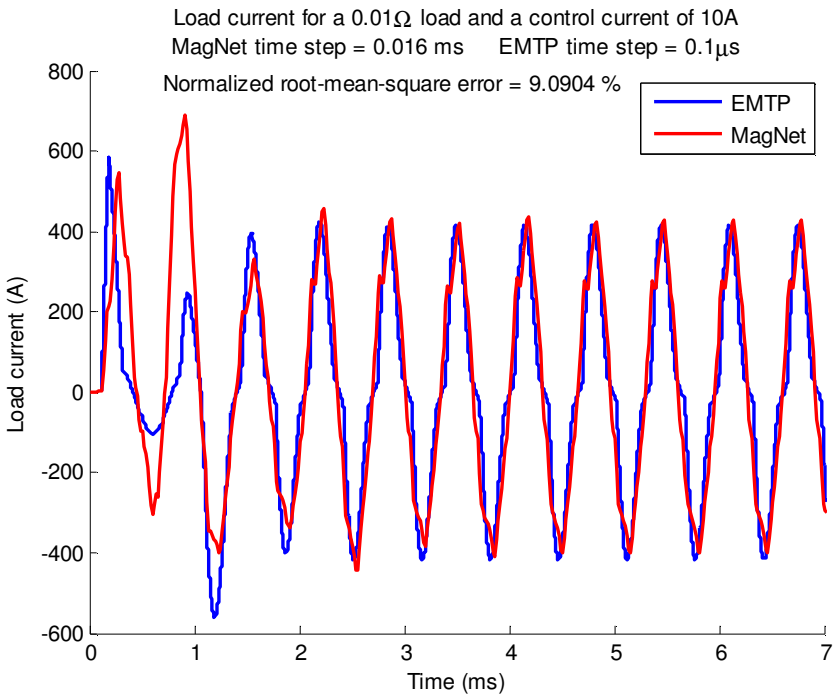

Figure 4-9 Load current for a control current of 10 A and a load of 4.6 p.u. (0,01Ω)

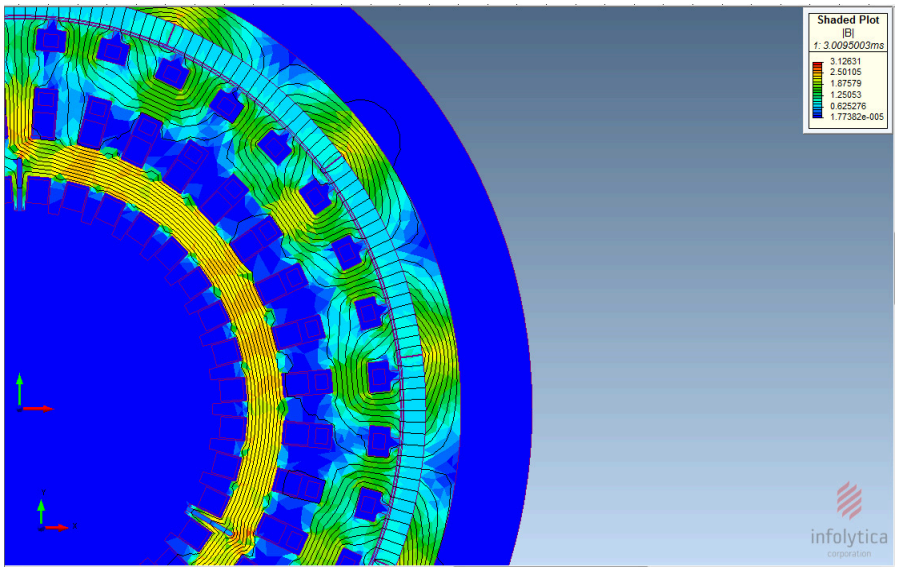

Figure 4-10 Flux lines and magnetic field magnitude calculated by MagNet for a control current of 10 A and a load of 4.6 p.u. (0,01Ω)

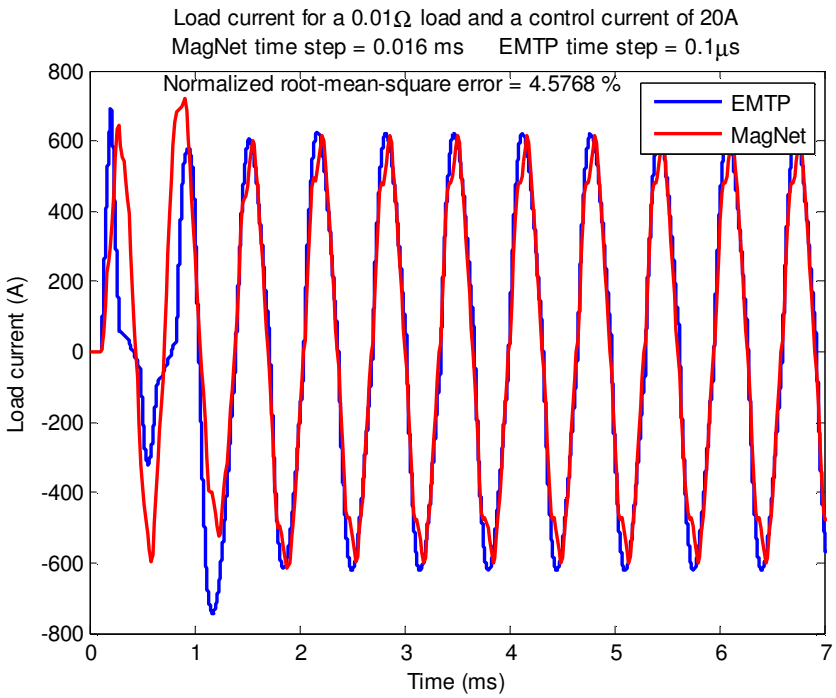

Figure 4-11 Load current for a control current of 20 A and a load of 4.6 p.u. (0,01Ω)

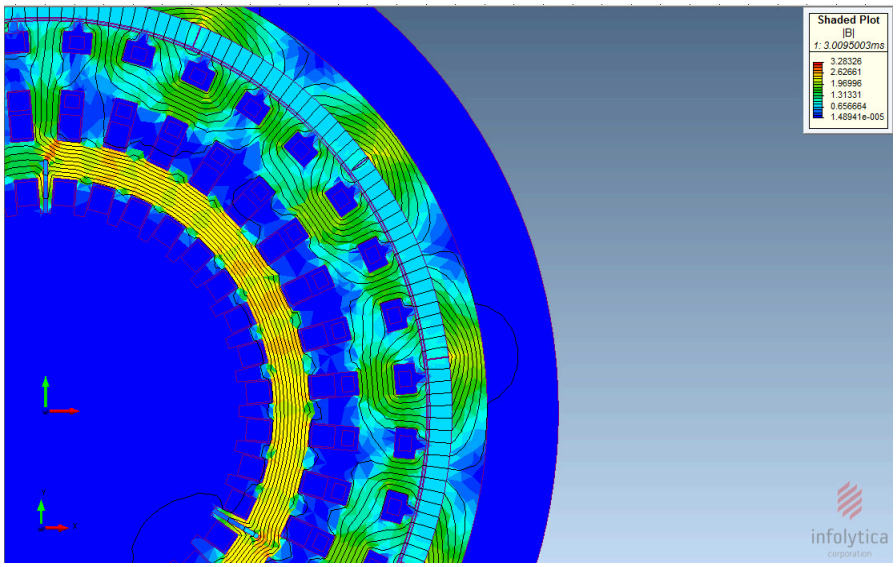

Figure 4-12 Flux lines and magnetic field magnitude calculated by MagNet for a control current of 20 A and a load of 4.6 p.u. (0,01Ω)

4.3 Test case #3: 0.1 Ω (0.5 p.u.) load

This last scenario puts the NAEM in a light-load condition. In this case, a 0.1 Ω load was used. This represents a case where the load is around half of the nominal load.

Figure 4-13 presents the results obtained for a control current of 0A. The next two figures, figure 4-14 and figure 4-15, present the output current of the machine for the same load for, respectively, a control current of 10 A and 20 A. In this loading scenario, a larger discrepancy is visible between the electrical and magnetic model results than in the two previous scenarios. This is due to the fact that, as the load decreases, the NAEM is approaching a no-load condition. In such condition, the output current is small compared to the nominal value and, thus, the effects of the space harmonics are more significant. This phenomenon is linked to the non-linear filter behaviour of the control inductance in the model as mentioned in section 4.1. This explains the increasing discrepancy, as the electrical model does not take their effects into account. Besides that, this scenario illustrates another loading condition where the developed model shows good performances. The EMTP-RV model therefore reproduces with a good consistency the behaviour of its magnetic counter-part as it was shown in these three loading scenarios.

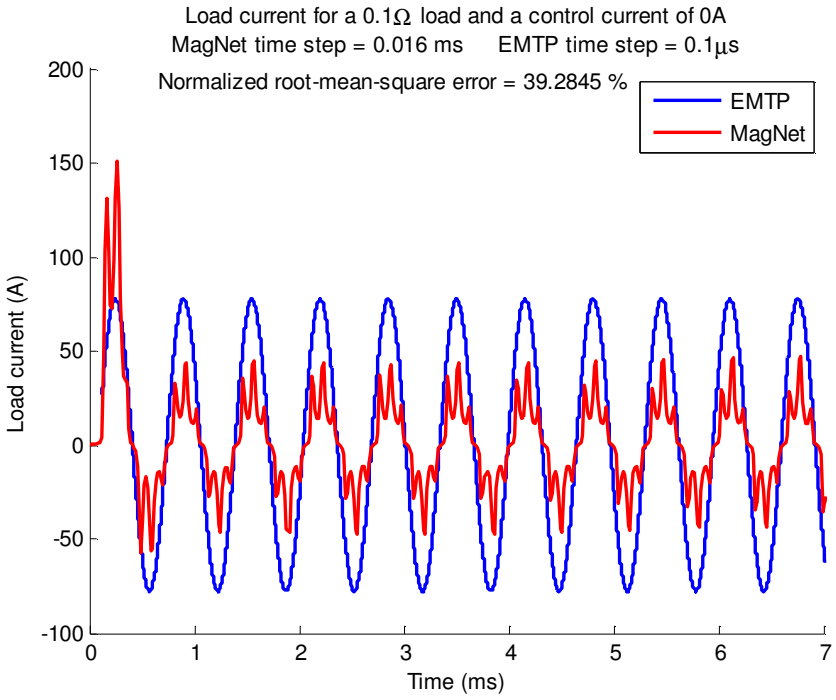

Figure 4-13 Load current for a control current of 0 A and a load of 0.5 p.u. (0,1Ω)

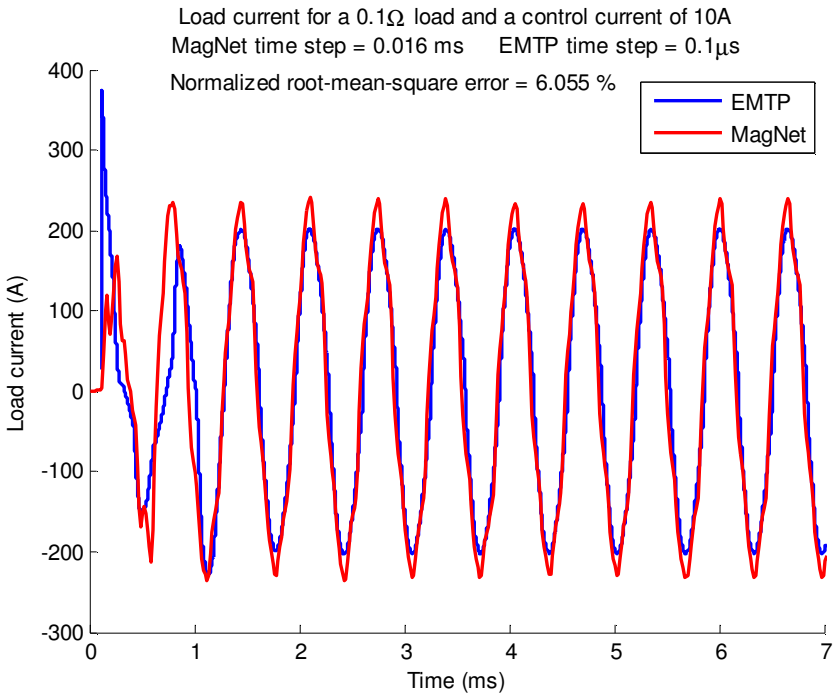

Figure 4-14 Load current for a control current of 10 A and a load of 0.5 p.u. (0,1Ω)

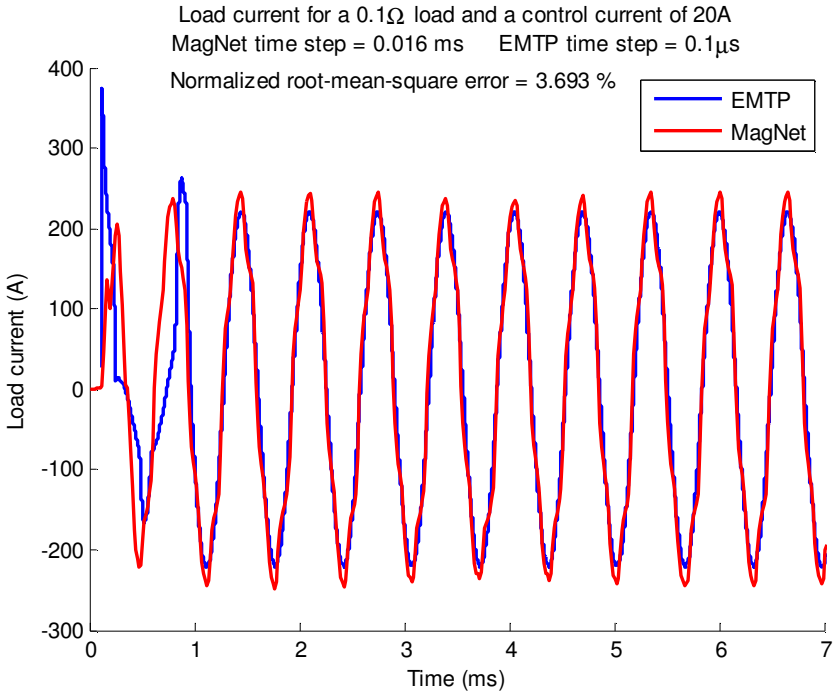

Figure 4-15 Load current for a control current of 20 A and a load of 0.5 p.u. (0,1Ω)

4.4 Test case #4: 5 Ω load (no-load condition)

For comparison and discussion purposes, it is relevant to see the behaviour of both models in a no-load condition. Here, this condition is simulated by a 5 Ω load. This value is sufficiently large to simulate an open-circuited NAEM while avoiding numerical instabilities caused by an actual open circuit in the magnetic model (in the circuit window of MagNet, it is not possible to let a node disconnected, but this can easily be avoided by connecting a large resistor at the NAEM output terminals). Only the results for a control current of 0 A and a control current of 20 A are shown here.

Under no-load conditions, one can observe that some assumptions taken previously are no longer correct (the same applies to the scenarios where the control current is set to zero). For instance, the influence of the space harmonics and the fluctuation of the internal voltage generation become significant here. These results justify the needs for future works in order to improve the performances of the electrical model as it will be discussed in the next few pages.

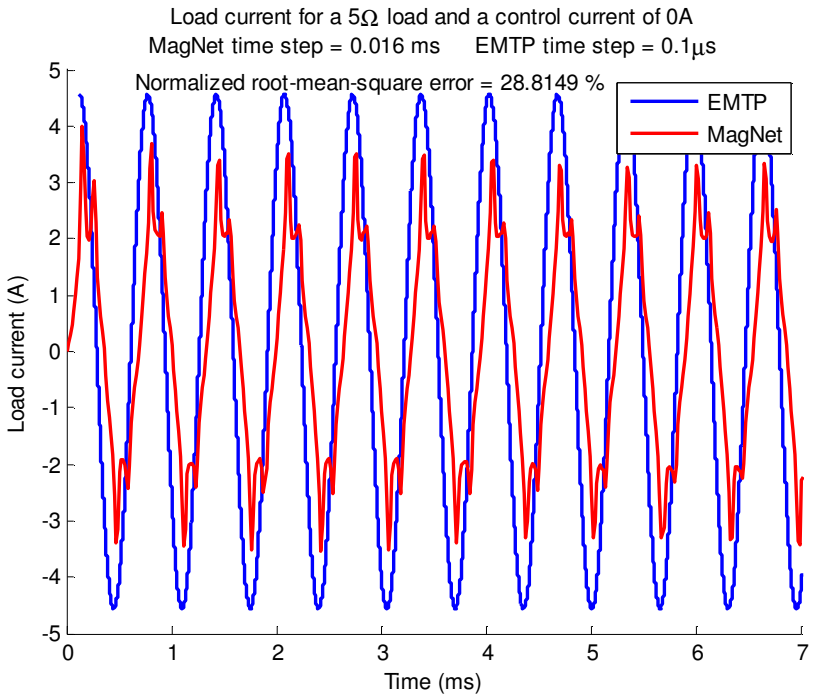

Figure 4-16 Load current for a control current of 0 A and a load of 5Ω (no-load)

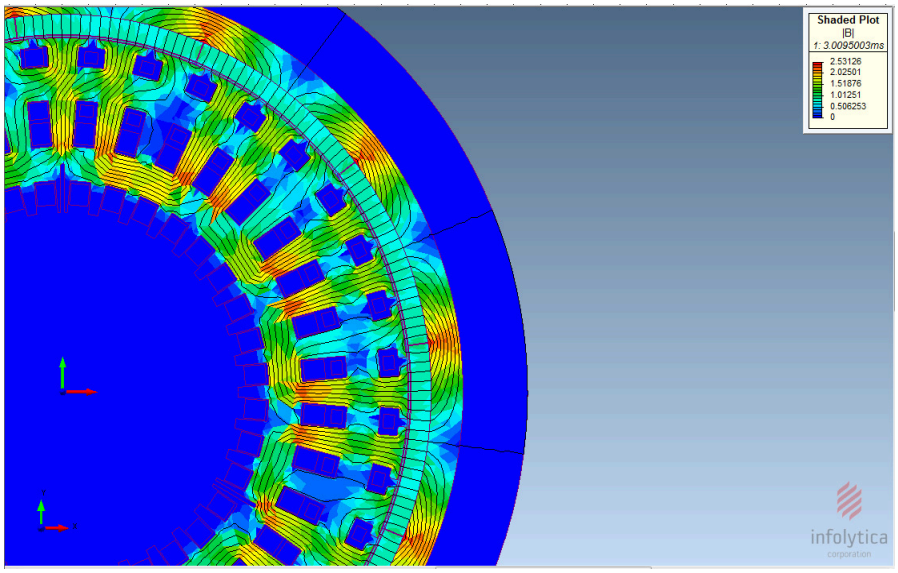

Figure 4-17 Flux lines and magnetic field magnitude calculated by MagNet for a control current of 0 A and a load of 5Ω (no-load)

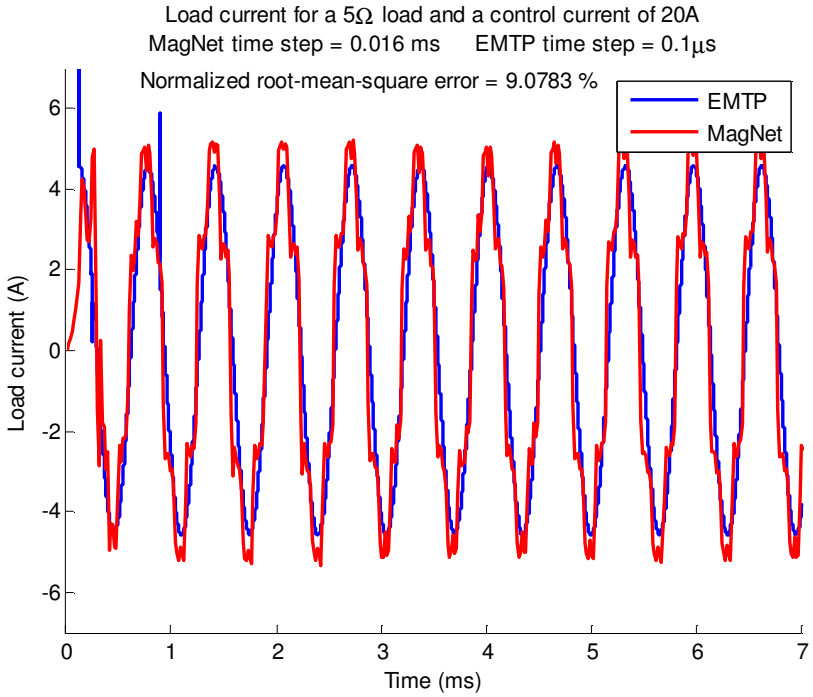

Figure 4-18 Load current for a control current of 20 A and a load of 5Ω (no-load)

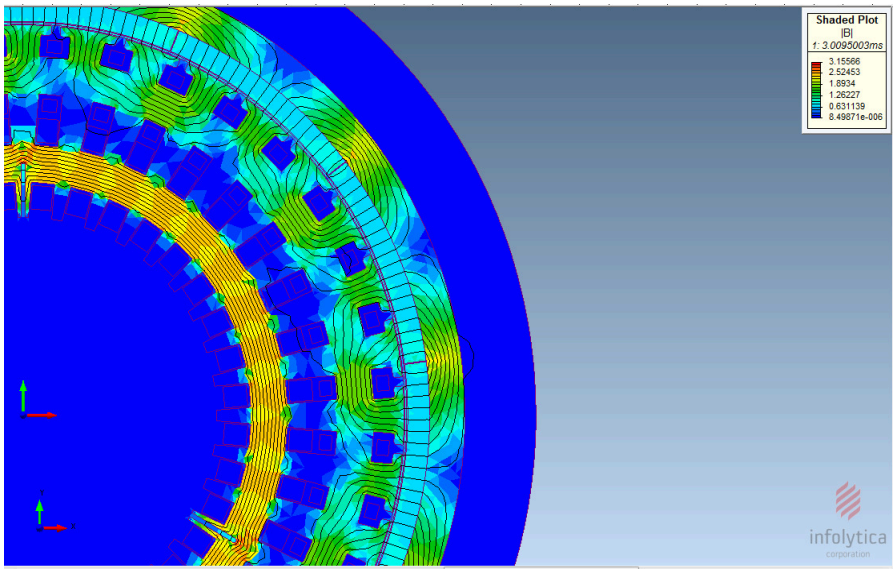

Figure 4-19 Flux lines and magnetic field magnitude calculated by MagNet for a control current of 20 A and a load of 5Ω (no-load)

CHAPTER 5 DISCUSSION

This last section of the document aims to present an analysis of the results presented in the previous section. As the reader is now aware, the EMTP-RV model shows good results in steady-state operation under a wide range of loading conditions. Some discrepancies, caused by different factors, were noted. The most relevant points of analysis are discussed here in the first sections. The last section presents the future work to be done on the current model in order to improve its representativeness and, eventually, to model the transient behaviour. Some possible technical avenues to achieve this are also presented.

5.1 Space harmonics

At the beginning of the modelling process, the decision to neglect space harmonics in the electrical model was taken (refer to section 3.2.3 for the justifications behind this assumption). This resulted in some discrepancies between the output current waveforms generated in EMTP-RV and in those generated by MagNet. It was also noted that the higher the output current value is, the less significant the effects of those space harmonics are. To explain the mechanisms behind this relationship and to be able to evaluate the importance of the space harmonics, the generated voltage inside the NAEM has been analyzed in the frequency domain. But first, figure 5-1 and figure 5-2 show a typical waveform for the generated voltage inside the generator for a fixed load in a partially-saturated state first (control current of 5 A) and in a fully-saturated state afterwards (control current of 20 A).

Space harmonics are directly linked to the stator winding arrangement in the generator. Referring to figure 2-5, it is possible to observe that the pole arrangement in the stator for each phase inside the machine is rather “rough”. For a given phase, the number of slots is low, and the number of slot per pole per phase is correspondingly low. This results in a staircase-like emf waveform which in turns results in a high harmonic content. One must note that one of the main reasons for this choice of design here is the fact the output of the NAEM is meant to be rectified and distributed to a DC power system throughout the aircraft afterwards. Thus, there is no particular need for a smooth sine emf waveform at the output of the generator. From an engineering point of view, the fact that the NAEM will mainly be used in a situation where its output will be directly rectified supports the assumptions taken at the beginning of the working process. As the

output is rectified in DC, it becomes less critical to have an accurate model of the NAEM in that regard as its main contribution to the aircraft's network will not be in AC but in DC. The discussed model here can therefore be incorporated in an aircraft electrical network as a first approximation of the NAEM in steady-state.

Looking at those figures (the data is coming from the MagNet model), it is possible to observe that the internal voltage waveform is significantly different depending on the control current value. This is explainable by the fact that the value of the control current dictates, under a given loading condition, the output current value of the NAEM. This fluctuation in the output current value influences the impact of the armature effect and thus influences the generated voltage of the NAEM. This represents a limit of the developed model that is due to the modelling assumption and will be discussed in more detail in the next subsection. In both cases, it is possible to observe a significant harmonic content in the waveforms. As the generated voltage waveforms are far from a pure sinusoidal waveform, this explains the discrepancies observed previously between MagNet and EMTP-RV results.

To better appreciate the order of magnitude of the influence of the various harmonics present in the voltage signal, figure 5-3 shows a Fourier decomposition of the flux induced in the winding of phase A in the NAEM. The method used here to perform the Fourier transform was the Fast Fourier Transform (FFT). This was used here in order to obtain an idea of the order of magnitude of each of the main harmonics present in the signal. In a machine, flux and voltage are directly linked together, remembering Faraday's law:

$$\epsilon = -\frac{d\lambda}{\mathrm{dt}}$$

From the equation above, one can conclude that the harmonic content of the voltage waveform can be significantly higher than the one of the generated flux waveform. Thus, for comparison purposes, the harmonic content of the voltage waveform is also shown. It appeared essential to observe the harmonic content of the flux and voltage waveforms as these waveforms characterize the potential difference generated across the phase coils in the generator.

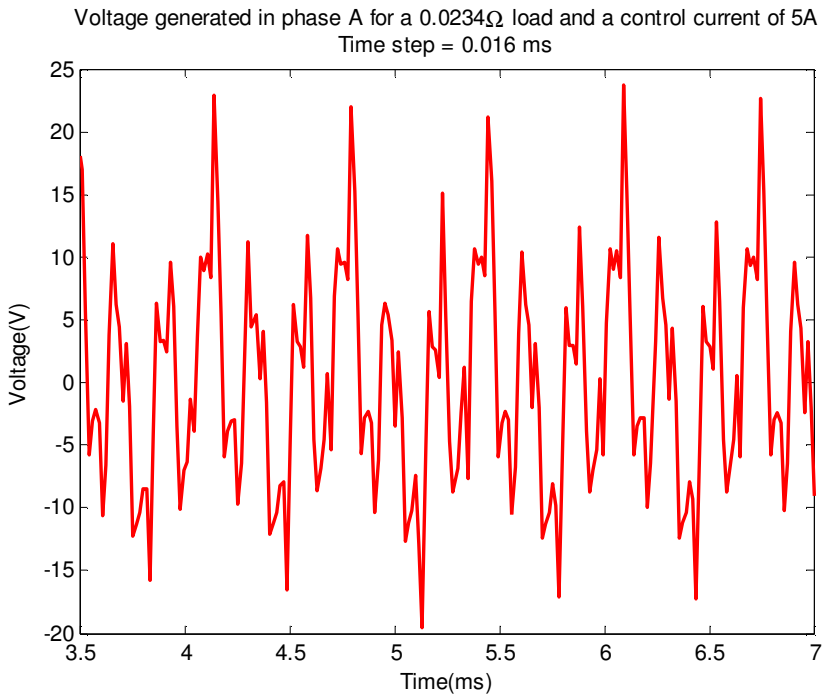

Figure 5-1 Internal voltage waveform for a 0.0234Ω load and a control current of 5A

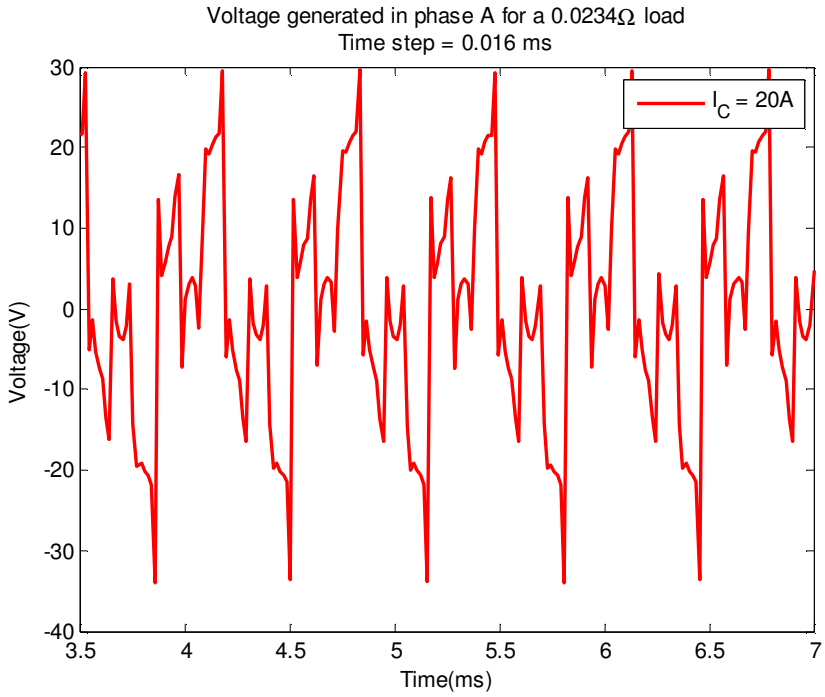

Figure 5-2 Internal voltage waveform for a 0.0234Ω load and a control current of 20A

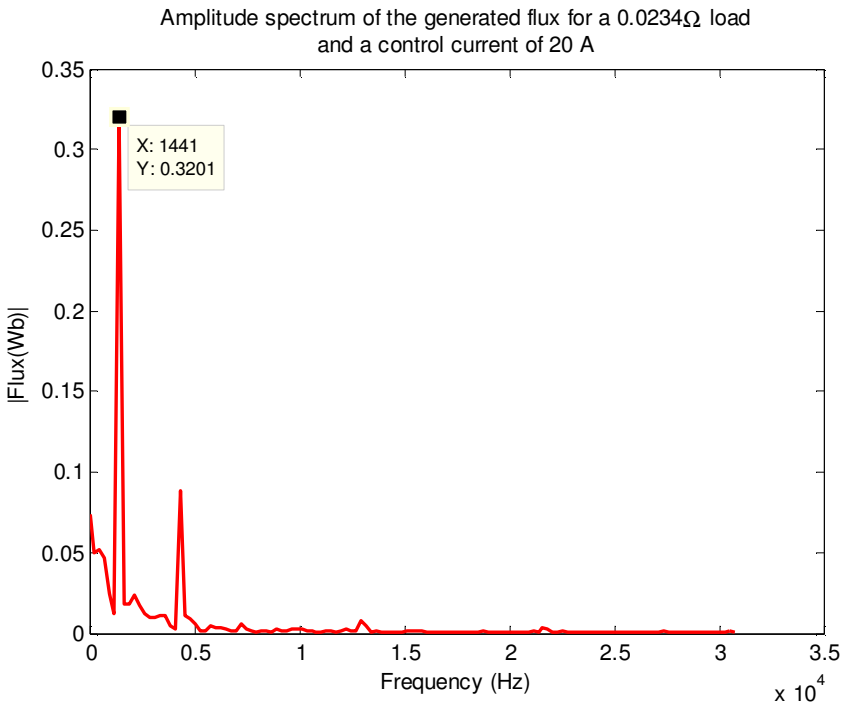

Figure 5-3 Amplitude spectrum of the generated flux in the NAEM for a 0.0234Ω load and a control current of 20A

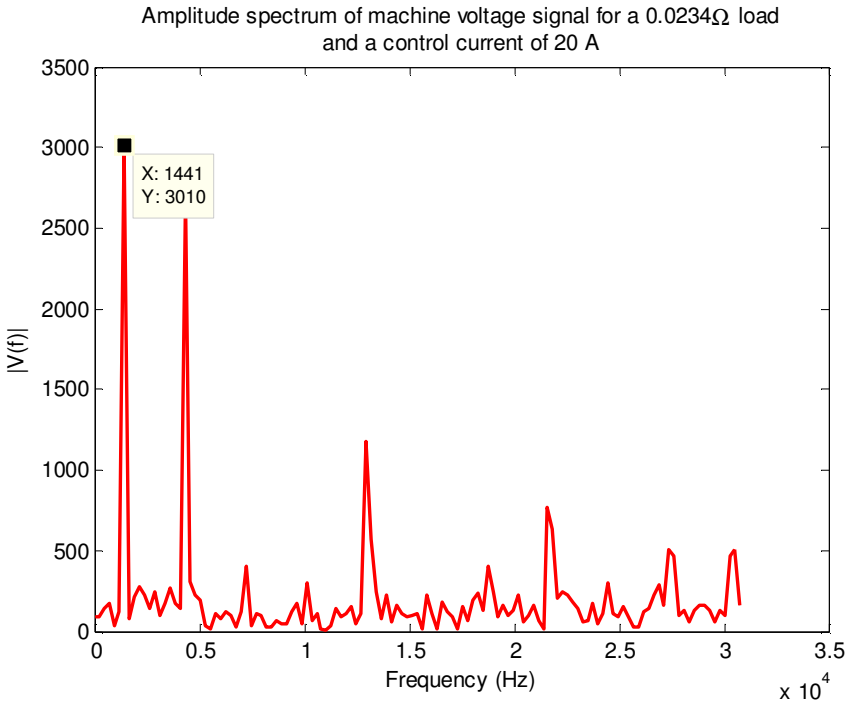

Figure 5-4 Amplitude spectrum of the generated voltage in the NAEM for a 0.0234Ω load and a control current of 20A

The resulting signals are composed of 240 points and come from figures 5-1 and 5-2. The points of the beginning and the end of a period were not repeated. However, the time step used in MagNet (0.016 ms) is not an integer of a period (0.65 ms), which causes some spectral leakage that can be neglected for this analysis.

Such analysis was done to confirm, first, whether or not the harmonic content of the generated voltage was significant. Second, it was performed to evaluate the importance of this harmonic content by quantifying it. From table 5-1, it can be seen that it will be needed to assess the harmonic content in order to obtain a more realistic model. This seems particularly true for light loading condition.

Table 5-1 Harmonic content of the generated voltage for a 5Ω load

Harmonic	$I_{control}$ = 0A		$I_{control}$ = 10A		$I_{control}$ = 20A	
	RMS value (V)	Angle (rad)	RMS value (V)	Angle (rad)	RMS value (V)	Angle (rad)
1	1.5658	-2.6389	15.4925	-1.7873	20.2769	-1.5295
2	0.3005	1.5574	0.7006	1.8030	0.4681	0.9524
3	2.2783	-0.7436	13.6043	-0.3245	9.2349	0.1474
4	0.0701	-0.9236	1.6489	-0.6940	0.1379	-1.8843
5	1.3568	0.4407	0.5313	0.5281	1.6188	0.6257
6	0.0793	-2.8248	1.3245	1.3068	0.1088	0.8116
7	1.0865	-3.0730	0.2304	1.1594	1.1890	2.0614
8	0.1130	-0.8009	0.5698	-0.7171	0.0676	-0.1928
9	1.4925	2.8053	0.4773	-2.6173	2.4709	-3.1346
10	0.0524	-2.9111	1.4316	0.4283	0.1382	-2.2950
11	1.1661	-2.4753	0.2450	2.5208	0.5654	-2.3928
12	0.0056	-0.3588	0.2892	-2.1367	0.1677	2.5685
13	1.0756	0.7552	0.7492	1.5038	0.5604	-0.6273
14	0.0439	2.8855	1.1403	1.3108	0.1107	2.8569
15	1.3203	-0.9274	0.4594	-0.7983	1.2925	-0.5529

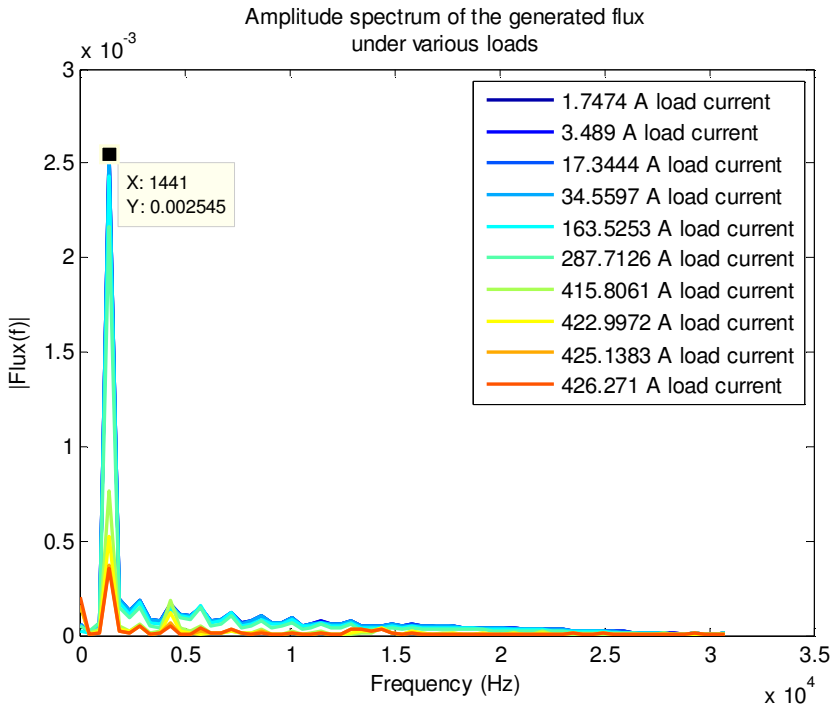

Figure 5-5 Amplitude spectrum of the generated flux under various loading conditions

For a more visual image of the evolution of the harmonic spectrum with the output current value, figure 5-5 shows a superposition of the FFT of the generated flux for various loading conditions. It is clear from this figure that the effect of the output current on the harmonic content is significant.

5.2 Effect of the output current on the generated voltage

Taking into account the effect of the output current on the generated voltage in the NAEM is one of the most significant improvements that have to be made on the current model in future work. This effect, also known as the armature effect, is the name given to the demagnetizing field that affects the inducer. In the case of the NAEM, it is the demagnetizing effect of the field of the output current acting on the permanent magnets. The armature effect is thus affecting various parameter of the generator such as changing the magnitude of the generated voltage and the harmonic content to name a few [29]. Furthermore, as it can be seen from the last section results, the impact on the internally generated voltage can be significant. This impact affects directly the output current waveforms of the generator.

As one can observe in table 5-1, the effect is particularly notable between no saturation and full saturation of the control coil. For instance, taking a look at the rms value of the fundamental of the generated voltage between I_c = 10A and I_c = 0 A, one can observe a diminution of around 90% of the fundamental magnitude. Furthermore, in the latter case, the magnitude of the third harmonic becomes greater than the fundamental. As saturation increases, the magnitude of the third harmonic (as well as the higher order harmonics) in regards to the fundamental decreases.

In addition to the effect over the harmonic content of the generated voltage, the output current magnitude also influences the magnitude of the internal voltage generation. In the table above, one has to recall that both speed and load are kept constant. The only parameter varying is the control current (which, in turn, has an impact the output current). This brief analysis indicates that the rms value of the generated voltage inside the machine is, therefore, subject to change depending on the loading conditions and the value of the control current.

Those two effects combined, of great importance between 10A and 0A for the same load for instance, explains why it is impossible to obtain good results for I_c = 0A and I_c = 20A with the current model using a constant internal voltage source. The choice was made to calibrate the model at or near its fully saturated state. The reason of this choice is that this is the preferred mode of operation of the NAEM; the generator normally should operate in this mode as long as there is no overheating or any kind of fault. To reach better results in those conditions, the internal emf of the machine should be expressed as a function of both the control current and the loading conditions (and thus the load current). To achieve an acceptable modelling of the emf of the machine would require additional simulations in MagNet in order to be able to characterize precisely the relationship that exists between the voltage generation in the machine, the output currents and the control current.

5.3 Control coil modelling

The modelling of the control coil was a delicate and important procedure in the modelling process of the NAEM. It is this portion of the generator that makes the NAEM a unique design and that controls, as its name implies, the output current of the machine. The modelling of the saturation curve of the control coil was also made using some assumptions as it was the case for previous components. For instance, the current version of the model uses a simplified version of

the saturation curve. This was useful in order to avoid getting too much time step dependant numerical imprecision in the model. Such instabilities have been experienced when trying to use a more detailed saturation curves (with around 14 different segments) instead of the simplified one currently implemented in EMTP-RV. Those imprecision can occur when the operating point shifts too much from one slope to another; creating therefore the need for a curve with less knee points. Figure 5-6 shows an example of such imprecision. It can be see here that the waveform is highly distorted and significantly far from the desired waveform presented in the last section and repeated here in figure 5-7 (note that the complete saturation curve in figure 5-6 is not calibrated which explain the discrepancy in the output current amplitude). In comparison, the waveform presented in figure 5-6 never enters saturation as it should be. Therefore, it was chosen to use a simplified saturation curves for the model built for this project.

As it was possible to see in the previous section, the simplified curve gave acceptable results in terms of the output current for the same loading scenario (refer to results of test case #2 in section 4.2). This was particularly true for the fully-saturated NAEM as the curve was calibrated to have the best fit as possible in this operating condition. The simplified curve that resulted of this process is given in figure 5-8; this is the curve that was used during this project.

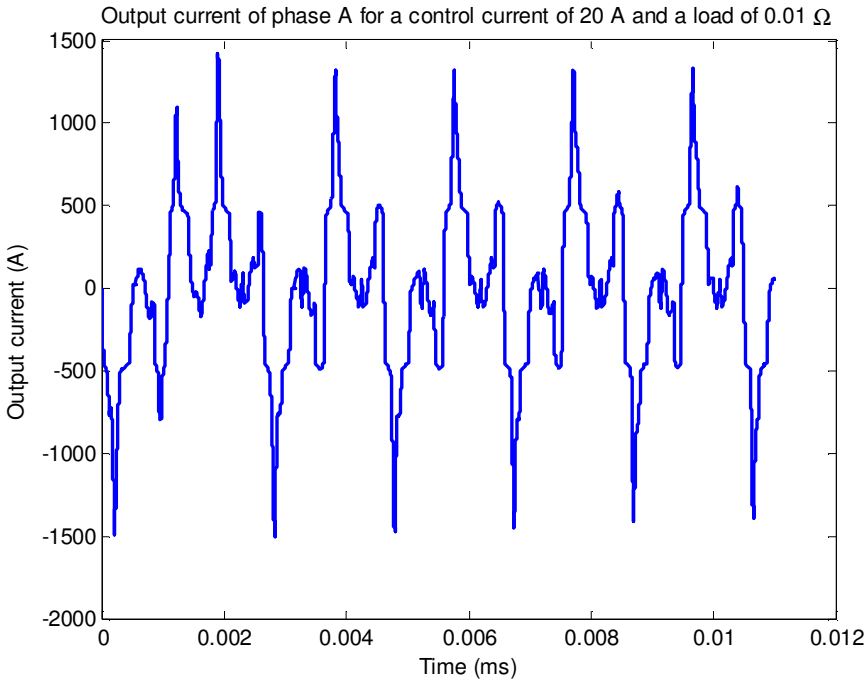

Figure 5-6: Example showing sudden numerical fluctuations (14-segments saturation curve)

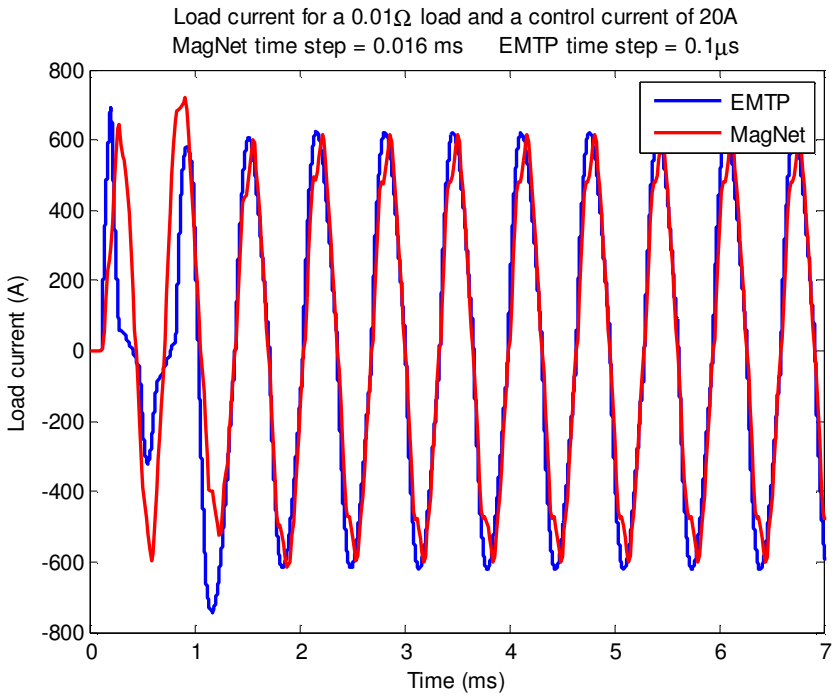

Figure 5-7 Load current for a control current of 20 A and a load of 0,01Ω

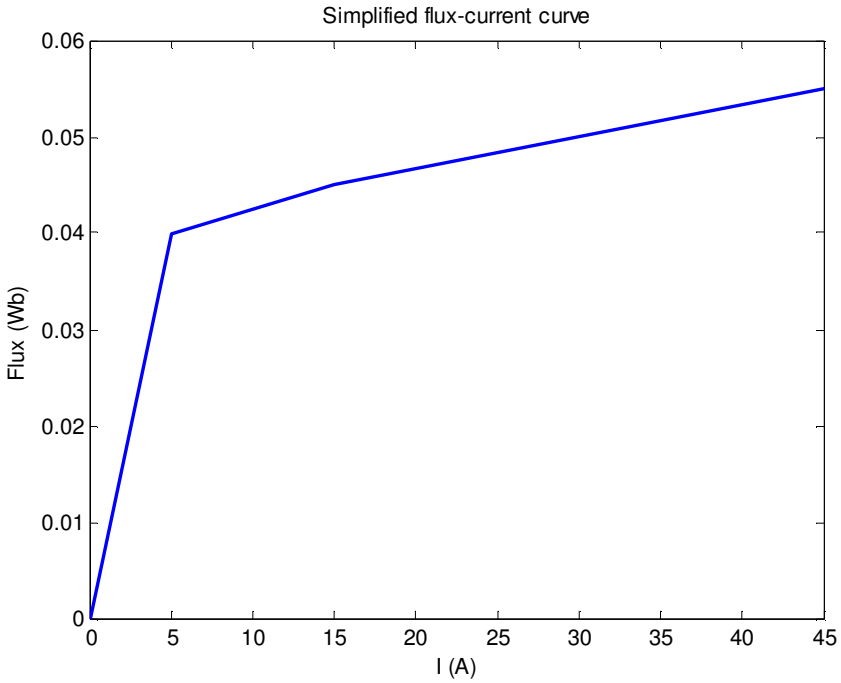

Figure 5-8 Simplified flux-current curve

5.4 Future works and improvements

The model created here is suitable to evaluate the behaviour of the NAEM in steady-state. The more saturated the secondary magnetic path is, the more accurate are the results given by the electrical model. As it was possible to understand throughout this section, one needs to make some improvements to the existing model in order to have an electrical model capable of simulating the behaviour of the generator both in transient and in steady-state operation. Some technical possibilities are introduced and discussed here.

5.4.1 Dependence between voltage generation in the generator and load current

One of the main improvements, if not the principal one, which needs to be done in the model, is the modification of the internal voltage sources in the machine to take into account the dependency that exists between the internal machine voltage, the output current and the control current. This addition to the model would significantly improve his behavior, mainly in light loading conditions (when the impedance of the load is high and/or when the control current is fixed at a small value).

Although it is a significant improvement that needs to be done in the future, it was left over in the scope of this project because of the amount of work required to achieve it. It may not seem so at first sight, but there is a complex relationship between the three quantities named above that would require a significant amount of simulation time and computational time to be able to characterize it. The complexity of the problem is coming from the fact that it is virtually impossible to decouple one variable from the two others: the internal flux is a non-linear function of the control current, the load current and the electrical phase angle of the rotor. Suggested approaches to model this relationship can be found in the literature regarding synchronous machines [30-33].

It would be possible to characterize this relationship in order to model it in EMTP-RV afterwards. To do so would require several weeks of continuous simulations in MagNet in order to be able to have as much operational points as possible for various operating conditions (various speeds, control currents and loads). This would allow the construction of surfaces in 3

dimensional plots that would characterize the relationship between the three values. It then would be possible to extrapolate an electrical relationship and implement it in the model.

The resulting EMTP-RV model would be more accurate and would reflect with more fidelity the actual behavior of the reference model. It would be mostly of substantial importance for one who wishes to model with more precision the behavior of the machine operating in the unsaturated region. Thus, this improvement is mandatory in order to achieve an electrical model capable of replicating the behavior of the NAEM in transient operation as well as in steady-state operation.

One possible avenue to characterize this relationship would be to fix one parameter and create a family of 3D curves by varying the three others (the fourth parameter in question here is the position of the rotor in relation to the stator which obviously influences the flux magnitude at a given time in the stator coils). The resulting curves would be similar to the one shown here as examples.

In the example below, two curves are produced for the flux, the output current and the position (or time) with a fixed control current. By superposing multiple curves together (in other words, by producing those curves for various levels of control current), it could be possible to develop a mathematical relationship between those parameters. Such relationship would make it possible afterwards to take into account the influence each one of the parameters has on others. This strategy represents a possible avenue to pursue the work that could be used in a future project.

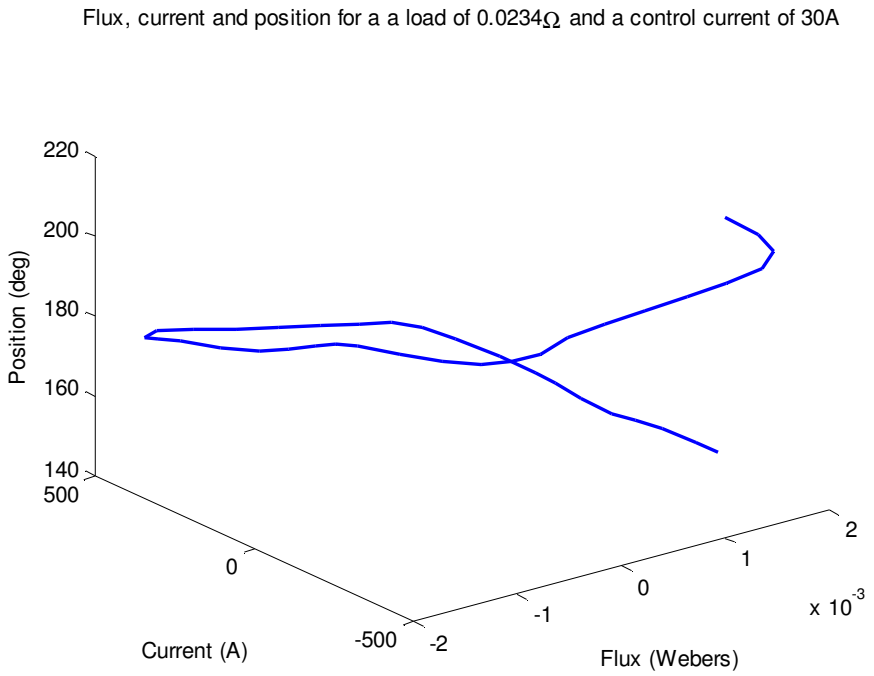

Figure 5-9 Flux, current and position for a load of 0,0234Ω and a control current of 30A

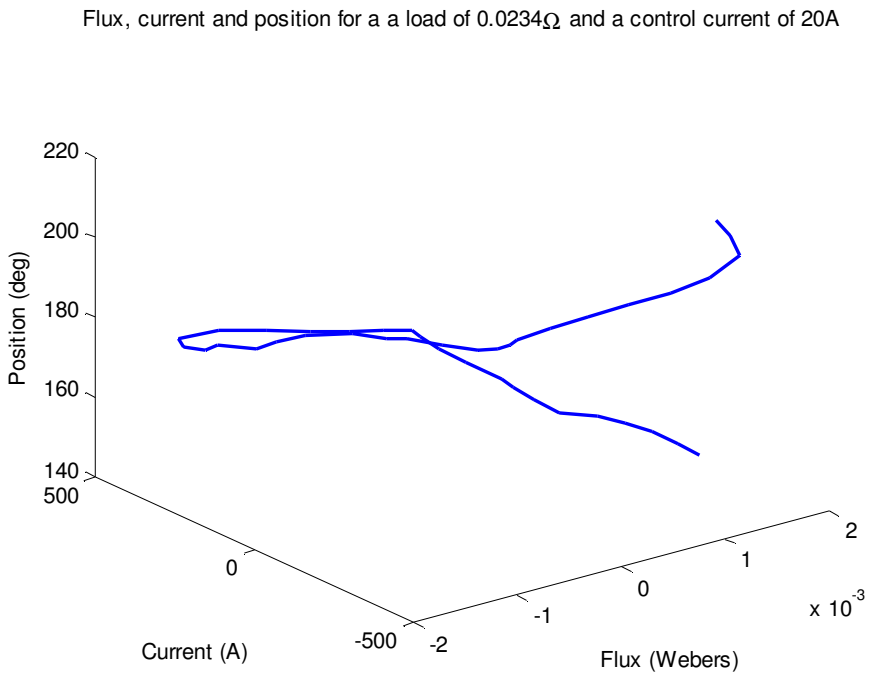

Figure 5-10 Flux, current and position for a load of 0,0234Ω and a control current of 20A

5.4.2 Inclusion of space harmonics

The following point also affects the internal voltage generation in the machine and is proposed as an alternative if the approach presented in the previous section is not implemented. As it was exposed in the section introducing the methodology of the project, the space harmonics were neglected for the EMTP-RV model. As a result, the machine's electrical model produces a purely sinusoidal voltage waveform and, therefore, a smooth current output (except for the harmonics induced by the non linear saturable elements and the distribution of the winding around the generator).

If one wishes to obtain a more faithful model that reproduces more accurately the output current waveform, the space harmonics should be included in the voltage generation modules in the model. To do so would require a more in depth analysis of the fem distribution characteristic around the machine stator. The ideal voltage sources then would be took off the model to be replaced by a module that includes the space harmonics effects. This improvement is not too significant on the magnitude of the output current though (this is the reason why it was neglected in the first place), but is of significant importance in order to reproduce more accurately the waveform of the load current. Different approaches are available in the literature to assess this problematic [34].

5.4.3 Improvement of the saturation characteristic curve

Some compromises were made regarding the saturation characteristic curve of the non linear inductances in order to reach an acceptable precision with the EMTP-RV model, in the saturated condition, with the assumptions taken in the modeling process. With the improvement mentioned above realized, the saturation curve will need to be adjusted to reflect to adapt to those changes. However, if a model is developed using the approach of section 5.4.1, this specific curve would not be mandatory (as the role of this curve in the model would already be taken into account).

Such curve would reflect with more precision the behavior of the magnetic model than the ones obtained with the simplified curve. Also, one could want to use a complete curve (with all the 14 segments that have been calculated for instance) in order to have a more sensible model in regards with waveform shapes. This is only fine-tuning thought and should not be considered until the final stages of the model; after all the suggestions above are completed.

CONCLUSION

This thesis presented the results obtained during this first attempt at building an electrical model of the New Architecture Electromagnetic Machine (NAEM) that was developed by Pratt & Whitney Canada. This project is in direct concordance with the MEE philosophy presented in chapter 1 and has been situated in its contemporary technological context with the literature review of this same chapter.

Throughout the whole project, the finite element model presented in chapter 2 was used as the reference. This model was built prior to the current project by Pratt & Whitney Canada. It was presented in details, firstly, for the reader to understand the technical innovations behind the design of the NAEM. Secondly, it allowed introducing the model which served as the foundations for this project and, at the same time, concluding the literature review. The presentation of the state of the art in this domain, as well as the theoretical concepts of the design of the NAEM, was the first objective pursued by this project.

The electrical model was afterwards presented in chapter 3. This electrical model was built in EMTP-RV using the available data in the finite element model. This is the main original contribution of this project. Prior to it, there was no model of the NAEM available in simulation software such as EMTP-RV, capable of modelling a complete electrical network. As this project was a first attempt at building an electrical model, some assumptions were made in order to restrain the amount of work to achieve the desired objectives.

The finite element model was then used to validate the electrical model in the fourth chapter. The results obtained with the EMTP-RV model were plotted against the ones obtained from MagNet (the reference). It was possible to see in this section that a good correspondence was achieved in steady-state with the electrical model despite some discrepancies that were later discussed. The results coming from the model show a normalized mean square error in steady-state as low as 2.6% in regards with the MagNet model in the scenarios presented. Therefore, this section confirmed that the second objective of the project was achieved: to obtain a first model of the NAEM in EMTP-RV, capable of reproducing with an acceptable accuracy the behaviour of the magnetic model of the generator in steady-state.

The fifth and last chapter contained an in-depth discussion of the results obtained with the electrical model. The main focus of the discussion was to explain the visible discrepancies between the obtained results and the reference in relation to the modelling assumptions that were made at the beginning of the project; keeping in mind that the model developed here was a steady-state model. Furthermore, an overview of some of the possible improvements to be achieved in future work was also presented, giving a starting point for a future project on this topic.

Due to the innovative nature of the work, some difficulties, unforeseen at the beginning, were encountered throughout the course of this project. As the work progressed, it became clearer that the objectives that were originally targeted had to be revised due to the magnitude of the technical challenges to undertake. The main objectives of the project were therefore adapted to best fit the scope of work of a master project. Even though the objectives of the project had to be revised and that difficulties were encountered, this project brings a technical contribution on the following aspects:

1. Outline a literature review of the state of the art regarding the MEE in its technical context: the more electrical aircraft.
2. Explain the technical innovations of the NAEM in relation with a typical permanent magnet synchronous machine. Prior to the NAEM, PMSM was not the preferred considered option for power generation due to the issue outlined in chapter 1: the destructive potential of an internal fault and the control capabilities of the NAEM overcome this limitation.
3. Demonstrate the behaviour of the NAEM in various scenarios. This contribution was done by performing an extensive number of FE simulations in MagNet. All the results obtained during those simulations are saved and archived; ready to be used in future projects.
4. Provide a first electrical model of the NAEM, built in EMTP-RV. The model that was built during this project is a first attempt at developing an electrical model of the NAEM in opposition to the existing FE model. One of the main improvements of the model developed in EMTP-RV is the possibility to integrate it easily to a complete network to perform simulations.

5. Present the performances of this first electrical model and explain the most significant discrepancies between the developed model and the reference.
6. Explore some of the most promising possible improvements that could be undertake in a future project to obtain a more accurate electrical model. This last section can be used as a base for future projects to improve the electrical model of the NAEM.

As it has been established earlier in this document, the more electrical engine and, more generally, the more electrical aircraft are two key concepts that will significantly influence the technical decisions to come in the aerospace industry. As the electrical portion of the total power generated and distributed in aircraft is expected only to increase in the future years (in relation to more typical sources of power already found in aircraft such as mechanical power, hydraulic power, ...), the need for electrical simulation tools is growing correspondingly. Thus, the necessity for the industry to be able to simulate a whole aircraft network is just around the corner. Using an electrical model as the one developed in this project for the electrical generator will facilitate the integration of said generator in a complete aircraft network, enabling the possibility of complete electrical studies of aircraft electrical networks. Such compatible-model with network simulation software of the NAEM was not available prior to the project. The results obtained during this project therefore contribute to take one step further toward the objective of simulating complete aircraft electrical networks.

REFERENCES

[1] J. A. Weimer, "Electrical power technology for the more electric aircraft," in *Digital Avionics Systems Conference, 1993. 12th DASC., AIAA/IEEE*, 1993, pp. 445-450.

[2] X. Roboam, "New trends and challenges of electrical networks embedded in "more electrical aircraft"," *2011 Ieee International Symposium on Industrial Electronics (Isie),* 2011.

[3] D. Izquierdo*, et al.*, "Electrical Power Distribution System (HV270DC), for Application in More Electric Aircraft," *2010 Twenty-Fifth Annual Ieee Applied Power Electronics Conference and Exposition (Apec),* pp. 1300-1305, 2010.

[4] C. R. Avery*, et al.*, "Electrical generation and distribution for the more electric aircraft," *2007 42nd International Universities Power Engineering Conference, Vols 1-3,* pp. 1007-1012, 2007.

[5] B. Mecrow*, et al.*, "Electrical Machines and Drives for the More Electric Aircraft," *Iet Electric Power Applications,* vol. 5, pp. 1-2, Jan 2011.

[6] K. Muehlbauer and D. Gerling, "Two-generator-concepts for electric power generation in More Electric Aircraft Engine," in *Electrical Machines (ICEM), 2010 XIX International Conference on*, 2010, pp. 1-5.

[7] K. Emadi and M. Ehsani, "Aircraft power systems: technology, state of the art, and future trends," *Aerospace and Electronic Systems Magazine, IEEE,* vol. 15, pp. 28-32, 2000.

[8] J. S. Cloyd, "Status of the United States Air Force's More Electric Aircraft initiative," *Aerospace and Electronic Systems Magazine, IEEE,* vol. 13, pp. 17-22, 1998.

[9] M. E. Elbuluk and M. D. Kankam, "Motor drive technologies for the power-by-wire (PBW) program: options, trends and tradeoffs. I. Motors and controllers," *Aerospace and Electronic Systems Magazine, IEEE,* vol. 10, pp. 37-42, 1995.

[10] M. Howse, "All-electric aircraft," *Power Engineer,* vol. 17, pp. 35-37, Aug-Sep 2003.

[11] I. Moir, "The all-electric aircraft-major challenges," in *All Electric Aircraft (Digest No. 1998/260), IEE Colloquium on*, 1998, pp. 2/1-2/6.

[12] M. J. Provost, "The More Electric Aero-engine: a general overview from an engine manufacturer," in *Power Electronics, Machines and Drives, 2002. International Conference on (Conf. Publ. No. 487)*, 2002, pp. 246-251.

[13] G. R. Sundberg, "Civil Air Transport - a Fresh Look at Power-by-Wire and Fly-by-Light," *Proceedings of the Ieee 1990 National Aerospace and Electronics Conference, Naecon 1990, Vols 1-3,* pp. 1365-1368, 1990.

[14] D. Weale and C. Whitely, "Power takes flight," *Power Engineer,* vol. 18, pp. 32-36, Jun-Jul 2004.

[15] Pratt & Whitney Canada, "Pratt & Whitney Canada New Architecture Electromagnetic Machine (NAEM)," Pratt & Whitney Canada, Mississauga, 2010.

[16] W.-K. Chen, *The electrical engineering handbook*. Amsterdam ; Boston: Elsevier Academic Press, 2005.

[17] K. A. Dooley and K. Dooley, "Thermal protection for electric machine e.g. directly driven permanent magnet generator and starter motor in aircraft, uses temperature sensitive stator material to prevent overheating during operation," WO200147091-A; EP1240702-A; WO200147091-A1; US6313560-B1; US2002047477-A1; EP1240702-A1; JP2003518896-W; US6664705-B2; US2004103520-A1; US2005082939-A1; RU2251195-C2; US7098561-B2; EP1240702-B1; DE60043265-E; CA2397635-C, 2001.

[18] K. A. Dooley and K. Dooley, "Current interrupter for electric machine of gas turbine engine, has conductor whose cross-sectional area is sized relative to threshold current such that generated magnetic field causes conductor to flow so as to open electrical circuit," US2005099250-A1; WO2005045870-A1; US7023307-B2; EP1680797-A1; EP1680797-B1; DE602004008957-E; JP2007534112-W; DE602004008957-T2, 2005.

[19] Infolytica corporation. (2010, 01/12/2011). *MagNet Live Docs*. Available: http://www.infolytica.com/secured/customer/elite/livedocs/

[20] S. J. Chapman, *Electric machinery fundamentals*, 4e éd. -- ed. Boston ; Montréal: McGraw-Hill Higher Education, 2005.

[21] HBM - Perception, "PNRF Reader Toolkit 32/64-bit," 6.18 ed: HBM Deutschland, 2011, p. Software programming tool to read the proprietary PNRF (Perception Native Recording File) file format.

[22] J. Mahseredjian*, et al.*, "On a new approach for the simulation of transients in power systems," *Electric Power Systems Research,* vol. 77, pp. 1514-1520, 2007.

[23] J. Mahseredjian, "Simulation des transitoires électromagnétiques dans les réseaux électriques," *Les techniques de l'ingénieur,* vol. Dossier no D4130, p. 12, 2008.

[24] A. E. Fitzgerald*, et al.*, *Electric machinery*, 6th ed. Boston, MA ; Montreal: McGraw-Hill, 2003.

[25] J. A. Martinez*, et al.*, "Parameter determination for modeling system transients-Part III: Transformers," *IEEE Transactions on Power Delivery,* vol. 20, pp. 2051-62, 2005.

[26] ASTM, "ASTM Standard B48-00 (2011) - Standard Specification for Soft Rectangular and Square Bare Copper Wire for Electrical Conductors," ed. West Conshohocken, PA: ASTM Internationnal, 2011.

[27] N. Mohan*, et al.*, *Power Electronics : Converters, applications and design*, third ed. Danvers, MA: John Wiley & Sons, 2003.

[28] R. J. Hyndman and A. B. Koehler, "Another look at measures of forecast accuracy," *International Journal of Forecasting,* vol. 22, pp. 679-688, 2006.

[29] L. Yan and Z. Chao, "Simulation of harmonic armature reaction in synchronous brushless excitation," in *Artificial Intelligence, Management Science and Electronic Commerce (AIMSEC), 2011 2nd International Conference on*, 2011, pp. 4304-4306.

[30] A. M. El-Serafi and J. Wu, "Determination of the parameters representing the cross-magnetizing effect in saturated synchronous machines," *Energy Conversion, IEEE Transactions on,* vol. 8, pp. 333-342, 1993.

[31] A. Bellara*, et al.*, "Two-Dimensional Exact Analytical Solution of Armature Reaction Field in Slotted Surface Mounted PM Radial Flux Synchronous Machines," *Magnetics, IEEE Transactions on,* vol. 45, pp. 4534-4538, 2009.

[32] T. Sebastian and G. R. Slemon, "Transient modeling and performance of variable-speed permanent-magnet motors," *Industry Applications, IEEE Transactions on,* vol. 25, pp. 101-106, 1989.

[33] G. Xiong and S. A. Nasar, "Analysis of fields and forces in a permanent magnet linear synchronous machine based on the concept of magnetic charge," *Magnetics, IEEE Transactions on,* vol. 25, pp. 2713-2719, 1989.

[34] C. Ong, *Dynamic Simulation of Electric Machinery Using Matlab/Simulink*. Upper Saddle River: Prentice Hall PTR, 1998.

ANNEX 1 – TYPICAL PROCEDURE TO CONNECT MATLAB TO MAGNET

```
%% Lunching/initialization of MagNet
disp('Initialization...')
% Create objects handles for MagNet
mn7 = actxserver('Magnet.Application');
set(mn7, 'Visible', 1);

% Set MagNEt constants
consts = invoke(mn7, 'getConstants');

% Open MagNet document
dev = invoke(mn7, 'openDocument', 'C:\Users\Bertrand\Desktop\MagNet
Simulations\Parametrical Study\ParametricalStudy.mn', ...
get(consts, 'infoFalse'));
view= invoke(dev, 'getView', int32(1));
invoke(view, 'setScaledToFit', get(consts, 'infoTrue'));
disp('Inialization completed')
```

ANNEX 2 – TYPICAL COMMANDS TO EXTRACT DATA FROM MAGNET TO MATLAB

```
                                                    %% Data extraction
% Retreiving of all the problem/solution IDs
invoke(mn7, 'processCommand', 'ReDim problemIDs(0)');
invoke(mn7, 'processCommand', 'problemID = getDocument().getSolution().getSolvedProblems()');
invoke(mn7, 'processCommand', 'Call setVariant(0, problemID, "MATLAB")');
problemID = invoke(mn7, 'getVariant', 0, 'MATLAB');

% Retrieving of all the solution time instants
invoke(mn7, 'processCommand', 'ReDim TimeInstants(0)');
invoke(mn7, 'processCommand', 'Call getDocument().getSolution().getFieldSolutionTimeInstants(1,TimeInstants)');
invoke(mn7, 'processCommand', 'Call setVariant(0, TimeInstants, "MATLAB")');
timeInstants = invoke(mn7, 'getVariant', 0, 'MATLAB');

%                       Flux linkage                          %
%-------------------------------------------------------------%
disp(' ')
disp('Extraction of flux linkage data...')
% Preallocation of memory
fluxLinkage = zeros(41,length(problemID)+1);

% Steady-state data extraction
% The following loop extracts the 41 last data point of each solution (41
% data points = ~360 electrical degrees)
for m=1:length(problemID)

    invoke(mn7, 'processCommand', 'ReDim solutionID(2)');
    invoke(mn7, 'processCommand', ['solutionID(0)=',num2str(problemID{m}x)]);
    l = 1;

    for k=length(timeInstants)-41:length(timeInstants)

        invoke(mn7, 'processCommand', ['solutionID(1)= TimeInstants(', num2str(k-1), ')']);
        invoke(mn7, 'processCommand', 'CALL getDocument().getSolution().getFluxLinkageThroughCoil(solutionID,"LowV1-     PhA
Coil", magnitude, phase)');
        invoke(mn7, 'processCommand', 'Call setVariant(0, magnitude)');
        fluxLinkage(l,problemID{m}+1) = invoke(mn7, 'getVariant', 0);

        if problemID{m} == 1  % The time data has only to be saved once
            fluxLinkage(l,1) = timeInstants{k};
        end

        l = l + 1;

    end
end
disp('Extraction of flux linkage data completed')
%-------------------------------------------------------------%
```

ANNEX 3 – FILENAMES CORRESPONDENCE TABLE

Filename	Contents	Format	Comments
NAEM.ecf	EMTP-RV model of the NAEM	EMTP-RV	Electrical model of the NAEM built using EMTP-RV
Matlab_scripts.zip	Matlab scripts	Matlab	Contains all the Matlab scripts used during the project
ParametricalStudy.mn	MagNet model	MagNet	Solved MagNet model for 130 test cases (refer to table 2-1 for details)
Recordings.zip	Real-time recordings	Perception	Real-time measurements of a prototype; data given by PWC